SAND2023-00384

SANDIA REPORT
SAND2023-00384
Printed March 2023

Sandia National Laboratories

Flammability and Dispersion of Tritium in Confined Release Scenarios

Randy C. Shurtz, Alexander L. Brown, Lynelle K. Takahashi

Prepared by
Sandia National Laboratories
Albuquerque, New Mexico
87185 and Livermore,
California 94550

Sandia National Laboratories
U.S. DEPARTMENT OF ENERGY NNSA

Sandia National Laboratories is a multimission laboratory managed and operated by National Technology & Engineering Solutions of Sandia, LLC, a wholly owned subsidiary of Honeywell International Inc., for the U.S. Department of Energy's National Nuclear Security Administration under contract DE-NA0003525.

Issued by Sandia National Laboratories, operated for the United States Department of Energy by National Technology & Engineering Solutions of Sandia, LLC.

Available to DOE and DOE contractors from
U.S. Department of Energy
Office of Scientific and Technical Information
P.O. Box 62
Oak Ridge, TN 37831

Telephone: (865) 576-8401
Facsimile: (865) 576-5728
E-Mail: reports@osti.gov
Online ordering: http://www.osti.gov/scitech

Available to the public from
U.S. Department of Commerce
National Technical Information Service
5301 Shawnee Rd
Alexandria, VA 22312

Telephone: (800) 553-6847
Facsimile: (703) 605-6900
E-Mail: orders@ntis.gov
Online order: https://classic.ntis.gov/help/order-methods/

ABSTRACT

Ignition of a flammable tritium-air mixture is the most probable means to produce the water form (T_2O or HTO), which is more easily absorbed by living tissue and is hence ~10,000 times more hazardous to human health when uptake occurs compared to the gaseous form (T_2 or HT; per Mishima and Steele, 2002). Tritium-air mixtures with T_2 concentrations below 4 mol% are considered sub-flammable and will not readily convert to the more hazardous water form. It is therefore desirable from a safety perspective to understand the dispersion behavior of tritium under different release conditions, especially since tritium is often stored in quantities and pressures much lower than is typical for normal hydrogen. The formation of a flammable layer at the ceiling is a scenario of particular concern because the rate of dispersion to nonflammable conditions is slowest in this configuration, which maximizes the time window over which the flammable tritium may encounter an ignition source. This report describes the processes of buoyant rise and dispersion of tritium. Accumulation of flammable concentrations of tritium next to the ceiling is a common safety concern for hydrogen, but this situation can only occur if dispersion rates are slow with respect to rates of release and rise. Theory and simulations demonstrate that buoyancy does not cause regions with flammable concentrations to form within buildings from sources that have previously been mixed to sub-flammable concentrations. A simulated series of tritium release events with their associated dispersion behavior are reported herein; these simulations apply computational fluid dynamics to rooms with three different ceiling heights and a variety of tritium release rates. Safety-related quantities from these simulations are reported, including the mass and volume of tritium occurring in a flammable mixture, the presence or absence of a flammable layer at the ceiling, and the time required for dispersion to nonflammable conditions after the end of the tritium release event. These safety metrics are influenced by the magnitude and rate of the tritium release with respect to the air volume in the room and also the momentum of the plume or jet with respect to the ceiling height. Several screening criteria are recommended to assess whether a specific tritium release scenario is likely to form a flammable layer at the ceiling. The methods and results in this modeling study have applicability to explosion safety analysis for other buoyant flammable gases, including the lighter isotopes of hydrogen.

ACKNOWLEDGEMENTS

Many thanks are due to Bill Weaver at the U.S. DOE for being supportive of this work. NA-19 funding for the simulations reported in this work was provided by Nanette Founds. Thanks also to Rick Karnesky, who helped expedite access to these funds to start work. Lynelle Takahashi and Rajan Tandon have guided and championed this work and provided supplementary funds required to finish analyzing the simulations, document the results in this report, and present these findings at the 43rd Tritium Focus Group. We also gratefully acknowledge reviews provided by Andrew Kurzawski, Mike Hobbs, Rick Karnesky, and Carlos Lopez.

CONTENTS

LIST OF FIGURES

LIST OF TABLES

ACRONYMS AND TERMS

Acronym/Term	Definition
A	Area of release surface
CF	Conversion fraction
CFD	Computational fluid dynamics
CV	Control volume
CVFEM	Control volume finite element mechanics
D	Hydraulic diameter
DOE	Department of Energy
Fr	Froude number
g	Gravity acceleration
h	Height or altitude in kilometers
H_p	Penetration height of a buoyant gas jet
H_R	Height of room
HC	Hazard category
ID	Internal diameter
ISF	Ignition safety factor
L	Large domain (9.36 m length by 6.24 m width by 7.62 m = 25 ft height)
LES	Large Eddy Simulation
LFL	Lower flammability limit (volume fraction, e.g., 0.04 for hydrogen)
M	Medium domain (7.85 m length by 5.23 m width by 4.1 m = 13.5 ft height)
MFLT	Maximum flammable layer thickness
NL	Nonlinear iterations
P_i	Partial pressure of gas species designated by subscript "i"
R	Refined meshes that transition in size from coarse to medium to fine
RANS	Reynolds-averaged Navier-Stokes
Re	Reynolds number
S	Small/standard domain (3.6 m length by 2.4 m width by 2.4 m = 7.9 ft height)
TFNS	Temporally filtered Navier-Stokes
UFL	Upper flammability limit (volume fraction, e.g., 0.74 for hydrogen)
v	Velocity
V_{LFL}	Volume at the LFL
V_P	Volume of released gas in purified form at standard pressure and temperature
V_R	Volume of room

Acronym/Term	Definition
α	Scaling parameter for jet penetration correlation
ρ	Density of fluid mixture
μ	Viscosity of fluid mixture

1. INTRODUCTION

Tritium is a radioactive isotope of hydrogen that has roughly three times the mass of hydrogen. It has a half-life of 12.3 years (DOE-STD-1129), and upon decay it releases a low-energy beta particle and produces ^{3}He. The low-energy beta decay product has insufficient kinetic energy to pose a hazard to the human body through external exposure; therefore, the radiological hazards result purely from tritium that has been taken into the body (i.e., via inhalation, ingestion, skin absorption, or injection).

The specific hazards posed by a given amount of tritium depend on the physical and chemical form that is absorbed into the body. Most tritium inventories in DOE facilities are stored in gaseous form (T_2) or in metal tritide (or hydride) beds that by design liberate T_2 upon heating. While both gaseous T_2 and metal tritides pose radiological hazards, one of the bounding hazards for tritium facility inventories is a fire scenario wherein T_2 is liberated and oxidized to tritiated water vapor. Tritiated water vapor (i.e., tritium oxide), has 10,000 times higher dose consequences than T_2 due to the improved ability for the human body to retain tritium in water form (Mishima and Steele, 2002). Due to this higher dose consequence and the ease with which tritiated water vapor can be absorbed into the human body, the conversion fraction (CF) of T_2 gas to tritiated water vapor in fire scenarios is a primary concern in tritium safety analyses.

A previous body of work was compiled at Sandia National Laboratories that focused on the oxidation behavior of gaseous T_2 in the regime below the lower flammability limit (LFL) in fire environments (SAND2022-4187, Brown et al. 2022). The report showed that, for T_2 releases of scales relevant to most tritium facilities, the gas plume will tend to be at concentrations below the LFL when it interacts with a fire or other ignition source simply due to the tritium quantities and the resulting length and time scales involved in dissipating flammable plumes of gas. The concept of an ignition safety factor (ISF) was introduced, which accounts for the volumes of both the tritium gas and the room to evaluate the probability of a rapid oxidation event. Values of the ISF significantly higher than 1 result in a safer environment for T_2 storage because there is sufficient air within the room to disperse all T_2 below the LFL. This ISF concept is pragmatic, conventional, and works well for evaluating the oxidation risk involved with tritium releases that are most common at DOE tritium facilities (i.e., relatively slow releases of low-pressure gas). However, this simple concept does not capture how hazards vary with the rate of a tritium release, which will be discussed in the current work.

The earlier work also investigated the behavior of sub-LFL concentrations of tritium gas in fire environments. Experiments were performed in a tube reactor with sub-LFL concentrations of H_2 and D_2 to identify the magnitude and isotopic trends in the oxidation onset temperature and oxidation kinetics in this concentration regime. Compared to oxidation kinetics for gases in the flammable regime, the oxidation onset temperature was found to be much higher for dilute H_2 and D_2, suggesting that sub-LFL H_2 must incur a greater exposure to a fire for any oxidation to occur compared to larger H_2 releases typical in industrial or laboratory settings. The sub-LFL kinetic model was extrapolated to T_2 and implemented into the modeling and simulation code, SIERRA/Fuego, (2022a, 2022b), an in-house CFD code developed and maintained at Sandia National Laboratories, which was used to simulate dilute releases of tritium into a small, 21 m^3 room. The principal source of air motion in the room was from the fire (buoyancy and thermal expansion). The CFs from simulations suggested that unless the tritium is constrained to pass close to the fire (< 1 m), ~10% or less of the release is expected to oxidize before it leaves the room with the fire.

The perspective provided by the experiments and simulations in the previous report (Brown 2022) indicates that the current regulatory assumption of CF = 100% for tritium in a fire scenario (DOE-STD-1129-2015) is only realistic when a tritium release occurs very close to a fire and/or in situations where a release exceeds the LFL and encounters an ignition source before it disperses. An example of a scenario with concentrations above the LFL that is often considered to be hazardous for buoyant flammable gases like hydrogen isotopes (molecular protium = $^1H_2$ or H_2, deuterium = $^2H_2$ or D_2, and tritium = $^3H_2$ or T_2) is a release that rises and forms a flammable layer just below the ceiling. This scenario is of concern because such a layer could plausibly persist for an extended period of time, which increases the space and time available for the mixture to be ignited. Flammable or ignitable ceiling layers are known to occur for industrial hydrogen releases involving gas volumes that are orders of magnitude larger than tritium volumes existing at most facilities where tritium is stored and used. Nuclear power plant hazards and other applications that produce, use and store large quantities of hydrogen are settings where such phenomena have been most commonly observed or anticipated as a credible threat to safety (*e.g.*, Kim et al. 2015, Kuznetsov et al. 2015, Liang et al. 2018, de Stefano et al. 2019).

This report extends the work from Brown 2022. Simulations without fires are used to identify and characterize the conditions associated with a release event that are required to create a layer with flammable (>LFL) tritium concentrations below the ceiling; protium is also considered. This situation is referred to as a flammable ceiling layer in this report. The specific conditions when this situation becomes a concern are outlined and associated with metrics for flammability and momentum. Dispersion is also investigated via the simulations to understand how any flammable region (including but not limited to a layer at the ceiling) becomes less hazardous over time. The simulations are used to quantify timeframes required for this dispersion below the LFL to happen. The roles of buoyancy, dispersion, the size of the release, the rate of the release, the dimensions and volume of the room in question, as well as the duration of the simulated release are considered as factors affecting the risks and hazards of a given release scenario.

The following subsection within this introduction reviews the physical mechanisms that govern changes in gas concentrations from a release event over time. Subsequently, the methods section describes computational methods for the simulations, the geometries and meshes, the definition of cases in the simulation matrix, and metrics used to interpret and correlate the results of the simulations. Preliminary comparisons of these metrics to experimental hydrogen release measurements from the literature are also included at the end of the methods section. The results of the simulations are presented thereafter; these results are grouped by the three room sizes investigated. The results section includes a section comparing the simulated behavior to the flammability and momentum metrics defined in the methods section, including commentary on the safety implications for release events with different sizes and rates. The results section wraps up with summaries of metrics, behaviors, and conservatisms associated with the simulations. Appendices are included after the conclusions to document mesh and time resolution studies as well as a checklist that summarizes recommended procedures as developed in this work to assess risk for release of a flammable gas such as tritium.

1.1. Mechanisms of Gas Stratification and Mixing

It is well known that gases with lower density have a propensity to rise above gases with higher density. This phenomenon is known as buoyancy, and it is the principle that enables flight of hot air balloons and dirigibles. A difference in density driving buoyant motion may be caused by a difference in concentration of species that have different molecular weights, a difference in

temperature, or both. Figure 1-1 is a simplified illustration of buoyant rise of a colored region consisting of light gas (representing an isotope of H_2) through a surrounding heavier gas (representing air); this representation ignores diffusion and advective mixing effects. A release of gas with low density occurs next to the floor in Figure 1-1a, and a bubble rich in H_2 rises to the ceiling in the subsequent panels; this evolution is the typical means by which a layer rich in hydrogen can form beneath the ceiling when a release occurs elsewhere in the room.

The illustration in Figure 1-1 is oversimplified to focus entirely on the motion of the light gas with respect to the heavier surrounding gas. In real situations with release of a hydrogen isotope, the light gas will rise as a buoyant plume. This plume will tend to break up and the region of light gas will mix with the surrounding air. Buoyancy is an important driving mechanism for motion and mixing of light gases (including tritium) with heavier gases such as air, but there are additional factors to consider, as described below.

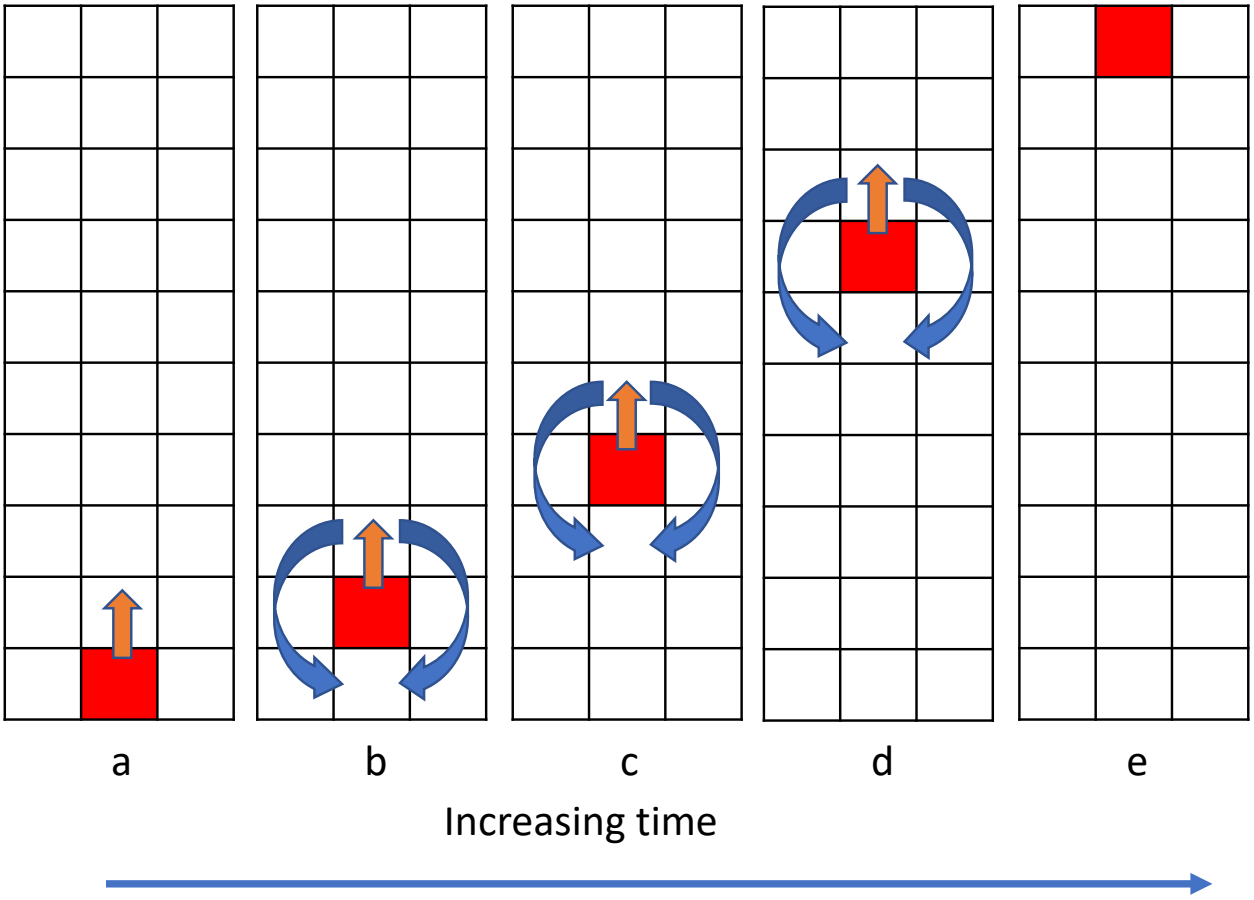

Figure 1-1. Illustration of buoyant rise of a low-density gas such as H_2 (red box) surrounded by a gas with higher density, such as air (uncolored boxes). The motion of the light gas is denoted by the orange arrows, and the motion of the heavy ambient gas is denoted with blue arrows.

Molecular diffusion is another means of mixing gases with differing compositions. Diffusion occurs because gaseous molecules are always in random motion, so there is a tendency for concentrations to become more equal within a container or room over time. Molecular diffusion occurs even when there is no bulk motion of the fluid. Diffusion rates may be calculated from differences in concentrations between two adjacent locations using Fick's Law, which includes a proportionality

constant known as the binary molecular diffusivity. Dispersion of H_2 in air from an initially enriched ceiling layer via molecular diffusion is illustrated in Figure 1-2.

The diffusion example in Figure 1-2 could occur after the buoyant rise shown in Figure 1-1. However, diffusion is not dependent on gravity, so diffusive mixing will also occur simultaneously with buoyant rise. This combination means that the bubble of light gas illustrated in the idealized buoyancy illustration in Figure 1-1 will partially mix with air and become less concentrated as it rises. This combination of buoyant and mixing behavior was observed in the 3D simulations presented in the main body of this report. Therefore, the concentration at the ceiling in a more realistic version of Figure 1-1e would be lower than the initial concentration near the floor in Figure 1-1a.

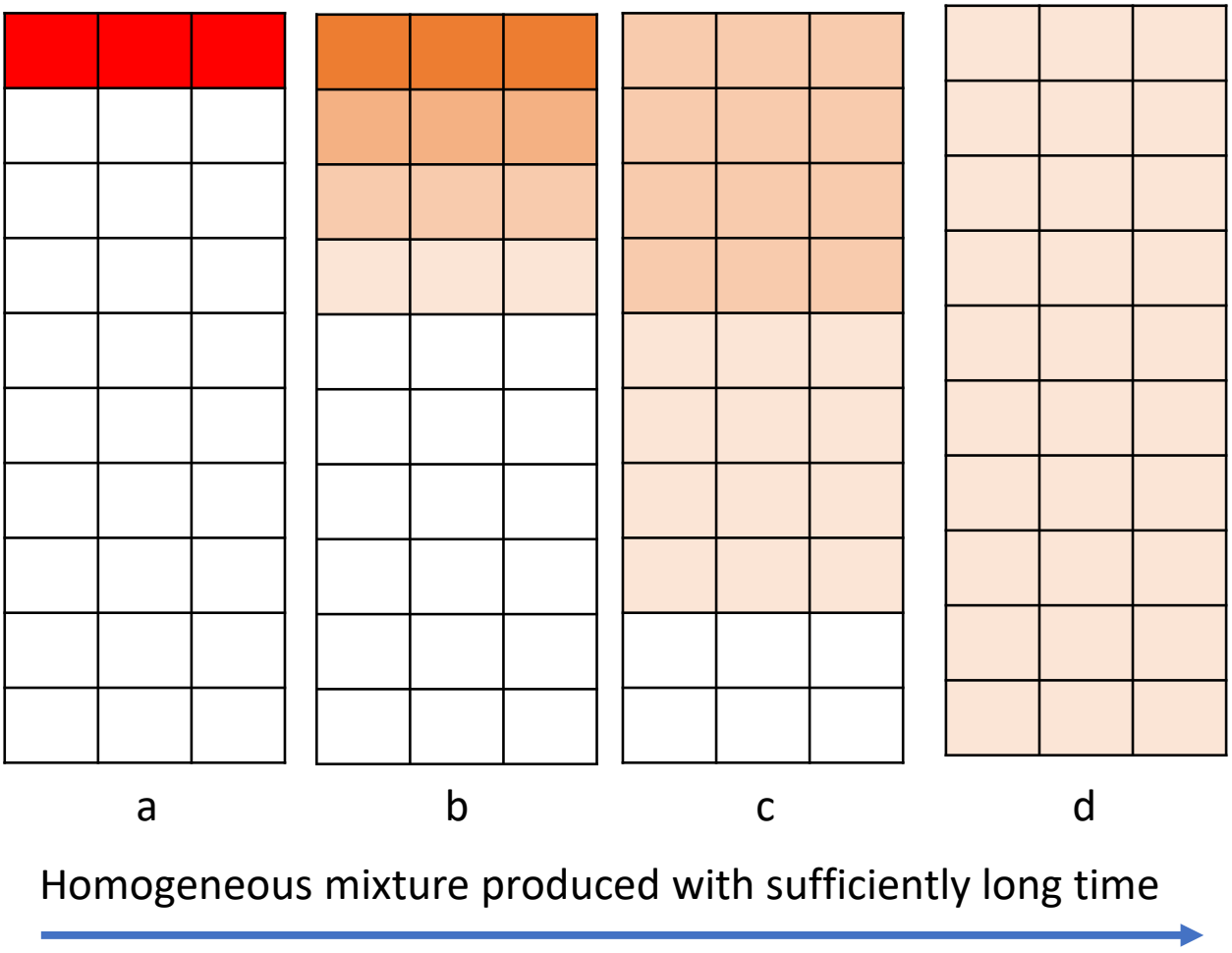

Figure 1-2. Illustration of mixing via molecular diffusion (and/or gas motion) from an initial layer of highly concentrated H_2 (red boxes) at the ceiling with air below. Lighter shades denote lower H_2 concentrations.

Any motion of the gas constitutes advection, which will enhance rates of mixing above the simple molecular diffusion rate, which is representative of the slowest physical mixing rate for gases. For conceptual simplicity, much of the analysis and discussion in this report assumes gases are initially stagnant and laminar conditions prevail. Faster motion of the gas with respect to surrounding regions will produce faster mixing rates, especially in the high-velocity turbulent regime. A completely stagnant gas environment is unusual, as air motion can originate from many sources, including ventilation systems, buoyant rise driven by release of light gas, thermally driven buoyancy from heat sources, motion of nearby objects, etc.

It is not uncommon for safety planners considering gas release events to assume that buoyancy will drive light gases up and heavy gases down, which leads them to recommend that detectors for the respective gases (or oxygen sensors) be installed near the ceiling or floor, respectively. However, this paradigm often neglects or greatly underestimates rates of dispersive mixing processes that have been observed in practical facilities and scenarios. Some relevant experimental trends are discussed here, and Section 3.4 includes more detailed consideration of specific experimental cases. Multiple experimental studies have shown various factors such as the size and rate of release affect the behavior of a release of light gas (Lacome et al. 2011). In some cases, dispersion can happen rather quickly, so that formation of a ceiling layer concentrated in light gases is avoided (Theilacker and White, 2005), or such a layer disperses quickly (Bauwens and Dorofeev 2014).

For example, a study by J. C. Theilacker and M. J. White (2005) showed that a release of helium in a real accident scenario mixed to vertical uniformity much faster than anticipated, and the gases stayed mixed for the full period of observation. A helium release was detected via O_2 sensors in a large tunnel, but the measurements at different heights were the same, regardless of distance or time from the source (Theilacker 2005). This rapid mixing was enhanced above the rate of pure diffusion by the 3 km/hr flow through the tunnel; we note from our experience that this velocity is of the same order of magnitude as air motion caused by a jetting or buoyant gas release, swinging doors, etc.

Theilacker's follow-up experiments of dispersion used a stagnant column with a 10 cm internal diameter (ID) and 1.8 m height. They investigated dispersion of pre-stratified scenarios as well as initially pure columns of light gases with a closed top and heavy gases with a closed bottom; they measured diffusion rates in the direction opposed to buoyant motion in both cases. In this worst-case stagnant scenario, the helium concentration at the closed top of an initially pure column (furthest from the open end) was reduced to 50% within 5.5 hours and 4% within 17 hours (Theilacker 2005). Releases of hydrogen isotopes are expected to disperse faster than helium due to the higher diffusivity, and this diffusivity trend is also demonstrated in Theilacker's experiments with heavy SF_6 gas in an inverted column. From an initially pure column of SF_6 with an open top, the time to achieve 50% dispersion at the closed bottom of the column was about 40 hours due to the much lower diffusivity of SF_6 in air compared to helium in air (the SF_6 concentration was reduced to 4% in 112 hours). Numerical simulations showed that the measured dispersion rates for both light and heavy gases were consistent with diffusion-limited mixing of the helium or SF_6 with ambient air exchanged through the open end of the stagnant column (Theilacker 2005). In summary, Theilacker's paper clearly shows that diffusive mixing occurs in the direction opposed to buoyancy, and gas motion typical of most release scenarios significantly enhances the rate of dispersion.

By investigating a hydrogen release scenario in an isothermal 80 m^3 chamber (7.2 m length, 8.78 m width, 2.88 m height) with no ventilation, another experimental study found that the size and rate of release have strong effects (Lacome et al. 2011). Lacome's measurements confirmed that the hydrogen release at floor-level near the center of the room initially stratified via buoyancy to create a ceiling layer and then dispersed via diffusion to form a homogeneous mixture within about 4 hours for all cases considered. The worst-case experimental release of 1 g/s H_2 over 4 minutes (240 grams total) yielded an estimated maximum flammable volume of about 40 m^3 (approximately half the chamber). Flammable concentrations persisted in the test cell beyond the two-hour duration of the test and extrapolating the dispersion trend suggests all concentrations would be sub-flammable (< 4%) in about 4 hours. The formation of a concentrated ceiling layer under similar conditions was confirmed visually using helium as a surrogate (the mass flow rate was doubled to account for the differences in molecular weight). In contrast, releases at a rate of 0.2 g/s over the same duration (49 grams total) did not result in flammable compositions for any of the locations measured (max of

2.2%, Lacome 2011). These results show that the magnitude and rate of a hydrogen release strongly affect the formation and dispersion of flammable zones.

An experimental study by C. R. Bauwens and S. B. Dorofeev (2014) coupled with CFD modeling demonstrated formation of a flammable ceiling layer from a buoyancy-driven release of H_2 in a 1/6 scale warehouse. 36.3 g of H_2 was released from a uniform 0.13 m square outlet over approximately 1.2 seconds, with the outlet located near the center of a room with a 2.72 m ceiling and a volume of 45.4 m^3 (Bauwens 2014). Measurements at three ceiling locations registered the rise in hydrogen concentration after 2 to 7 seconds, and the concentrations remained marginally flammable (between 4% and 7%) up to at least 20 seconds after the release. The trend from this scenario (Bauwens 2014) suggests that dispersion of the ceiling layer to nonflammable conditions (< 4%) would occur on the order of seconds up to a few minutes rather than hours as in the Lacome (2011) scenario. This difference is probably due to the fact that the release size from the Bauwens study is about 15% of the Lacome study, while the room volume from Bauwens is closer to the room volume from Lacome (about 57%) and the ceiling heights are very similar.

No combination of diffusion and/or buoyancy in open air should produce concentrations of released light gas (H_2 isotope) at any location or time that are higher than the initial concentration at the point of release. This assertion is a consequence of the second law of thermodynamics, which dictates that dispersion or mixing is spontaneous (i.e., formation of a more disordered state), but formation of enriched concentrations is not. The second law requires energy to be expended for the creation of regions in a miscible fluid that are enriched in specific components and depleted in others with respect to the initial conditions. For this reason, enrichment to any significant degree requires an engineered separation system that exploits characteristic phase-change temperatures, pressure gradients through a selective membrane, differential rates of diffusion, different binding affinities on a surface, or very high g-forces in a centrifuge. In the absence of a configuration resembling an engineered separation system with significant energy input, any control volume or "pocket" containing a light gas such as a hydrogen isotope with a concentration below the lower flammability limit (LFL) cannot spontaneously re-concentrate to form a flammable mixture.

Badino (2009) showed mathematically that Earth's gravitational force acting on a mixed gas system does not exploit a property difference with sufficient energy to cause detectable separation or enrichment of specific gaseous components within height differences on the scale of buildings. When a column of gas has a density gradient due to gravity, the partial pressures of the components vary differently with increasing altitude. For the H_2-air system, the ratio of partial pressures at any altitude with respect to the ratio at sea level (denoted by subscript "0") in a stagnant gas column is given by:

$$\frac{\left(\frac{P_{H_2}}{P_{air}}\right)}{\left(\frac{P_{H_2}}{P_{air}}\right)_0} = exp\left(\frac{h}{8.5} - \frac{h}{122.2}\right) = exp\left(\frac{h}{9.1}\right), \quad (1)$$

where h is the altitude in kilometers and the characteristic length scales for H_2 and air are 122.2 km and 8.5 km, respectively (Badino 2009). According to this relationship, a very large altitude of 6.3 km in a stagnant column of air is required for the concentration at the top be to double the ground-level concentration of H_2 under static equilibrium conditions.

As an example, if an initial uniform H_2 concentration is 3.8% by volume (slightly below the LFL), Equation (1) indicates that an altitude of 1 km is required to produce a very modest enrichment at the top equal to the LFL of 4.0% while depleting the ground-level concentration to 3.6%. Equation (1) refers to equilibrium conditions, so it says nothing about the time scale required for this highly

inefficient enrichment process to occur. Measurements of helium diffusion (a reasonable surrogate for hydrogen and especially tritium; see Lacome 2011 and Brown 2022) from a stagnant 1.8-m column with an open bottom equilibrated with the surroundings in about 24 hours (Theilacker 2005); linear scaling of this result suggests that the required equilibration time for stratification of hydrogen in a hypothetical 1-km column could be on the order of 18 months. Such a configuration would require the 1-km column of air to be completely stagnant and sealed off from outside air. Any bulk motion in the column will mix the gases so that stratification via gravity is suppressed, and some motion is virtually guaranteed over such a large height unless a space is specifically designed to suppress it.

The implication of Equation (1) and the example above is that auto-stratification of gases from an initially dispersed condition via gravity alone within either a single-story laboratory or a multi-story building has no physical basis, especially if the timescale under consideration is on the order of several weeks or less. This implication makes sense because gas centrifuges achieve relatively modest single-stage changes in concentration by inputting significant energy to create g-forces that are large multiples of normal gravity. The tallest buildings in the United States are all less than 0.5 km, and any realistic laboratory space is more than two orders of magnitude shorter (this study considers ceiling heights between 2.4 m and 7.62 m). These observations indicate that layers of light gas observed to accumulate and persist for long periods near ceilings (or heavy gases near floor-level) have explanations other than auto-enrichment. A plume of light gas originating from a concentrated source may arrive at the top of a room via some combination of buoyancy, high-velocity jets, or other means. However, once this stratified configuration has been achieved, the buoyant force becomes dormant. Thereafter, dispersion of a stagnant light gas from the ceiling layer (or a heavy gas from the floor) will inevitably occur (Badino 2009, Theilacker 2005). In the absence of bulk motion, such dispersion is controlled by very slow rates of molecular diffusion. Hence, for low-quantity gases like tritium, the maximum ignition risk occurs during and immediately after the most rapid phase of release from containment. Except for cases where the storage area is small compared to the quantity of the release, the hazard diminishes with time.

To summarize the case of interest for this report in the context of the relevant physics, a release of hydrogen (or tritium) in an indoor space can occur either rapidly or slowly. A release of hydrogen gas at high concentration will result in a buoyant plume that rises towards the ceiling; this plume can also be designated as a jet if the initial velocity of the release is high enough. The plume begins to disperse via molecular diffusion as well as more rapid mixing driven by the motion of the plume rising through the surrounding air. If the room is sufficiently tall and the hydrogen is not released too quickly, the plume can be largely or even entirely dispersed to sub-flammable concentrations as it rises. However, a high rate of hydrogen release and/or a shorter ceiling can cause the buoyant plume or jet to reach the ceiling with a relatively high concentration, although still inevitably at a lower concentration than at the point of release. If a thick layer that is rich in hydrogen covers the whole ceiling and no sustained sources of gas velocity are present (i.e., there is no active ventilation), the flammable ceiling layer has the potential to persist for an extended period on the order of minutes or perhaps even hours. If only a thin flammable layer forms or if the layer does not cover the whole ceiling, dispersion to sub-flammable concentrations is likely to occur quickly. Once any control volume of gas is dispersed below the LFL, it will not spontaneously concentrate to form a flammable mixture, regardless of its location.

This page left blank

2. METHODS

2.1. Computational Methods

Computational Fluid Dynamics (CFD) can be used to simulate fluid mechanics processes that include diffusion, buoyancy, and other forms of mixing (including turbulent mixing). SIERRA/Fuego (2022a, 2022b) is a low-Mach number CFD code originally designed for simulating heat transport for objects in fires and is generalized and consequently used to support a variety of additional problems of interest to Sandia and affiliates who use the code. A major differentiating factor compared to most other CFD codes is that SIERRA/Fuego is a control volume finite element mechanics (CVFEM) code rather than a more traditional control volume (CV) code. This distinction has implications for the software design, but is of more minor consequence to the user, who should be aware of how this affects mesh volume sizing at interfaces. A variety of mesh elements are available to the unstructured solver; however, the meshes used in this study are all hexahedral and regularly orthogonal, which would be suited to a structured code solver as well. Fuego is massively parallel, permitting jobs to scale and run on thousands of processors on laboratory computational resources, and the resolved scale for simulations typically is in the range of 1−100 cm.

The continuum approach used for gases in SIERRA/Fuego and many other similar codes relies on the bulk gas density (including all species) for buoyant motion. This computational approach is not expected to capture subtle variations of species occurring over large elevation changes described by Equation (1). However, Section 1.1 shows that the length scales where this physics mechanism could be relevant are much larger than the heights of buildings and rooms that are of interest for hydrogen and tritium safety. A column of gas must be completely stagnant for a very long time (many months) for the gravitational process described by Equation (1) to apply and cause any significant level of enrichment for light gases at high elevations, which differs substantially from conditions in real buildings.

All cases were run with version 5.6.1 of the SIERRA/Fuego code. Designed under the governance of DOE order O 414.1D, version control, nightly testing, and verification are inherent in the code design and maintenance practices that lend to the credibility of the results. Besides verification, validation is the other aspect of scientific computing that provides credibility to the predictions. Validation is generally demonstrated in published data comparisons over the lifetime of the code's use and is more specifically demonstrated in our prior work with the code for the tritium safety problem for a buoyant He plume (Brown et al., 2022).

Turbulence involves multiscale rotating motion that enhances mixing significantly with respect to the lower limit for mixing rates, which is molecular diffusion in stagnant gas. One of the functions of turbulence models is to approximate the large-scale effects of the momentum transfer and mixing that occurs for turbulent flows on the sub-grid scale. For most of the simulations described in this work, laminar solvers were used instead of turbulent solvers to produce dispersion rates that are conservatively low because they neglect the mixing attributable to turbulent motion on the sub-grid scale.

A variety of turbulence models are available in SIERRA/Fuego, and the Temporally Filtered Navier-Stokes (TFNS) (Tieszen et al. 2005) model (a hybrid LES/RANS capability) was selected for this study to model turbulence when applicable. The use of a turbulence model was considered necessary for cases where the principal source of momentum (the hydrogen isotope inlet) was sufficiently high. Simulations with tritium inlet boundary conditions having $Re > 2300$ were assumed to be

turbulent in this study (Re is the Reynolds number as defined in Section 2.3), and the remainder were assumed to be laminar. The three cases using the turbulent TFNS model also used a simplified Schmidt number approach to predict mixing via turbulent diffusion. A Schmidt number of 0.34 (with an equivalent Prandtl number) was implemented, as derived for tritium-nitrogen mixtures near 1% tritium concentration by volume (see Chapter 3 of Brown 2022).

2.2. Simulation Geometries, Meshes, and Case Definition

The baseline mesh geometry shown in Figure 2-1 was used in our previous simulation study of hydrogen isotope release events co-located with an ISO9705 standard room fire (see Chapter 5 of Brown 2022). This room has dimensions of 3.6 m length by 2.4 m wide with a 2.4 m ceiling height. A door frame in the center of one end is 2.0 m tall and 0.8 m wide with a wall thickness of 0.17 m. The open door leads to an outer region with the same 2.4 m square cross section and a depth of 1.2 m. This outer region has a coarser mesh and open boundaries that allow the hydrogen isotope contaminant to be dispersed away from the vicinity of the room after passing through the door.

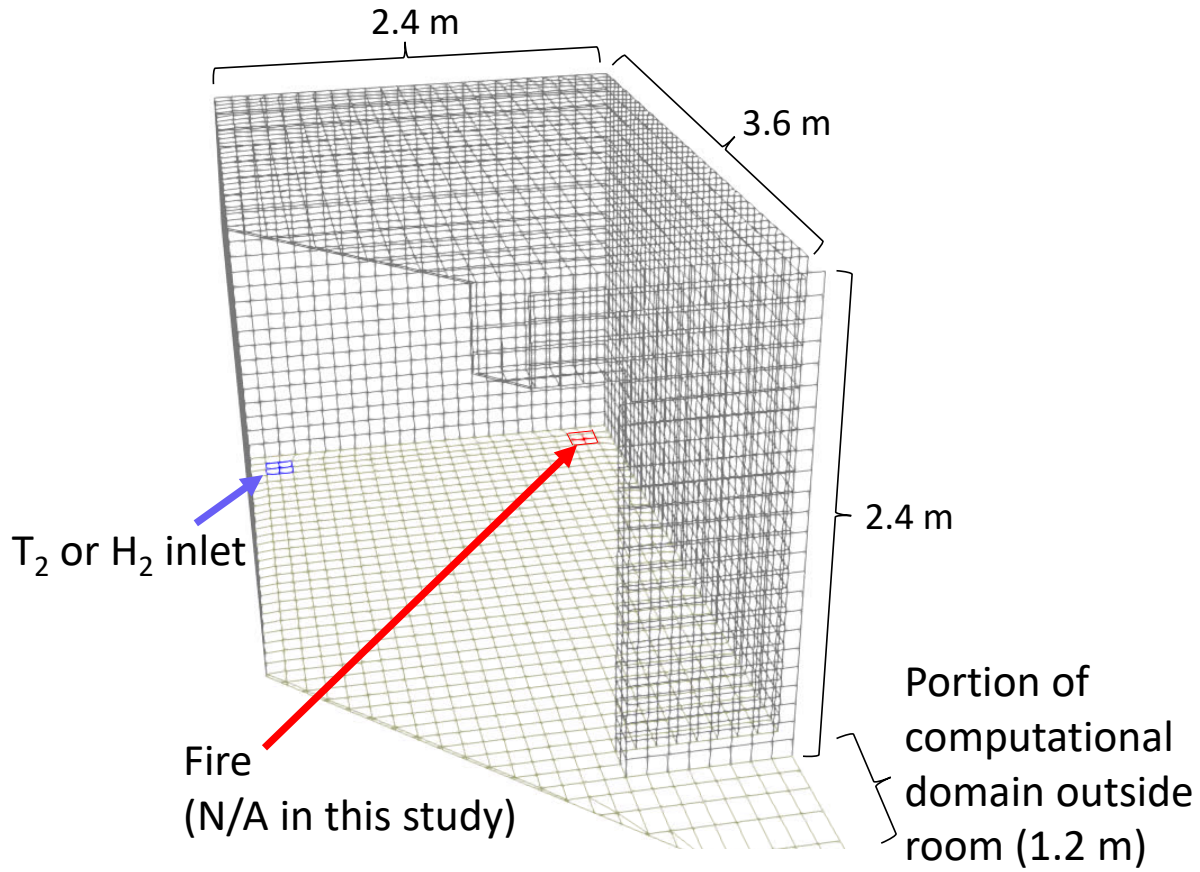

Figure 2-1. Illustration of the coarse ISO9705 mesh (smallest or standard domain size "S") with front left corner cutaway (Brown 2022); the gas inlet is highlighted blue in the back left corner.

For reference, the standard room height shown in in Figure 2-1 is slightly shorter than the experimental hydrogen venting studies of Lacome et al. (2011) and Bauwens and Dorofeev (2014), with 25% to 46% of their reported experimental room volumes. The red square region with a length of 0.17 m in the back right corner in Figure 2-1 was designated as the fire source in the previous

report (a gas burner) based on the ISO-9705 standard, but the fire is turned off for the purpose of this dispersion study. The square blue region in the back left corner of Figure 2-1 with the same dimensions prescribed for the fire is designated as the inlet surface for a hydrogen isotope gas release. The size and placement of this gas inlet was chosen for convenience and for compatibility with the existing mesh scale.

In the simulations, some hydrogen isotope exits the room due to buoyancy, mixing, and ambient motion or diffusion through an open door (see Figure 2-1 and Figure 3-31). The presence of this door is a feature of the ISO9705 standard fire scenarios simulated in the previous study (Brown 2022). For the purpose of this study the open door is representative of a variety of features common to most laboratory and storage locations that allow tritium to escape via passive airflow and/or diffusion, even when there is no literal open door. Such features include ventilation ducts, drop-tile ceilings with connections to adjacent spaces, ducts or conduits for various utilities, and closed doors with gaps around the edges. The space between the top of the open door frame and the ceiling make the simulations in this work conservative in the sense that flammable ceiling layers are retained longer than would be the case if there were openings in the ceiling (with or without active ventilation). For most of the scenarios considered in this study, <15% of the released gas left the room before the remaining gas was dispersed to nonflammable conditions, and <40% of the release was lost from the domain before the most aggressive (largest and fastest) releases were similarly dispersed. These results suggest that the open door does not dominate the simulated dispersion behavior.

Simulations with various hex-mesh resolutions are compared in Appendix A and Appendix B to verify that the solutions are sufficiently converged for this plume and dispersion scenario. Predicted metrics of interest were found to be sensitive to mesh resolution in locations with the highest velocities and tritium concentrations, which was the region around the plume and near the ceiling. These metrics of interest included maximum flammable mass (or volume) and dispersion time. Therefore, the coarse mesh used in (Brown 2022) and shown in Figure 2-1 was locally refined near the hydrogen isotope plume (back left corner around blue surface) and also near the ceiling. These meshes are designated by the prefix "R" in this work to indicate that refinement with respect to the coarse mesh shown in a Figure 2-1 has been applied to produce a mixture of coarse, medium, and fine mesh elements. The numerical mesh designations in Figure 2-2 and the Table 2-1 generally increase to denote meshes with smaller minimum dimensions (finer resolution near the ceiling and the tritium plume). The mesh size was transitioned gradually between the coarsest scale shown in Figure 2-1 (included to reduce computational expense) and the most refined regions surrounding the plume in Figure 2-2, with the same minimum mesh dimension imposed in the vertical direction near the ceiling. The surface designated as the tritium gas inlet boundary condition is highlighted in each view of Figure 2-2 (square with 0.17 m length) to indicate differences in mesh scale (the floor is shown at the top of each view); this inlet corresponds to the blue surface in Figure 2-1.

The meshes in Figure 2-2 for the small or standard ISO9705 domain (S) defined above were scaled to create medium (M) and large (L) domain sizes; these letters are used as suffixes for numbered meshes in Table 2-1 and elsewhere in this report to distinguish cases with different domain sizes and mesh resolutions. The medium and large room sizes were created from the ISO-9705 geometry with vertical and horizontal scale factors that differ somewhat in order to match both the ceiling height and volume of real spaces where tritium is stored that were identified or requested for assessment from within the U.S. DOE complex of laboratories. The scale factors for the medium room (M) with respect to the standard room (S) are 1.71 vertically and 2.18 horizontally. The scale factors for the large room (L) with respect to the standard room (S) are 3.175 vertically and 2.6 horizontally.

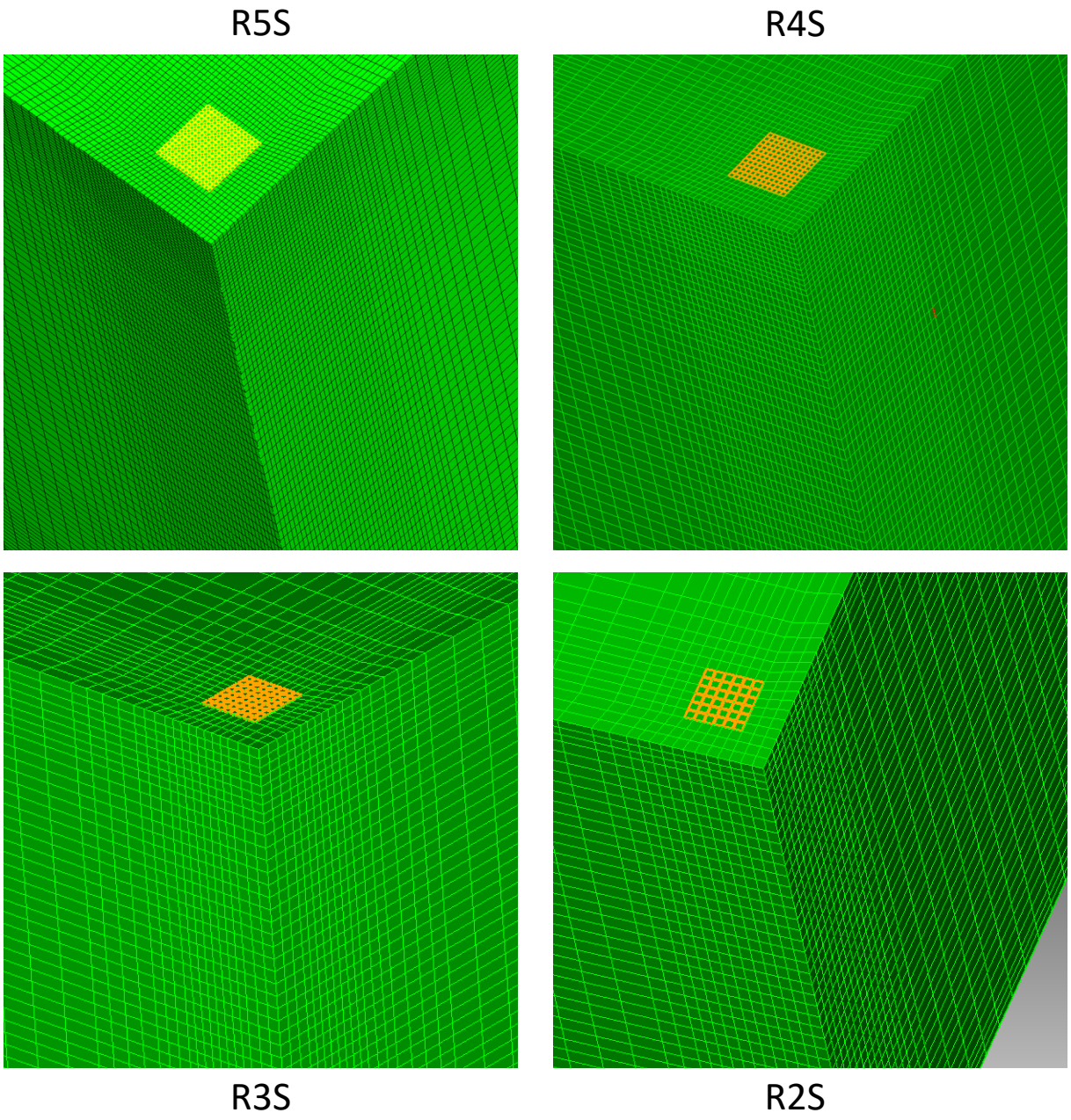

Figure 2-2. Examples of meshes in the smallest domain size (ISO9705 = "s"), highlighting gas inlets with 6 edge elements for R2S, 8 for R3S, 12 for R4S, and 16 for the R5S inlet edge.

Table 2-1 provides the room and tritium inlet dimensions for each mesh. The third column in Table 2-1 identifies the square length (equal to width) for the tritium inflow, which results from the horizontal scale factors for all medium and large meshes except R6M, which uses a ¼-length region from the center of the R5M inlet. The central columns of Table 2-1 list the smallest and largest mesh dimensions within the room. The dimensions in Table 2-1 are for the room only; they exclude the coarsest mesh in the region outside the open doorway as shown on the lower right of Figure 2-1.

Table 2-1. Simulation mesh dimensions and nonlinear iterations used for best solutions

Mesh Name	Room Size	Square Inlet Length = Width	Vertical Mesh Size Range (Min and Max)	Horizontal Mesh Size Range (Min and Max)	Nonlinear Iterations	Associated Simulation Case Numbers
R4S	L = 3.6 m W = 2.4 m H = 2.4 m	17 cm	1.42 cm 8.5 cm	1.42 cm 8.5 cm	6	S1
R5S	L = 3.6 m W = 2.4 m H = 2.4 m	17 cm	1.06 cm 8.5 cm	1.06 cm 8.5 cm	4	S2, S3
R5M	L = 7.85 m W = 5.23 m H = 4.1 m	37.06 cm	1.8 cm 14.535 cm	2.3 cm 18.5 cm	6	M1, M2, M4, M5, M6
R6M	L = 7.85 m W = 5.23 m H = 4.1 m	9.265 cm	1.8 cm 14.535 cm	2.3 cm 18.5 cm	6	M3 (reduced inlet size)
R4L	L = 9.36 m W = 6.24 m H = 7.62 m	44.2 cm	4.5 cm 27.0 cm	3.7 cm 22.1 cm	6	L1, L2

Additional mesh resolutions were also used for the mesh resolution study summarized in Appendix A. These are mostly coarser, including the uniform base mesh from our previous report (Brown et al. 2022) and scaled versions of it; the base mesh has twice the resolution of the coarse mesh shown in Figure 2-1. The maximum flammable mass and volume decreased as the mesh was refined until converged solutions were achieved for all three domain sizes. Appendix A shows that convergence of the residuals improved with increasing nonlinear iterations as well as mesh refinement; the best refined mesh dimensions and nonlinear iterations for computational solutions of practical durations (computational expense) are listed in Table 2-1. The mesh resolution study in Appendix A also shows that the differences in mesh size and aspect ratio for the three domain sizes were not large enough to significantly affect the solution quality, especially for the small and medium domains. The right column in Table 2-1 identifies simulations names that use the meshes designated in the left column; the characteristics defining these simulations are defined in subsequent tables.

2.2.1. Simulation Case Matrix Definition

The size, shape, and rates of real release events are expected to vary widely with the conditions of storage and the nature of a proposed accident scenario. At this writing the most probable failure modes and release characteristics for tritium vessels are unknown; a follow-up study has been proposed to characterize failure modes of containers that are most common for tritium storage applications. Given the lack of such information when these simulations were defined, the boundary condition for a hydrogen isotope release were defined for this computational study as simple step changes in velocity on the blue square surface shown in Figure 2-1.

Four surface sizes were used for the hydrogen isotope inlet in this study, including one for each room size (Small, Medium, and Large) plus a ¼ linear scale variant in the medium room (1/16 area); the dimensions of these inlets are provided in the third column of Table 2-1 and inlet areas are provided in the fifth (center-right) column of Table 2-2. These square inlet areas are an arbitrarily

chosen boundary condition, but they can be thought of as representing a release occurring from one or more pressurized vessels stored within a box-shaped container with an open top. The specified inlet areas have the advantage of being large enough to avoid extreme mesh refinement in the vicinity of a small jetting orifice.

The velocity was varied on the different inlet surfaces so that general observations could be made regarding effects of inlet momentum. Velocities are specified indirectly in Table 2-2 in terms of release durations (third column) with respect to the total mass of the release (second column). The actual velocities of these releases that were used as boundary conditions in the inlet surface are listed with other metrics in the next section (see Table 2-3).

It is reasonable to assume larger inventories of tritium gas would be stored in larger facilities, so Table 2-2 specifies a release of 30 g T_2 (maximum for a Hazard Category 3 or HC3 facility) for simulations in the small room (S), with 240 g T_2 for the medium room (M) and 1.5 kg T_2 for the large room (L). The medium and large releases correspond to inventories in Hazard Category 2 (HC2) facilities as currently defined (see DOE-STD-1027-2018). As noted above, the medium and large room sizes were sized to represent real laboratory spaces where tritium is stored. The mass of the release in the second column of Table 2-2 corresponds to a pure volume of released hydrogen isotope shown in the fourth column (at standard temperature and pressure). Note that the pure volume of gas released for cases S2 and S3 with different hydrogen isotopes is equivalent, even though the mass differs by a factor of 3 due to the molecular weights. The room volumes and heights corresponding to the three size designations are listed in the columns at the far right of Table 2-2. The case numbers in Table 2-2 include the letter designating the room size. The rows of Table 2-2 are also color-coded by room size (Small = blue, Medium = green, Large = orange). Darker shades of these colors designate distinctive characteristics, including a different isotope for case S3 (H_2 instead of T_2), a smaller inlet size for case M3, and turbulent rather than laminar models for cases M3, M5, M6, and L2.

Table 2-2. Tritium and hydrogen release simulation matrix

Case Number	Release Mass	Release Duration	V_p (Pure Gas Volume) of T_2 or H_2	Inlet Area	Turbulent or Laminar	V_R (Room Volume)	H_R (Room Height)
S1	30 g T_2	122 s	0.1217 m^3	0.0289 m^2	Laminar	20.7 m^3	2.4 m
S2	30 g T_2	30 s	0.1217 m^3	0.0289 m^2	Laminar	20.7 m^3	2.4 m
S3	10 g H_2	30 s	0.1217 m^3	0.0289 m^2	Laminar	20.7 m^3	2.4 m
M1	240 g T_2	180 s	0.9734 m^3	0.1373 m^2	Laminar	168.5 m^3	4.1 m
M2	240 g T_2	60 s	0.9734 m^3	0.1373 m^2	Laminar	168.5 m^3	4.1 m
M3	240 g T_2	30 s	0.9734 m^3	0.0086 m^2	Turbulent	168.5 m^3	4.1 m
M4	240 g T_2	45 s	0.9734 m^3	0.1373 m^2	Laminar	168.5 m^3	4.1 m
M5	240 g T_2	45 s	0.9734 m^3	0.1373 m^2	Turbulent	168.5 m^3	4.1 m
M6	240 g T_2	30 s	0.9734 m^3	0.1373 m^2	Turbulent	168.5 m^3	4.1 m
L1	1.5 kg T_2	300 s	6.1 m^3	0.1954 m^2	Laminar	445.1 m^3	7.62 m
L2	1.5 kg T_2	8 s	6.1 m^3	0.1954 m^2	Turbulent	445.1 m^3	7.62 m

The release sizes in Table 2-2 were chosen to be conservative rather than typical representations of different hazard categories (see DOE-STD-1027-2018). The inventories specified here are conservatively large with respect to the associated room sizes, and the assumption that the entire T_2 mass specified is released from a single location is a further conservatism. The degree of this conservatism becomes apparent by considering the example of a Hazard Category 3 facility (HC3), where a maximum total inventory of smaller than 30 grams is stored in several containers that are scattered across multiple rooms, where each room is larger than the smallest room simulated in this study. Another conservatism was to assume the full release durations in Table 2-2 were limited to less than 5 minutes (300 s), whereas many credible release scenarios could occur much more slowly.

The largest and most rapid release in Table 2-2 approximates a large gas cylinder at high pressure in catastrophic failure (case L2 with a duration of 8 seconds). Case L1 represents a much slower leak over 5 minutes from the same type of source. It is assumed that a large facility (with 25-foot ceilings) is more likely to contain tritium inventories on the order of kilograms. The remaining cases can be thought of as representing smaller tritium containers, where storage and handling in smaller facilities is assumed to be more likely. Comparisons and commentary in the results section consider how the behavior of the simulated release events would differ in rooms with different ceiling heights.

2.3. Analysis Metrics and Methods

2.3.1. LFL Selection and Flammable Regions from Simulations

In this work, simulated release events are characterized in terms of how much flammable volume (with concentrations above the LFL of 4% by volume or moles) exists during and after the release. This metric is of interest because flammable regions with larger volumes that persist for longer durations have higher probabilities of encountering an ignition source, which is the scenario where a large tritium-to-water CF (near 100%) is most likely to occur. The amount of tritium mass contained within flammable regions is also presented, as this quantity relates directly to the amount of the more hazardous T_2O that can be formed if the flammable region is ignited. Dispersion times required to achieve non-flammable conditions after the release event ends are noted. The locations of flammable regions with respect to the original plume and the ceiling are also identified visually from the simulations, along with shape-based features that may affect dispersion rates.

The LFL varies with direction of flame propagation; the minimum LFL of 4% occurs in the upward direction for H_2 where buoyancy enhances flame propagation (Shapiro and Moffette 1957, Kumar 1985, Cashdollar et al. 2000, Bauwens and Dorofeev 2014). The LFL is also expected to vary with isotope type; the LFL for D_2 is expected to be higher than H_2 at ≈5.5% (Koroll and Kumar, 1991; Cashdollar et al., 2000) and the LFL for T_2 is expected to be highest of all at 6.6% (Cadwallader and Petti, 2002). Therefore, using the minimum LFL from H_2 measurements for all isotopes is conservative (see Chapter 2 of Brown 2022). An additional aspect of this conservatism is that concentrations near the LFL are not expected to combust or oxidize with high efficiency (Shapiro and Moffette, 1957). Therefore, for T_2, the concentration bins between about 4% and 6% are not expected to be flammable, and the concentration bins between 6% and 10% should not yield full conversion to the oxidized form (T_2O or HTO).

Postprocessors in Fuego were set up to output various metrics at each timestep, including masses and volumes of various concentration bins near the minimum LFL for hydrogen (4%). A step function is defined based on a volume concentration c_j for species j (where j = T_2 or H_2) between c_{min} and c_{max} is defined in the Fuego postprocessors as (SIERRA/Fuego 2022b):

$$step(c_j,c_{min},c_{max}) = \begin{cases} 0, & c \le c_{min} \\ 1, & c_{min} < c < c_{max} \\ 0, & c \ge c_{max} \end{cases}. \quad (2)$$

This step function is used within volume integrals over the whole computational domain to sum up only the mass of species *j* that occurs within a concentration bin (defined as between c_{min} to c_{max}) and only the volume containing gas within this concentration bin for species *j*:

$$Mass_j(c_{min},c_{max}) = \int \rho Y_j step(c_j,c_{min},c_{max}) dV \quad (3)$$

$$Volume_j(c_{min},c_{max}) = \int step(c_j,c_{min},c_{max}) dV \quad (4)$$

where ρ is the bulk gas density and Y_j is the mass fraction of species *j*. Equations (3) and (4) were written into the postprocessor section of the Fuego input file for a variety of bins designated by different combinations of c_{min} and c_{max}. Fuego output the results of these calculations to a text file that was updated for each timestep as the simulations were running.

The upper flammability limit (UFL) is not utilized as a safety metric in this work; it has a value for normal hydrogen of about 74% to 76% in air on a volumetric or molar basis (Shapiro and Moffette 1957, Cashdollar et al. 2000). The following sections show that the simulated scenarios identified in Table 2-2 have sufficient air for dispersion of the full release below the LFL to occur given enough time. Therefore, any released hydrogen isotope that occurs in a region with concentrations above the UFL (typically near the source) will become ignitable as it mixes with the surrounding air to concentrations below the UFL. This flammable mixture will always occur before dispersion drives the concentration still lower to non-ignitable conditions below the LFL. The UFL is most useful as an ignition safety metric for scenarios where a flammable gas is released into an enclosure with very limited air volume, which is less representative of the small typical inventories for tritium gas.

2.3.2. Additional Flammability Metrics

This section defines additional metrics used to analyze the simulation results that account for the LFL as well as effects of room volume and in some cases room height. The next section defines other metrics used to consider effects of momentum and includes tabulated metrics for flammability and momentum for the simulations presented in this study. The ignition safety factor (ISF) was introduced as a metric in Chapter 2 of our recent report (Brown 2022). The ISF is the ratio of the room volume V_R to the maximum volume that a flammable mixture can occupy; for hydrogen isotopes this parameter is defined as the volume occupied when diluted in air to the conservative lower flammability limit of 4% (from protium). Since the volume at the LFL, V_{LFL}, is the volume of a pure gas V_P divided by the LFL, ISF can be obtained from either of the following expressions:

$$ISF = \frac{V_R}{V_{LFL}} = \frac{V_R LFL}{V_P}. \quad (5)$$

The ISF can be thought of as a measure of excess air with respect to the magnitude of the gas release. Although the ISF does not address transient hazards before released gases reach equilibrium concentrations, larger ISF values indicate greater safety, with ISF > 1 indicating that there is sufficient air volume in the room for the full release to be dispersed below the LFL. The inverse of

the ISF is also conceptually useful, as it is the maximum fraction of a room's volume that can be at a flammable composition. The ISF for the three sizes of release considered in this study can be calculated easily from the LFL and the fully mixed room concentrations. For a 30-g release of T_2 (or 10 grams of H_2) in a room with 20.7 m^3 (2.4 m ceiling, Small cases) the ISF = 4%/0.59% = 6.8. For a 240-g release of T_2 in a room with 168.5 m^3 (4.1 m ceiling, Medium cases) the ISF is similar at 6.9. For a 1.5-kg release of T_2 in a room with 445.1 m^3 (7.62 m ceiling, Large cases) the ISF is somewhat worse at 2.9, but still above the critical value of 1 required for full dispersion. These ISF values are tabulated for the full simulation matrix in the next section (Table 2-3).

To help analysts better gauge the potential for transient flaming hazards, another idealized metric introduced here is designated as the maximum flammable layer thickness (MFLT). MFLT can be used to rank risk for different quantities of hydrogen isotope in rooms with known dimensions. The MFLT as illustrated in Figure 2-3 assumes that all released hydrogen (tritium in most cases considered here) collects on the ceiling in a layer with a composition of 4% (the conservative LFL for hydrogen), which is the thickest possible layer that can be ignited. When this worst-case layer thickness is compared for a given release and room size, thin layers indicate that flammable regions are more likely to disperse quickly (possibly before ever reaching the ceiling). Thick values for MFLT indicate that flammable regions are more likely to reach the ceiling and persist for long periods before dispersing. If ISF >1, then the MFLT will be less than the height of the room, and MFLT can be calculated as the room height divided by the ISF. The MFLT can also be calculated from the room height H_R, pure volume of released hydrogen V_P, the LFL, and room volume V_R:

$$MFLT = \frac{H_R}{ISF} = \frac{H_R V_P}{LFL \cdot V_R} \quad , \tag{6}$$

which is 0.35 m for the simulations in the small room, 0.59 m for the medium cases and 2.61 m for the large cases. These MFLT values are tabulated for the full simulation matrix in the next section (Table 2-3), and smaller values of MFLT are better from a safety perspective. The MFLT metric assumes a flat ceiling. A slanted or arched ceiling or a ceiling with segmented regions may collect buoyant light gases within a region of reduced horizontal extent and greater vertical thickness, which will probably disperse more slowly than a flat-ceiling scenario.

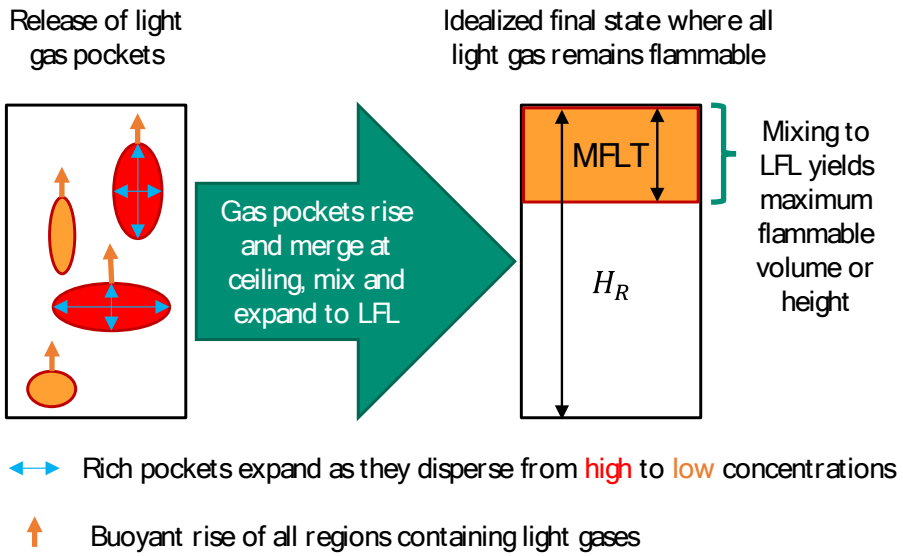

Figure 2-3. Maximum flammable layer thickness (MFLT) concept.

2.3.3. Momentum Metrics

This section presents metrics related to the momentum of a release event for tritium gas, which may also be applied to releases of other light flammable gases such as normal hydrogen and methane. In this study, these metrics are used to characterize transient effects such as release rate and plume dimensions, which are only factors of concern for ignition if the flammability metrics defined in the previous section indicate that the release is large enough for flammable concentrations to exist in a substantial fraction of the room volume (e.g., ISF close to 1 or lower, or MFLT of about 0.5 m or higher, see Appendix C). The need to consider such metrics became apparent when the simulations reported in this work exhibited very different behaviors in terms of the presence or absence of flammable ceiling layers when the tritium release rate was varied.

The Reynolds number is defined as the ratio of inertia and viscous forces, which suggests that it may be useful for correlating jet penetration lengths. Jets with higher Reynolds numbers have greater potential to reach the ceiling (Re > 2300, modeled in this work as turbulent), assuming the worst-case scenario wherein the gas jet is oriented upward. Releases with lower momentum (Re < 2300, modeled in this work as laminar) that tend to mix to non-flammable conditions before reaching and/or covering the ceiling are usually designated as "plumes" rather than "jets" in this study. The inlet Reynolds number Re is defined as

$$Re = \frac{\rho v D}{\mu}, \tag{7}$$

where ρ is tritium density, v is velocity, D is the hydraulic diameter, and μ is tritium viscosity. The hydraulic or effective circular pipe diameter was inferred from the area A of the tritium release:

$$D = 2\sqrt{\frac{A}{\pi}}. \tag{8}$$

The standard Reynolds number for turbulence transition (Re = 2300) defined for pipes was used for the hydrogen isotope inlet because the scenario considered in this report was designed so that the release of flammable gas was the only significant source of velocity in the room. Case M5 was an exception to this rule, with a Reynolds number of 1812 (21% below the turbulence threshold) that was deliberately modeled as turbulent to see how much difference it made in the simulation results.

Another dimensionless parameter known as the Froude number is a ratio of inertia to gravity effects. The Froude number as used in this work is defined from the inlet velocity v, the acceleration due to gravity g, and the hydraulic jet diameter D as

$$Fr = \frac{v}{\sqrt{gD}}. \tag{9}$$

The Froude number is often used to correlate jet penetration behavior in the literature (e.g., Blake et al. 1990, Briens et al. 2010, Kazachkov 2011, Philippe et al. 2005, Svantesson et al. 2021). Some of these correlations use a definition of the Froude number that is squared with respect to Equation (9), which eliminates the square root in the denominator. Some authors use a squared reciprocal of Equation (9), which is designated as the Richardson number. When considering release scenarios for real pressurized containers, calculating the Reynolds or Froude numbers *a priori* typically requires knowledge of the source pressure and reasonable estimates of the orifice size to determine the size and velocity of the jet; a common approach is summarized in Lacome (2011).

When standardized to the definition of the Froude number specified in Equation (9), it is typical to correlate the ratio of jet penetration lengths to jet diameter in terms of Froude number with an exponent between 0.5 and 1, regardless of the orientation and fluid type (Blake et al. 1990, Briens et al. 2010, Philippe et al. 2005, Svantesson et al. 2021). Some of these correlations also include the Reynolds number and a ratio of density terms, which is not included in this work because of the limited number of gases considered. The comparison of simulations in this work (especially in Section 3.2.1) indicates that momentum, buoyancy, and viscous drag are all important, which suggests some combination of the Reynolds and Froude number is appropriate for scaling.

A relationship of the form suggested by Philippe et al. (2005) appears reasonable when considering the trends of the simulations in this report with respect to the available metrics as defined above. This scaling relationship for dimensionless penetration length H_p/D uses an exponent near 0.5 for the Reynolds number and an exponent of 1 for the Equation (9) definition of the Froude number:

$$\frac{H_p}{D} = \alpha Re^{0.5} Fr \ . \tag{10}$$

The penetration height H_p in Equation (10) can be defined for the purpose of this report as the maximum ceiling height that the plume or jet will reach with sufficient momentum to form a layer that can endure on the order of minutes. Once the scaling constant α in Equation (10) is specified based on the simulations in this work (see Section 3.4), this equation can be used to estimate whether this penetration distance H_p exceeds the actual ceiling height H_R. $H_p < H_R$ is desirable from a safety perspective, as this condition signifies that the hydrogen plume at the height of the ceiling is sufficiently dispersed in terms of both momentum and concentration so that the gas mixture spreading from the plume across the ceiling will be nonflammable on average (sub-LFL). In other words, $H_p < H_R$ indicates near-complete dispersion below the LFL while the plume is rising. In contrast, $H_p > H_R$ signifies that a high-momentum release propels light gas upward so quickly that only a small fraction of is dispersed below the LFL while in transit to the ceiling.

Table 2-3 is a collection of metrics that were considered for the simulation matrix to assess risk *a priori* and correlate trends once the results became available. The same color scheme based on room size from Table 2-2 is used in Table 2-3 (Small = blue, Medium = green, Large = orange). All of the numbers in Table 2-3 were calculated from the case definitions; none depend on CFD results. The three columns on the right are flammability metrics; the mixed room concentration is used to define the ISF and MFLT as described above. These assume the room has no inflow or outflow and plenty of motion and/or dispersion time. All the simulations in this study have an ideal mixed room concentration on the order of 1% hydrogen isotope by volume, which is less than the conservative LFL of 4%. This sub-flammable mixed criterion is also reflected through ISF > 1 and MFLT > H_R for all cases in Table 2-3. These metrics indicate that given enough time, all of these releases will become a uniform, nonflammable mixture, even without ventilation. This implication is noteworthy given that all three rooms are sized conservatively small with respect to the magnitude of the tritium release specified for each. The middle columns of Table 2-3 are momentum metrics intended to correlate the behavior of plumes and jets as described in the paragraphs above; these are discussed in Section 3.4 of the results with respect to the observed behavior of the simulated plumes and jets.

The momentum metrics defined in this section assume a quasi-continuous release, but it should be remembered that the momentum effects included in both the Froude number and the Reynolds number couples with the release size, as reflected in either the ISF or the MFLT. Very high values of the Froude and Reynolds numbers may cause almost all the released mass to accumulate at the

ceiling, but if the released mass is small enough, the resulting flammable layer will be thin and the residual motion from the rapid release event will cause it to disperse quickly.

Table 2-3. Idealized flammability and inlet momentum metrics for tritium and hydrogen releases

Case Num.	Release Mass (Duration)	Inlet Velocity	Inlet Reynolds Number (Re)	Froude Number (Fr)	$Re^{0.5}FrD$	Mixed Room Conc.	Ignition Safety Factor (ISF)	Max Flammable Layer Thickness (MFLT)
S1	30 g T_2 (122 s)	0.035 m/s	183	0.025	0.065 m	0.59%	6.8	0.35 m
S2	30 g T_2 (30 s)	0.140 m/s	741	0.102	0.534 m	0.59%	6.8	0.35 m
S3	10 g H_2 (30 s)	0.140 m/s	248	0.102	0.309 m	0.59%	6.8	0.35 m
M1	240 g T_2 (180 s)	0.039 m/s	453	0.019	0.173 m	0.58%	6.9	0.59 m
M2	240 g T_2 (60 s)	0.118 m/s	1359	0.058	0.899 m	0.58%	6.9	0.59 m
M3	240 g T_2 (30 s)	3.780 m/s	10874	3.733	40.7 m	0.58%	6.9	0.59 m
M4	240 g T_2 (45 s)	0.158 m/s	1812	0.078	1.385 m	0.58%	6.9	0.59 m
M5	240 g T_2 (45 s)	0.158 m/s	1812	0.078	1.385 m	0.58%	6.9	0.59 m
M6	240 g T_2 (30 s)	0.236 m/s	2719	0.117	2.544 m	0.58%	6.9	0.59 m
L1	1.5 kg T_2 (300 s)	0.104 m/s	1425	0.047	0.886 m	1.37%	2.9	2.61 m
L2	1.5 kg T_2 (8 s)	3.903 m/s	53420	1.765	203.4 m	1.37%	2.9	2.61 m

Outlined cases (M4 through M6) were designed to investigate questions that arose through consideration of results from the remaining cases, which were the initial simulations for this study.

The ISF values quoted here for a 30-gram release in the small room (S1 through S3) differ slightly from the value presented in Table 2-1 of Brown 2022 (6.8 vs. 7.1). The difference arises from using slightly different dimensions to calculate room volume V_R. The previous report used dimensions 12 ft x 8 ft x 8 ft rather than the more exact 3.6 m x 2.4 m x 2.4 m from the ISO-9705 standard.

2.3.4. Comparison of Metrics to Experimental H_2 Releases Events

As a demonstration of how the flammability and momentum metrics defined in the previous section relate to each other and experimental measurements, the data of Lacome et al. (2011) with a room volume of 80 m^3 and ceiling height of 2.88 m are presented in Table 2-4 using a format similar to the simulations in Table 2-3. These experimental hydrogen releases used a pressurized source and a small orifice; the first column of Table 2-4 is an effective area ($A \cdot C_d$) that assumes a discharge

coefficient C_d = 0.68 (the corresponding orifice diameters from Lacome 2011 are 20 mm, 10 mm, 20 mm and 5 mm). The velocities quoted by Lacome as reproduced in Table 2-4 are 3% to 8% lower than what would be calculated from the effective areas, but this discrepancy is not material in terms of evaluating the performance of Equation (10).

Table 2-4. Metrics for the experimental H_2 release measurements of Lacome (2011) and Bauwens (2014)

Effective Inlet Area	Release Mass H_2 (Duration)	Inlet Velocity	Inlet Reynolds Number (Re)	Froude Number (Fr)	$Re^{0.5}FrD$	Mixed Room Conc.	Ignition Safety Factor (ISF)	Max Flammable Layer Thickness (MFLT)
Lacome et al. 2011								
0.000214 m^2	240 g (240 s)	53 m/s	8038	132	195 m	3.65%	1.1	2.63 m*
0.0000534 m^2	240 g (240 s)	210 m/s	15925	738	768 m	3.65%	1.1	2.63 m*
0.000214 m^2	48 g (240 s)	11 m/s	1668	27	18 m	0.73%	5.48	0.53 m
0.0000134 m^2	48 g (240 s)	170 m/s	6446	845	280 m	0.73%	5.48	0.53 m
Bauwens and Dorofeev 2014								
0.0169 m^2	36.3 g (~1.2 s)	22 m/s	29385	18	457 m	0.97%	4.11	0.66 m*
*Flammable layer detected at the ceiling								

Lacome's group measured 16 concentrations on a 2-D plane through the center of their release chamber, where this measurement plane was offset 0.2 m from the H_2 release location (Lacome 2011). From these measurements they estimated a flammable volume of about 40 m^3 (half of the chamber volume) for the first two rows in Table 2-4 with an H_2 release of 240 grams. The presence of a large flammable region, including a flammable layer next to the ceiling, is consistent with the fact that the MFLT for the first two entries is 2.63 m, which is 91% of the room height.

However, Lacome's group did not detect any flammable concentrations for the smaller release of 48 grams listed in the 3rd and 4th rows of Table 2-4, which had MFLT equal to 18% of the room height. The parameter $Re^{0.5}FrD$ for all cases in Table 2-4 is much higher than the room height of 2.88 m, so using $\alpha > 1$ in Equation (10) (as suggested from the simulation results in this work, see Section 3.4) predicts formation of a flammable ceiling layer for all four scenarios rather than just the first two with higher mass release. However, the MFLT is much lower for the last two entries from Lacome (where no flammable volume was detected in the measurement plane) Hence, the effect of momentum appears to be subsidiary to the total magnitude of release with respect to the surroundings, as reflected in the ISF and MFLT metrics based on the measurements of Lacome (2011). This trend may be enhanced for the Lacome measurements with respect to the simulations in this work given that H_2 has higher diffusivity compared to T_2, which allows it to disperse faster (see Chapter 3 of Brown 2022).

Metrics associated with the measurements of Bauwens and Dorofeev (2014) are also summarized in Table 2-4; these correspond to a room volume of 45.4 m^3 and a ceiling height of 2.72 m. The

Bauwens scenario formed a flammable region at the ceiling and started dispersing towards nonflammable conditions (< 4% H_2) by about 1 minute (extrapolation from the 20 seconds of data that were reported). The ISF is about 4 and the MFLT is well under 1 m, which are consistent with the relatively fast dispersion of the ceiling layer. The Bauwens case used a square inlet (0.13 m) with near-uniform velocity, similar to the simulations in this work (0.17 m for the smallest/standard ISO-9705 room). The reported release duration and hence the velocity-related terms are approximate (the concentration graphs nearest the source suggest 1 to 2 seconds), but the orders of magnitude for the Reynolds number and $Re^{0.5}FrD$ show that the Bauwens (2014) release in Table 2-4 had high momentum, with metrics on the same order of magnitude as the fastest releases from Lacome (2011). This high initial momentum for the Bauwens case explains why a flammable ceiling layer formed.

In summary, Equation (10) is useful as a conceptual screening tool to estimate momentum effects and has the advantage of being simple to implement. With an initial estimate of $\alpha > 1$ (which is refined further in Section 3.4 based on simulation results), it yields a correct assessment for the H_2 release measurement of Bauwens and Dorofeev (2014). It is conservative when used to assess flammability safety for the H_2 release measurements of Lacome et al. (2011). Flammability metrics such as MFLT may take precedence over momentum metrics by ruling out formation of a semi-stable flammable layer below the ceiling when the quantity of flammable gas is sufficiently low.

3. RESULTS: PREDICTED DISPERSION OF A TRITIUM RELEASE

3.1. Small Room with 2.4 m (7.9 ft) Ceiling

The cases in the small room are defined in the first three rows of Table 2-2 and are designated with case numbers that start with "S." The mesh geometries for these cases are summarized in the first two rows of Table 2-1, and metrics are identified in the first three rows of Table 2-3. The rows pertaining to these cases in all three tables are shaded blue.

Two simulations were executed to predict the behavior of a 30-gram release of T_2 in the smallest room with standard ISO9705 dimensions (S, 2.4 m ceiling). 30 grams of T_2 constitutes the maximum inventory for a Hazard Category 3 facility (HC3) at the time of this writing (see DOE-STD-1027-2018). The only difference between the first two cases with 30 g of T_2 is the rate of release; the 122-second release (S1) corresponds to 1 L/s and the 30-second release (S2) corresponds to 4.1 L/s. A third simulation was executed for a comparable volumetric release of normal hydrogen or protium (H_2), with a mass of 10 g released over 30 seconds (4.1 L/s, S3).

This room size is conservative (small) for a 30-gram inventory size, which is unlikely to be stored in a single container within a single room. Therefore, these cases constitute a reasonable worst-case assessment for a gaseous T_2 release event at an HC3 facility. The simulated release rate for case S3 exceeds the fastest experimental release of hydrogen studied by Lacome's group by a factor of 80, and the ISO-9705 standard simulated room has a volume that is 25% of Lacome's volume (Lacome 2011) and 46% of Bauwens' volume (Bauwens 2014). Hence, the release rates considered in these simulations are conservatively high with respect to the cited experimental hydrogen isotope release studies, especially since tritium containment vessels used for small inventories are usually charged to pressures that are much lower than normal hydrogen storage applications.

Figure 3-1 shows the flammable mass and flammable volume versus time for these three simulations. The conservative H_2 LFL of 4% by volume is used, so $c_{min} = 0.04$ and $c_{max} = 1.0$ are used with Equation (3) for flammable mass and Equation (4) for flammable volume at each timestep to produce these plots. Within a few seconds, the flammable region approaches an equilibrium condition, where the dispersion rate and the release rate are approximately equal. The slower release (122 seconds, S1) yields a lower maximum flammable mass (2% of release) than a faster release over 30 seconds (13.4% of release for T_2 in case S2 and 10.7% of release for H_2 in case S3). Once the release ends, zoomed-in versions of Figure 3-1 indicate that full dispersion below the LFL occurs in 2.4 seconds for the 122-second T_2 release (S1), 7.3 seconds for the 30-second T_2 release (S2), and 4.8 seconds for the 30-second H_2 release (S3). Dispersion is predicted to be fastest for the lowest release rate, and it is faster for normal hydrogen than it is for tritium.

Figure 3-1 shows that the flammable mass during the equilibrium "plateau" is higher by a factor of 3.5 for T_2 compared to H_2 under the same conditions (at 30 seconds), although the molecular weights and mass flow rates differ by a smaller factor of 3. The flammable volumes for T_2 and H_2 increase at essentially the same rate initially, but the flammable volume ratio for T_2 versus H_2 is 1.17 at 30 seconds, and the flammable H_2 disperses about 23% faster after the release. These isotopic trends are all consistent with the fact that the lighter H_2 molecule has greater buoyancy with respect to air and higher diffusivity or molecular mobility than does T_2. Therefore, T_2 has a propensity to disperse slower than normal hydrogen, which may balance somewhat with the higher LFL for T_2. This isotopic difference is small and probably becomes negligible under conditions where advection or turbulent mixing rather than diffusion dominates. The bottom panel of Figure 3-1 also shows that flammable volume for the two faster release events is on the order of 1% of the total room volume

identified in the caption. The flammable volume for the slower release is on the order of 0.1% of the room volume.

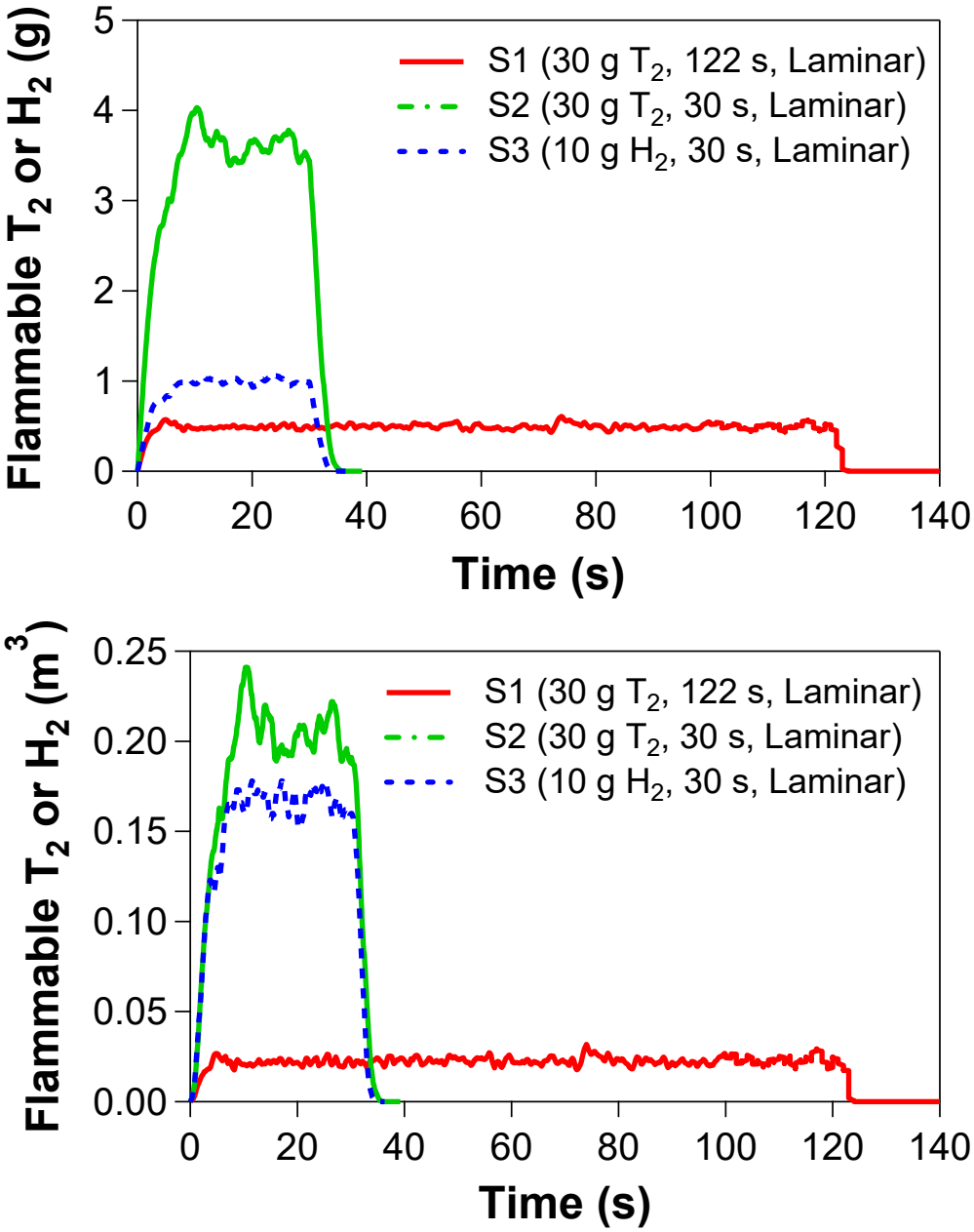

Figure 3-1. Flammable mass (top) and volume (bottom) for simulations S1, S2, and S3 in the small domain with room volume of 20.7 m^3

Iso-contours are a helpful way to illustrate where the gas is predicted to exceed the LFL. Figure 3-2 shows two views of such thresholds for the plume with the slowest release of T_2 (122 seconds, S1). Figure 3-2 shows the 1% concentration contour colored by velocity magnitude in m/s. Figure 3-3 is a similar visualization of the 4% concentration contour (the conservative LFL). The contour in Figure 3-3 at 117 seconds encompasses the tritium mass and volume that are plotted versus time as the solid red line in Figure 3-1. The left views in these figures are looking through the doorway into the room and the right views are looking upwards through the floor of the room. Figure 3-2 shows

that the buoyant plume does result in a ceiling layer that is enriched in T_2, while Figure 3-3 shows that the ceiling layer is nonflammable (concentrations below the hydrogen LFL of 4%). The portion of the plume containing flammable concentrations in Figure 3-3 reaches the ceiling at 2.4 meters only intermittently because the plume breaks up and disperses as it rises. The coloring in both figures indicates that the plume gains velocity as it rises; this acceleration promotes faster mixing with the surrounding air. For the 122-second release of 30 grams of tritium in the smallest room size (S1), Figure 3-3 indicates that the dispersion behavior to concentrations below the LFL is not slowed by the presence of the 2.4-meter ceiling.

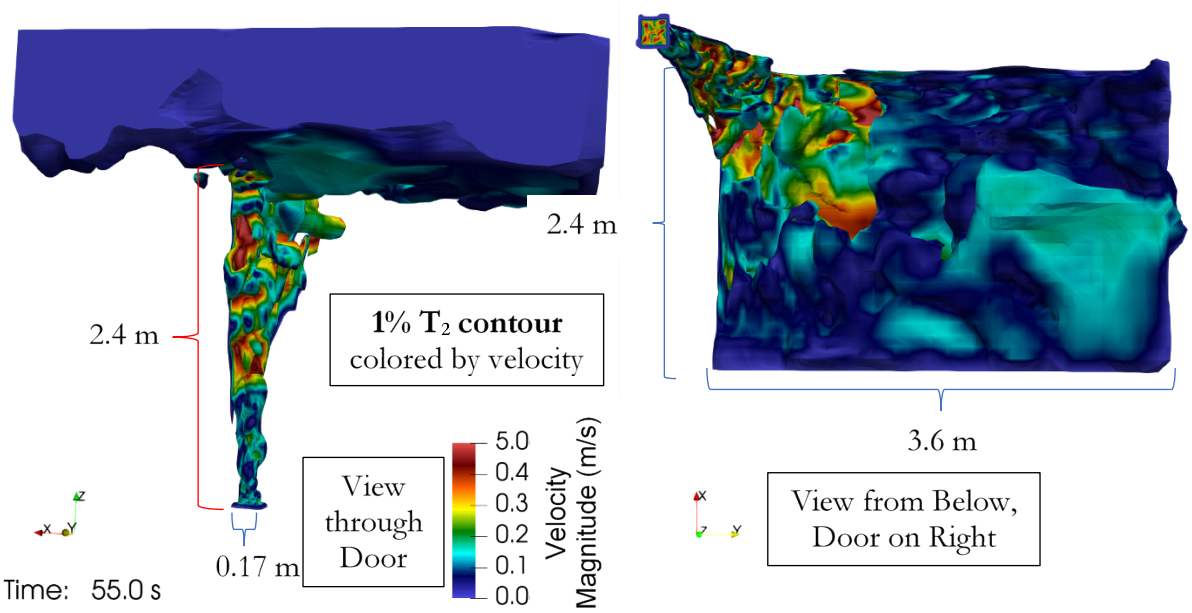

Figure 3-2. 1% T_2 contour for 122 s release of 30 g T_2 into small room with 2.4 m ceiling (S1)

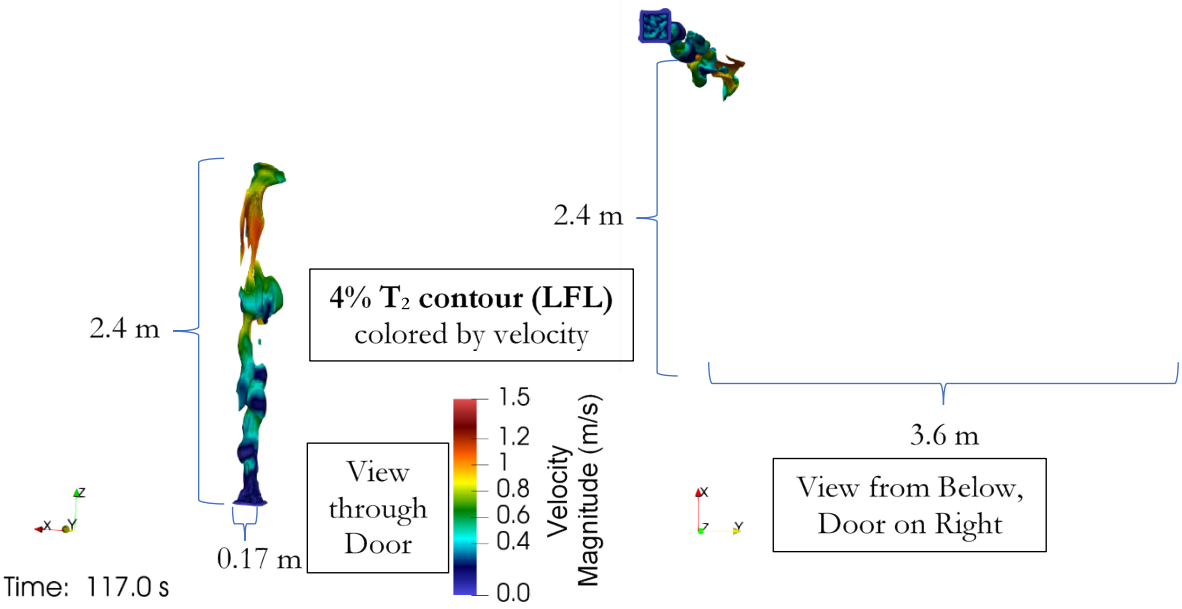

Figure 3-3. Flammable region (>4% T_2) for 122 s release of 30 g T_2 into small room (2.4 m ceiling, S1)

Figure 3-4 shows the LFL concentration (4%) colored by velocity magnitude (m/s) for the faster 30-second release of T_2 (S2). In this case, the buoyant plume continuously impinges on the ceiling, where it forms a thin localized flammable layer that disperses rapidly. The view shown in Figure 3-4 was selected at a time to be representative of the maximum ceiling coverage, which is limited by the fast dispersion rate to <25% ceiling coverage. The impingement on the ceiling stretches the flammable plume in a manner that may actually enhance the dispersion rate with respect to a comparable release in a larger (unconfined) space. For the scenarios considered in this section that lack an extensive flammable ceiling layer, the risk of an effective ignition event is almost entirely limited to the region directly above the tritium source, as the horizontal spreading and movement of the flammable plume is quite limited.

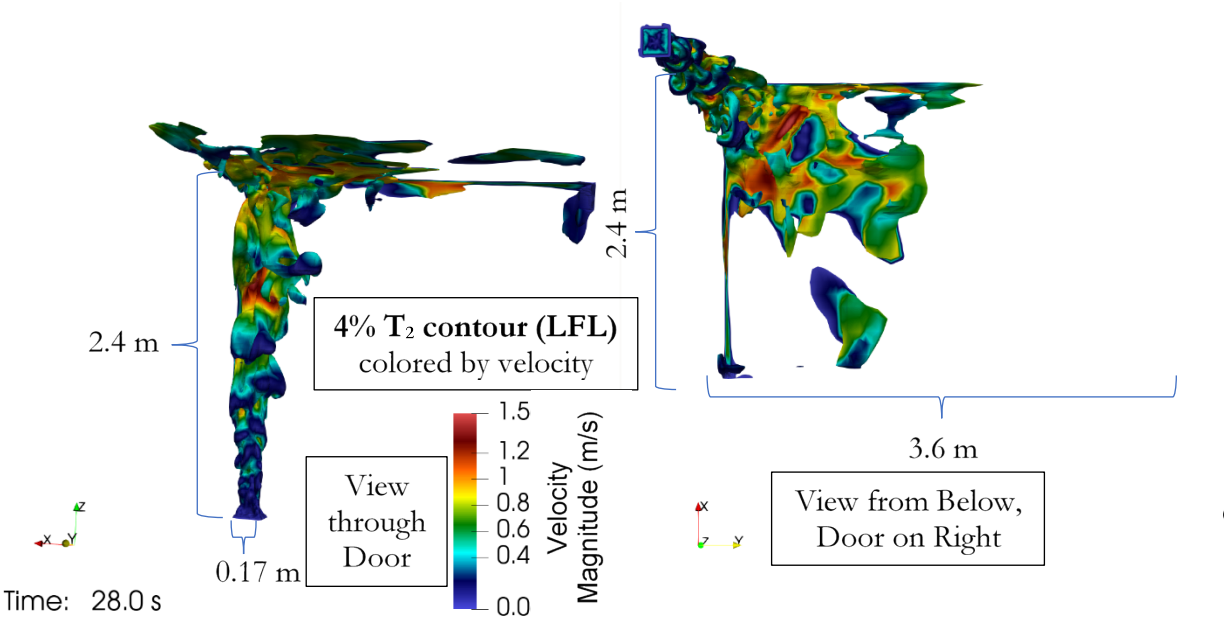

Figure 3-4. Flammable region (>4% T_2) for 30 s release of 30 g T_2 into room with 2.4 m ceiling (S2)

Figure 3-5 shows a 30-second release of 10 grams of H_2 (S3); it is directly comparable in terms of molar or volumetric release to the 30-gram release of T_2 over the same duration shown in Figure 3-4 (S2). Different times during the release were chosen for these images to yield views representative of the maximum ceiling coverage for the flammable region. Visual differences between the H_2 release and the T_2 release in terms of plume size, velocities (color maps use the same scale), and ceiling surface coverage are very minor, which is consistent with the small differences shown in the flammable volume line plot (bottom of Figure 3-1). This absence of major differences suggests that a release of tritium gas may be adequately represented in an experimental setting by H_2 or preferably the deuterium isotope (D_2), which is of intermediate molecular weight. Helium also has a similar molecular weight and may be considered as a safer surrogate for tritium in situations where chemical reactions (oxidation) are not central to the experiment objectives.

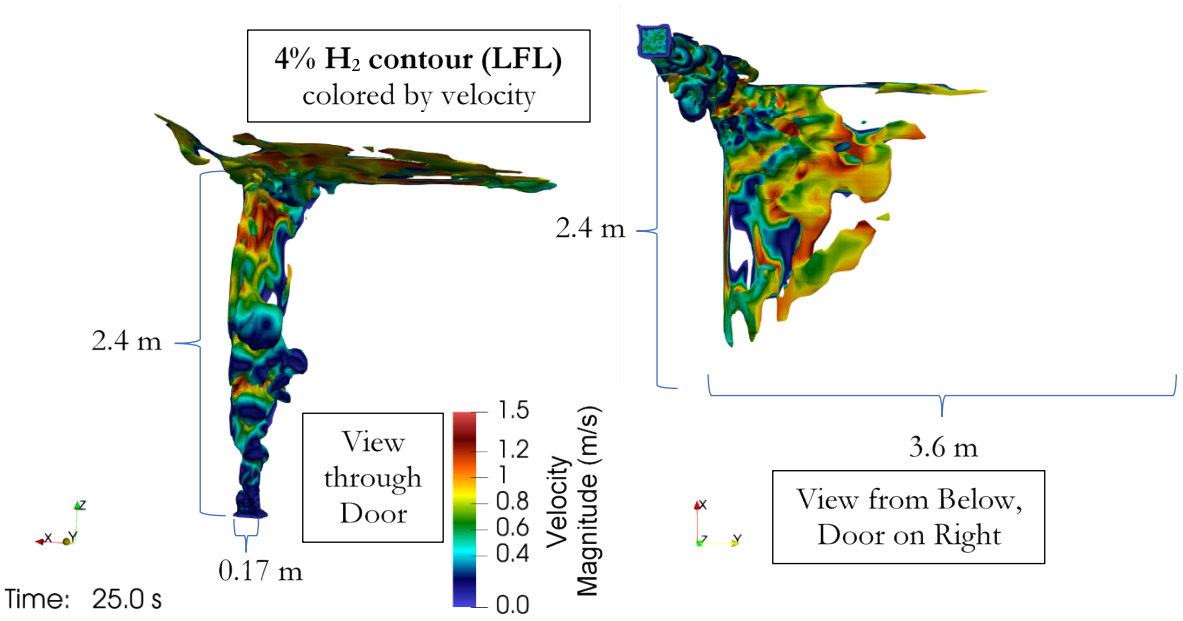

Figure 3-5. Flammable region (>4% H_2) for 30 s release of 10 g H_2 into room with 2.4 m ceiling (S3)

Figure 3-6 is a more detailed view in the style of Figure 3-1 for the simulated 122-second T_2 release (S1). To produce these curves, c_{min} to c_{max} are specified according to the legend in Figure 3-6; mass bins from Equation (3) are plotted in the top panel and volume bins from Equation (4) are plotted in the bottom panel. The nonflammable mass (<4%) that has been released is designated as the purple curve on the top panel of Figure 3-6; this curve tracks how much tritium is present within the domain in the least hazardous state. The nonflammable released T_2 increases monotonically during the release and peaks at 1.3 seconds after the release ends (121.3 s), which is within 1.1 seconds of when the dispersion below the flammability limit becomes complete. At this peak shortly after the injection termination time, the maximum nonflammable T_2 is 26.28 grams out of the 30-gram total injection. After 124 seconds the nonflammable mass decays, which indicates that tritium begins to exit the domain through the door before the release is finished. This exit is confirmed by a slight decrease in the positive slope of the <4% nonflammable mass curve after about 70 seconds.

The two largest contributions to the flammable mass (>4%) in Figure 3-6 (the most hazardous state for the released gas) are the >12% bin (blue curve), which is 36% of the total flammable mass at 122 seconds, and the 4% to 6% bin (red curve), which is 27% of the total flammable mass at 122 seconds. The >12% bin is most likely to ignite in a manner that produces efficient combustion and hence high conversion to the water form. The other flammable concentration bins shown include much less mass and volume individually. Even though the >12% bin has the most flammable mass of any bin shown (top panel of Figure 3-6), it occupies a small volume of 4.5 L (bottom panel of Figure 3-6) because the >12% bin is the most concentrated. The remaining simulations that did not form a ceiling layer reported in this work are consistent with the trend shown in Figure 3-6, where the volume of the 4% to 6% bin is larger than any of the others. For brevity, only the mass distributions are shown for most remaining cases in this work, as the flammable volume distributions do not provide much additional information when the total flammable volume (as in the bottom panel of Figure 3-1) and the mass distribution (as in the top panel of Figure 3-6) are already available.

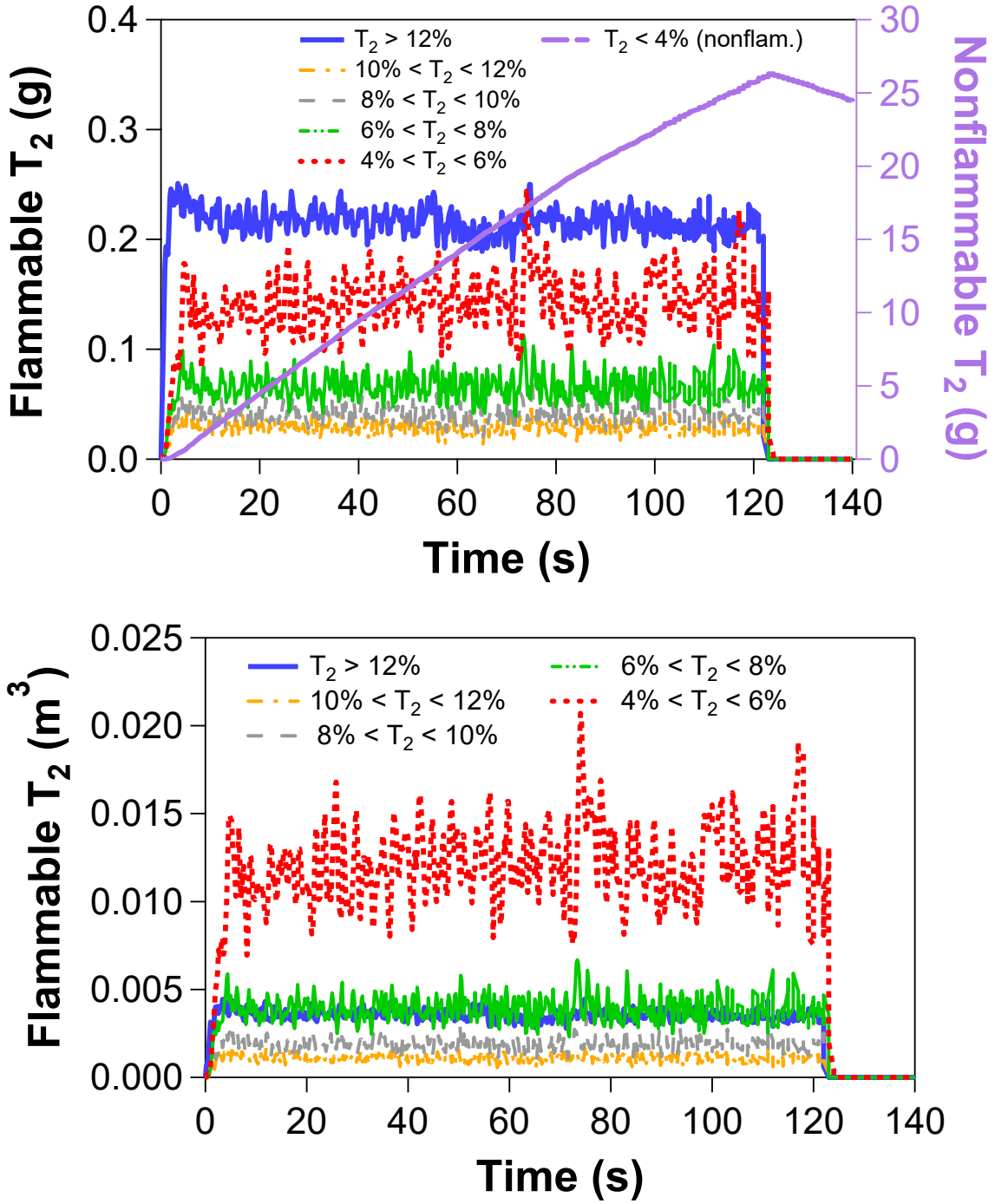

Figure 3-6. Concentration bins for 122 s release of 30 g T_2 in room with 2.4 m ceiling and 20.7 m^3 volume (S1) based on mass (top) and volume (bottom)

Figure 3-7 is a more detailed view in the style of Figure 3-1 showing the 30-second T_2 release (S2) with concentration bins included. The mass in the nonflammable bin (<4%) for this 30-second release in Figure 3-7 has trends similar to the 122-second release in Figure 3-6, with the peak occurring 4.7 seconds after the end of the release event. However, it appears that the initial decay rate of the nonflammable mass after the release ends is lower in Figure 3-7 than Figure 3-6, because

there has not been as much time for tritium to reach the door with the shorter release duration. For this faster release rate, the least flammable bin with 4% to 6% concentration contains more T_2 mass than the >12% bin, which is opposite the trend observed for the slower release. This difference can be explained in terms of enhanced mixing that occurs with a higher velocity injection. All the mass distribution trends shown for the 30-second T_2 release in Figure 3-7 (S2) are similar for the comparable H_2 release shown in Figure 3-8 (S3).

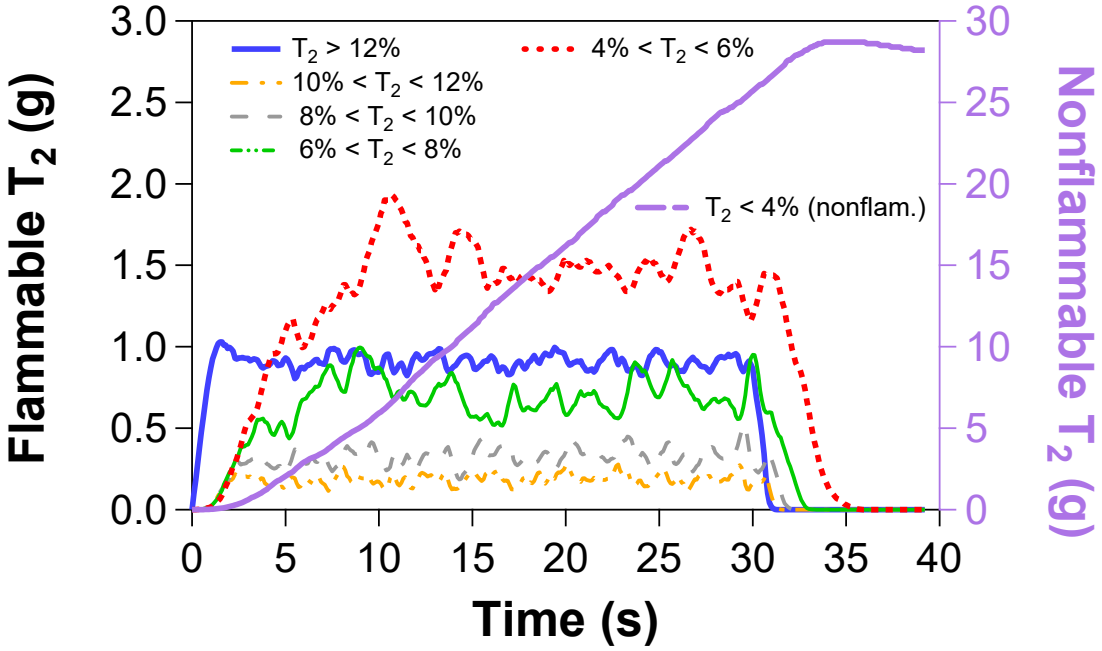

Figure 3-7. Mass concentration bins for 30 s release of 30 g T_2 in room with 2.4 m ceiling (S2)

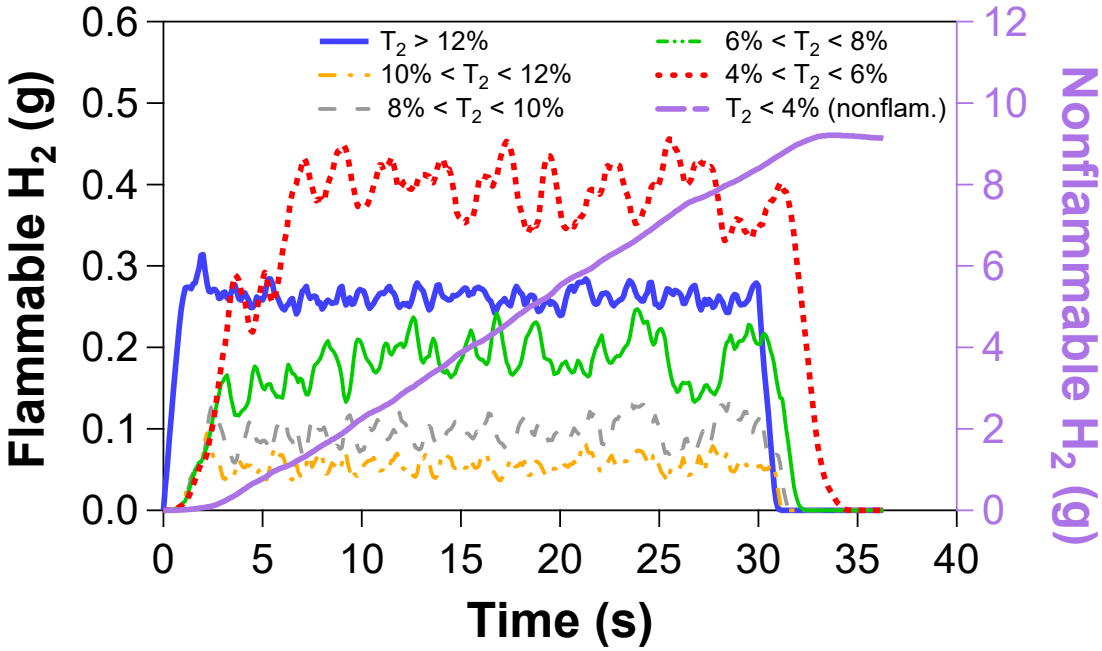

Figure 3-8. Mass concentration bins for 30 s release of 10 g H_2 in room with 2.4 m ceiling (S3)

The three simulations detailed in this section are insufficient to cover the full range of potential releases, however, the trending for a faster/slower release can be deduced based on the two cases that are identical except in the time for release (S1 and S2). The slower release represents a smaller hazard based on the lower volume and mass fraction of the inventory being above the LFL, in a state where ignition is possible. There will be less volume that can find an ignition source, but it will have longer to achieve the ignition. If it ignites, it will be a smaller flaming event, with reduced probability of sustaining a flame. Because ignition sources are spatially distributed, the larger volume scenario involving the faster release is considered more hazardous.

In all likelihood, these scenarios will not be strong candidates for ignition. Probable ignition sources in operational environments include sources of heat or spark like incandescent bulbs, switches, motors, etc. Whether an ignition source overlaps with a flammable mixture will be scenario dependent, but the probability of ignition is reduced when the flammable volume is reduced and also when the duration that a flammable region persists is reduced. These are also very conservative scenarios in terms of the magnitude of the inventory (30 g of T_2 represents the upper bound facility inventory for HC3 facilities) being released from a single region of a small room, as well as in terms of the flammability assumption at concentrations ≥4%.

3.2. Medium Room with 4.1 m (13.5 ft) Ceiling

The cases in the medium room are defined in the middle section of Table 2-2 and are designated with case numbers that start with "M." The mesh geometries for these cases are summarized in the middle of Table 2-1, and metrics are identified in the middle of Table 2-3. The rows pertaining to these cases in all three tables are shaded green.

Three simulations were initially executed to predict a 240-gram release of T_2 in the medium room with a 4.1-meter ceiling (designated as M1 through M3 in the tables specified above). At the time of this writing, the released quantity of tritium in these simulations corresponds to a Hazard Category 2 (HC2) facility (see DOE-STD-1027-2018). Two of these cases with releases occurring over 180 seconds (5.4 L/s, M1) and 60 seconds (16.2 L/s, M2) were modeled using laminar solvers, and the third with the highest velocity (30 seconds or 32.4 L/s with 1/16 the nominal inlet area, M3) was modeled as turbulent. Additional cases were added in a second round of simulations to answer questions that arose from the initial cases described in this section; the additional cases are described in Section 3.2.1.

The tritium mass and volume corresponding to the flammable portion of the computational domain for these three cases are shown in Figure 3-9. The methods used to produce the metrics shown in this plot are described in Section 2.3.1 and the beginning of Section 3.1. Slower inlet velocities yield lower maximum flammable mass because the tritium has more time to mix with the air. The two laminar cases with lower inlet velocities rapidly increase their flammable volume and mass to achieve plateaus and then disperse to a nonflammable condition almost immediately after the tritium release ends. The dispersion time to < 4% after the release ends is 6.2 seconds after the 180-second release (M1) and 13.6 seconds after the 60-second release (M2).

The turbulent case with high-velocity injection (M3) was initially included for completeness; it is an exploration of a more extreme scenario and may not be reflective of conditions at any real facility. Consequently, it behaves differently from slower (and possibly more realistic) release events of the same size (M1 and M2). A much larger fraction of the released tritium ends up in the flammable regime for M3 (62% of the total release at peak compared to 1.7% for M1 and 8% for M2) because the injection velocity is high enough for a large fraction of the tritium to reach the ceiling before

significant dispersion occurs. Much of the initial rapid dispersion before about 100 s corresponds to mixing of tritium from the plume or other regions below the level of the door frame (see Figure 2-1), while the slower rate after 100 s corresponds to dispersion of the ceiling layer via diffusion and residual gas motion in the room. Dispersion to < 4% for M3 occurs 570.1 seconds after the release ends, or about 10 minutes with the release time included.

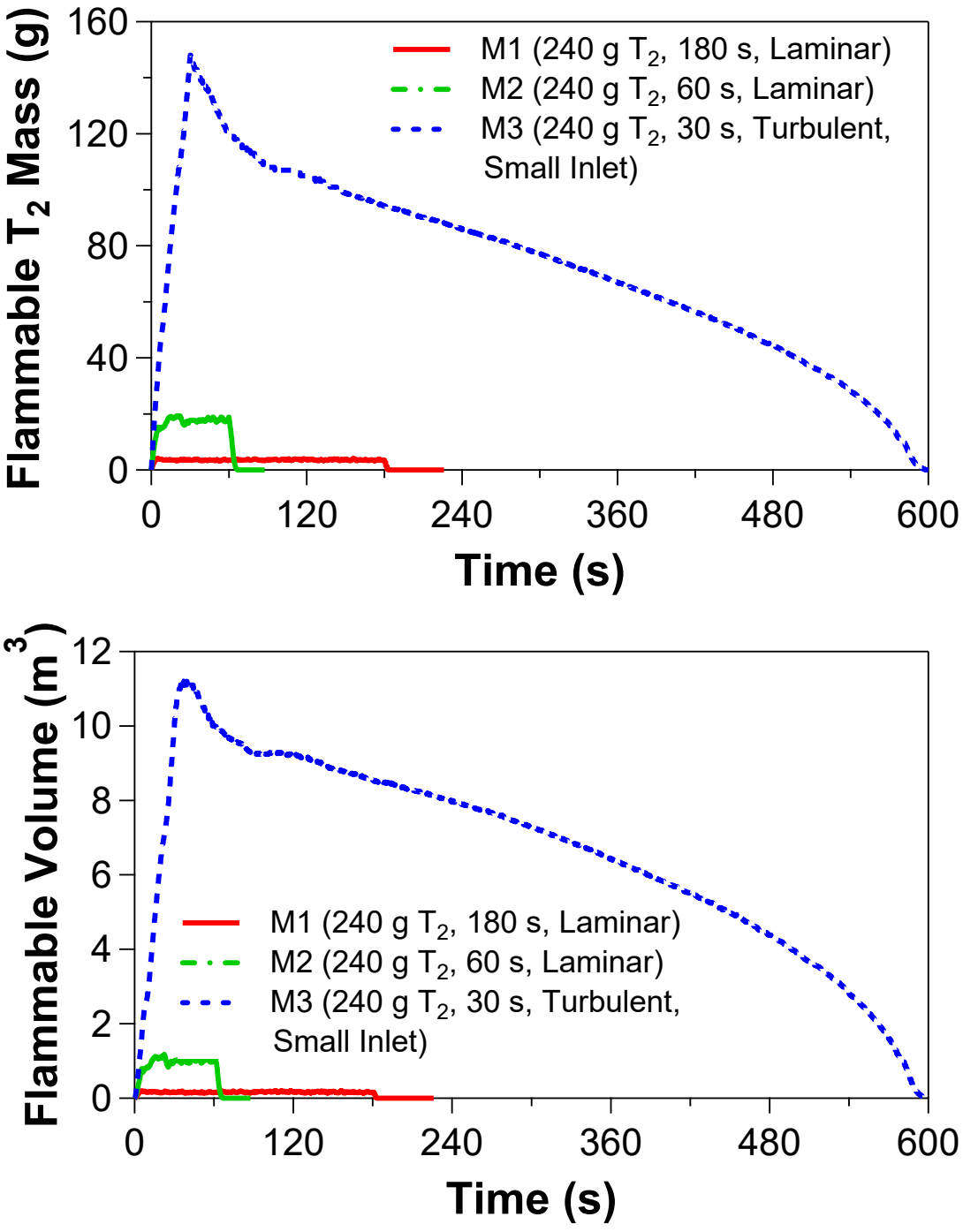

Figure 3-9. Flammable mass (top) and volume (bottom) from three initial simulations releasing 240 g T_2 (M1, M2, and M3) in the medium domain with room volume of 168.5 m^3

The bottom panel of Figure 3-9 shows that the high-velocity release (M3) produces a maximum flammable volume that is about 7% of the medium room volume listed in the caption. The maximum flammable volume for M2 is about an order of magnitude lower than M3, and the maximum flammable volume for M1 is about two orders of magnitude below M3. This observation shows that the relationship between flammable volume and release rate or velocity is not linear.

Figure 3-10 shows 4% tritium contours of the buoyant plume for the slowest release colored by velocity (180-second duration, M1), and Figure 3-11 shows a similar plot corresponding to the intermediate 60-second release (M2). For the slowest rate in Figure 3-10 (M1), flammable gas pockets only occasionally reach the ceiling, so the ceiling does not slow down the dispersion behavior and a flammable ceiling layer never forms. It appears unlikely that the M1 plume would have sufficient momentum to form a full ceiling layer even if it occurred in a room with the shorter ceiling height of 2.4 m. Both of these images are taken at a time of 36 seconds during the release.

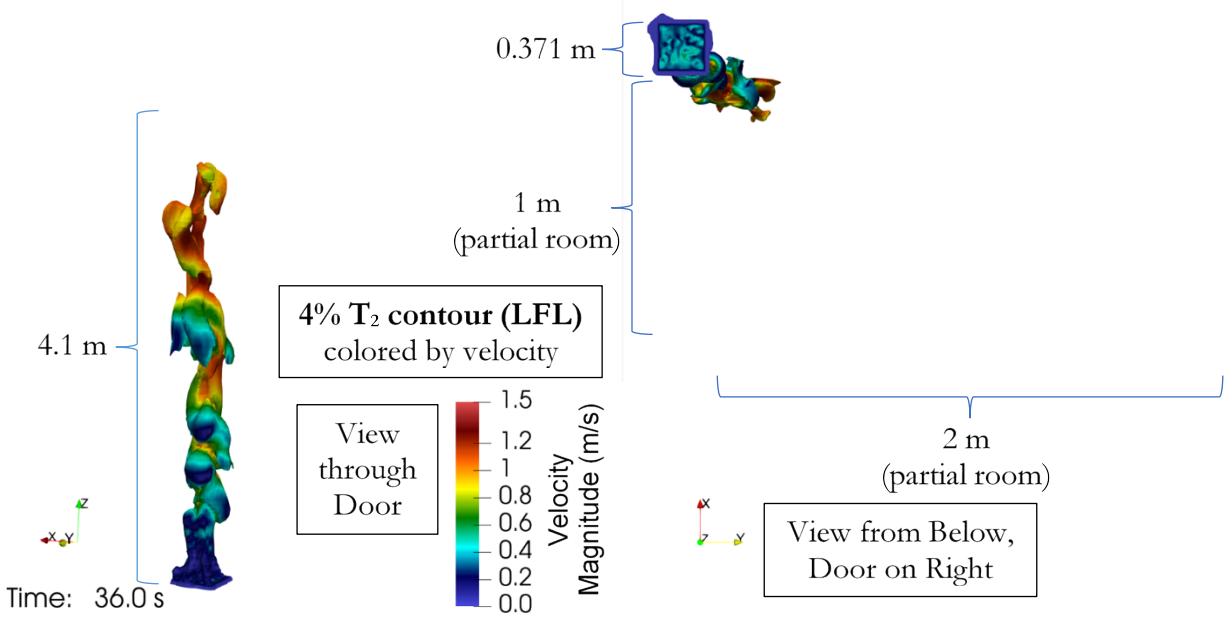

Figure 3-10. Flammable region (>4%) for 180 s release of 240 g T_2 into medium room (4.1 m ceiling, M1)

For the faster release shown in Figure 3-11 (M2), the plume does reach the ceiling and a limited ceiling layer forms near the plume. The layer for M2 is thin and never comes close to covering the whole ceiling (similar to S2 in Figure 3-4). Much of the dispersion for M2 in Figure 3-11 still occurs as the plume rises. The plume behavior observed in the animated results from which Figure 3-11 is drawn suggests that the ceiling may actually enhance dispersion slightly through a "splash effect." In other words, the impingement of the plume on the ceiling appears to shear the gas in a manner that makes flammable regions thinner, which promotes mixing. Note that the 4% tritium surfaces in these figures are colored by velocity magnitude, which increases as the plume gains altitude. This acceleration of the buoyant plume promotes more efficient mixing as the plume rises.

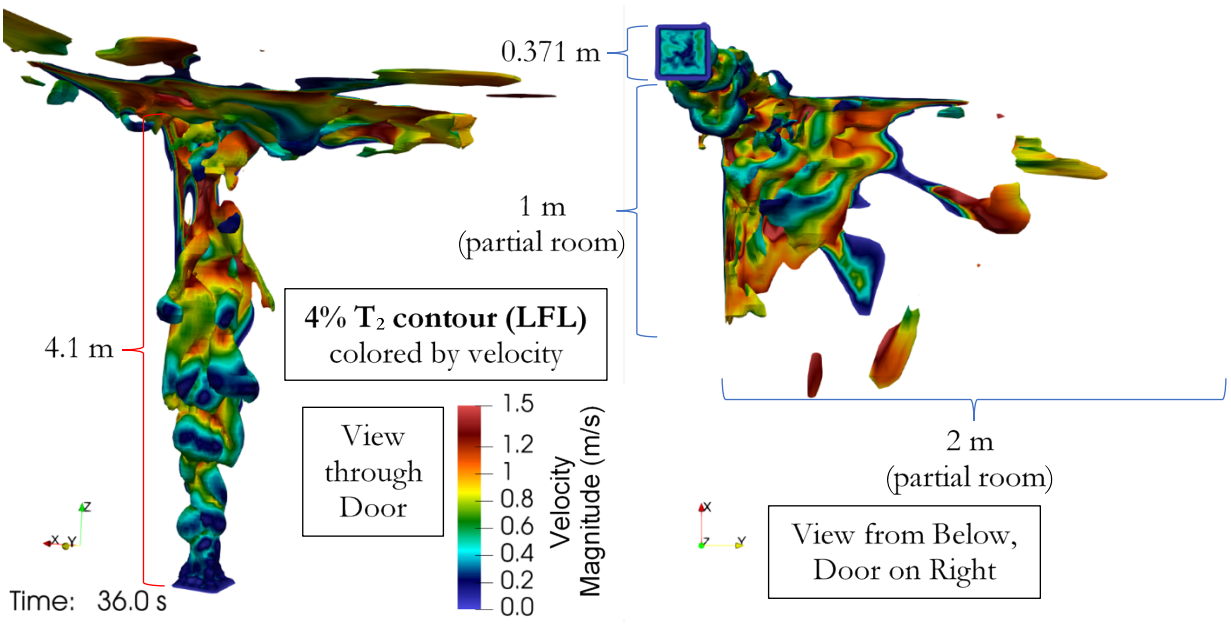

Figure 3-11. Flammable region (>4%) for 60 s release of 240 g T_2 into medium room (4.1 m ceiling, M2)

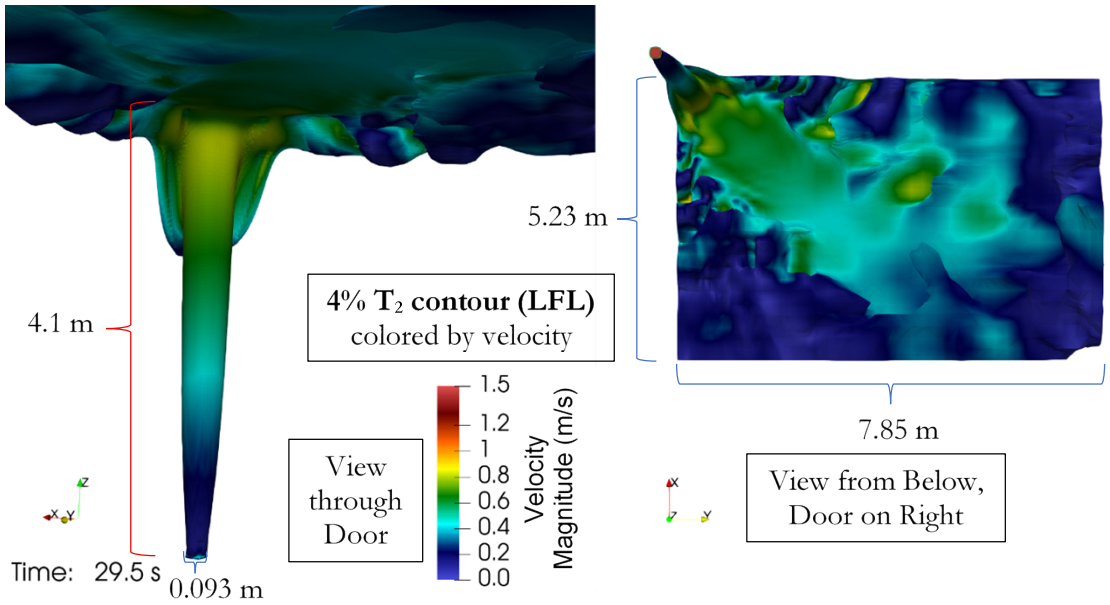

Figure 3-12. Flammable region (>4%) for 30 s release of 240 g T_2 through small inlet (4.1 m ceiling, M3)

Figure 3-12 is a similar visualization for the turbulent case with the highest injection velocity (M3, half the injection time and 1/16 the injection area shown for M2 in Figure 3-11, so M3/M2 injection velocity ratio is 32), shown 0.5 seconds before the end of the release. The distinct appearance of the M3 release is attributable to a combination of time averaging inherent in the turbulence model and the fact that the jet is primarily driven by the high initial velocity rather than the buoyancy alone. However, buoyancy still has a visible effect, as the velocity increases with height. The jet for case M3 has very high velocities near the centerline, as shown in Figure 3-13, and much greater symmetry than the plumes formed with lower injection velocities (e.g., M2 shown in Figure 3-11). The M3

velocities at the 4% concentration level on the jet periphery shown in Figure 3-12 are lower than the highest shown for the lower injection velocity in Figure 3-11. The velocities at the core of the M3 jet shown in Figure 3-13 are 2 to 3 times higher than the maximum velocities associated with the buoyant plume in Figure 3-11.

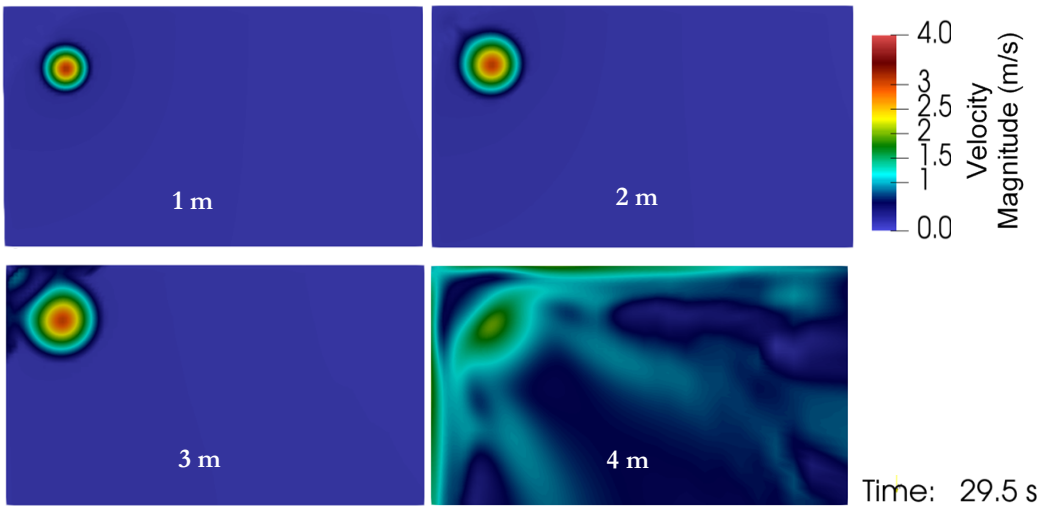

Figure 3-13. Horizontal slices of velocity magnitude through the jet from the 30 s release of 240 g T_2 into medium room (4.1 m ceiling, M3); heights from floor are designated in each frame

Figure 3-14 is a more detailed view of the same style as Figure 3-9 with binned concentrations for the M1 case with a release occurring over 180 seconds. The maximum flammable mass (sum of all bins >4%) for case M1 is 4 grams, or 1.7% of the total release. The nonflammable T_2 mass increases steadily until 3 seconds after the end of the release; the decline thereafter indicates that tritium is already leaving the computational domain through the door. Figure 3-14 indicates that about 40% the flammable mass during the release occurs at concentrations >12% (blue curve), but this bin accounts for only 14% of the flammable volume. The masses in the intermediate concentration bins (between 6% and 12%) are all much less than the red 4% to 6% bin for case M1, as are the corresponding volumes. The sum of the T_2 mass in the intermediate bins shown in Figure 3-14 (35% of the total flammable gas at 180 s) is higher than the 4% to 6% bin (24%).

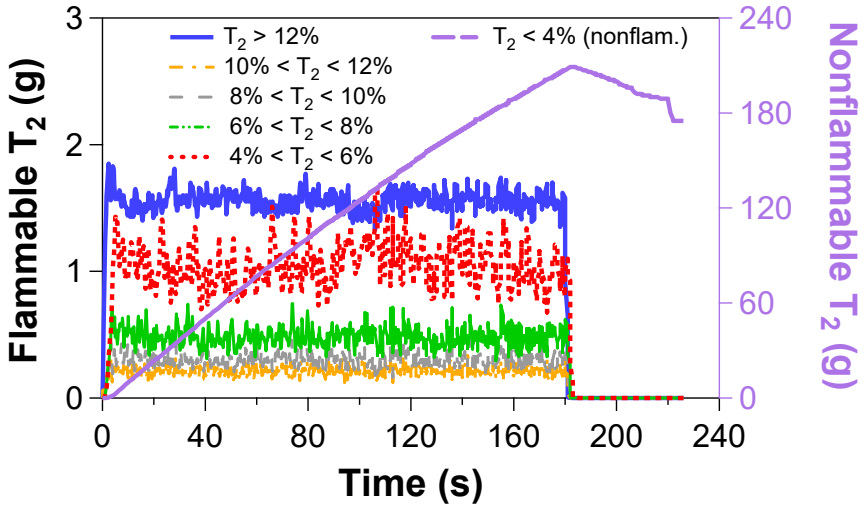

Figure 3-14. Concentration bins for 180 s release of 240 g T_2 into medium room (4.1 m ceiling, M1)

Figure 3-15 is a more detailed view in the style of Figure 3-9 with binned concentrations for the M2 case with a release occurring over 60 seconds. The maximum flammable mass from Figure 3-9 is 19 grams, or 8% of the total release. The nonflammable T_2 mass rises monotonically in Figure 3-15 until the end of the M2 release and begins to decline 6 seconds later as the tritium leaves the computational domain through the door. The steps just before the end of the nonflammable mass line (<4%) in both Figure 3-14 and Figure 3-15 are caused by a nonflammable pocket of air containing tritium being wafted out of the domain, which occurs because the tritium-rich layer at the top of the room is thick enough to spill out through the top of the doorframe. This exit of air containing tritium is shown with the (nonflammable) 1% T_2 contour in Figure 3-16 (warm-colored bump at top center of left panel and far right of right panel).

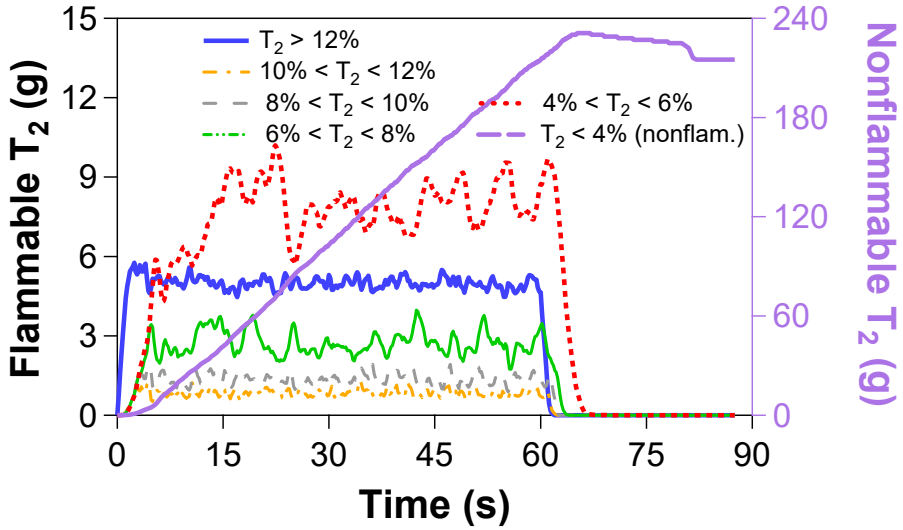

Figure 3-15. Concentration bins for 60 s release of 240 g T_2 into medium room (4.1 m ceiling, M2)

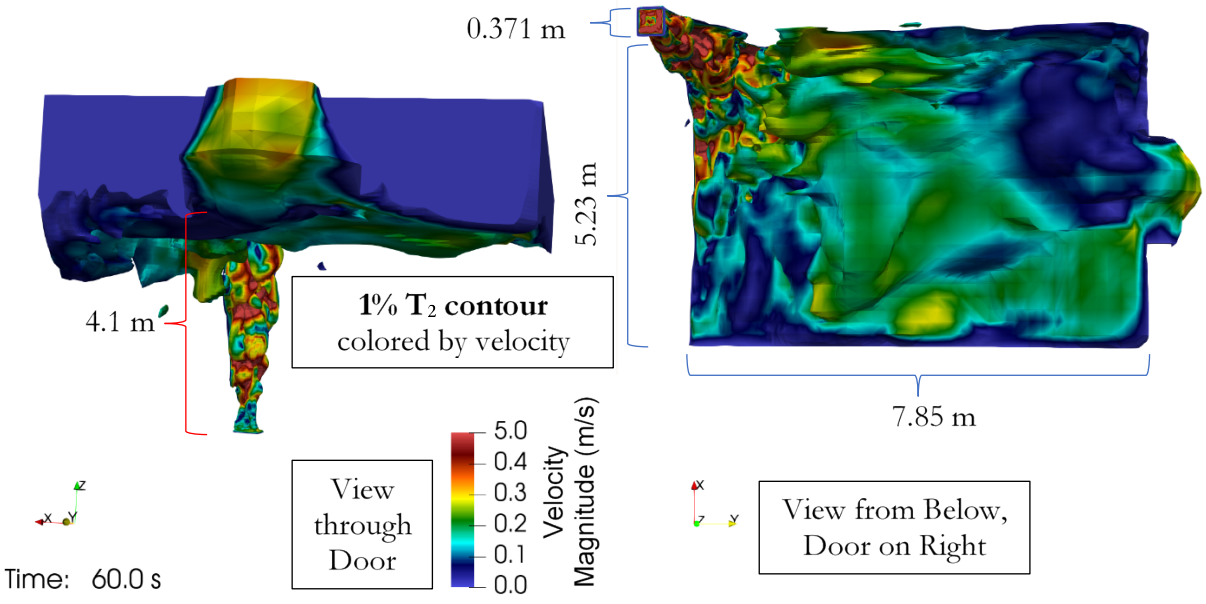

Figure 3-16. 1% tritium iso-contour colored by velocity magnitude for 60 s release of 240 g T_2 into medium room (4.1 m ceiling, M2)

The flammable masses at 60 seconds (the end of the release) in Figure 3-15 indicate that 46% of the total flammable mass during the M2 release corresponds to the lowest concentration bin between 4% and 6% (or 67% of the flammable volume). Figure 3-15 indicates that about 25% the flammable mass during the release occurs at concentrations >12% (blue curve), but this concentration bin occupies only 6% of the flammable volume. The volumes and masses in the bins between these extremes (6% to 12%) are all much less than the red 4% to 6% bin. The mass in the intermediate bins is 29% of the total flammable mass (>4%) at 60 s.

Figure 3-17 is a more detailed view of M3 in the style of Figure 3-9 with binned concentrations for the high-velocity release occurring over 30 seconds. The top frame in Figure 3-17 has a reduced timescale to focus on the initial behavior of M3. The maximum flammable mass (from Figure 3-9) is 148 grams, or 62% of the total release. This observation confirms that the maximum amount of flammable mass increases at faster flow rates (up to the total mass released). Unlike the slower releases (M1 and M2), the nonflammable T_2 mass in M3 does not begin to decline immediately after the release terminates. Instead, most of the flammable mass becomes trapped in a ceiling layer, and the nonflammable T_2 mass in the room continues to increase as this flammable ceiling layer disperses over about 10 minutes. Figure 3-17 indicates that 61% of the flammable mass at 30 seconds for M3 (73% of the flammable volume) corresponds to the lowest concentration bin between 4% and 6%. The high residual velocities cause the higher concentration bins to disperse so quickly that all flammable mass is in the 4% to 6% bin by 80 seconds; all concentrations greater than 8% are dispersed earlier, by 50 seconds. Note that if a less conservative and more appropriate LFL of 6.6% is assumed for tritium (Cadwallader and Petti, 2002), all flammable regions are still dispersed within ~1 minute (20 to 50 seconds after the release ends), consistent with the final dispersion time of the intermediate 60-second release (M2).

The simulations in this section (M1, M2 and M3) are releases of 240 grams of tritium with a 4.1-meter ceiling and excess volume sufficient to preclude flammability once the room is fully mixed. Under these conditions, flammable regions disperse within seconds if the release takes the form of a buoyancy-driven plume (M1 and M2), as was the case for smaller releases in the smaller room (S1, S2 and S3). If the release occurs as a high-velocity jet that is directed towards the ceiling (3.8 m/s at the inlet for M3), then the formation of a flammable layer on the ceiling that disperses slowly to a nonflammable condition over many minutes becomes more likely. However, dispersion to concentrations sufficiently low to preclude efficient oxidation to T_2O or HTO still occurs very rapidly for the M3 simulation with a high-velocity tritium jet.

The formation of a flammable ceiling layer appears unlikely for a release similar to M3 if the tritium jet is not oriented towards the ceiling, since the high velocity of the jet also promotes rapid mixing. Likewise, releases of the same total quantity of tritium occurring from multiple locations and multiple directions would tend to mix with air more rapidly. Therefore, tritium releases with magnitudes and room sizes similar to those considered in this section are unlikely to form a flammable ceiling layer (undesirable because it disperses slowly) unless deliberately engineered to do so. Worst-case scenarios similar to M3 require a confluence of unlikely events, wherein (1) the 240 grams is stored in a single container, (2) which is pressurized, and (3) breaches in a manner that forms a single high-velocity jet that is (4) directed towards the ceiling and (5) ignites or encounters a fire source (this last item is not explicitly considered in this analysis). Lower ceilings, larger inventories, faster release rates, and vertically directed releases all increase the probability of a flammable layer forming on the ceiling.

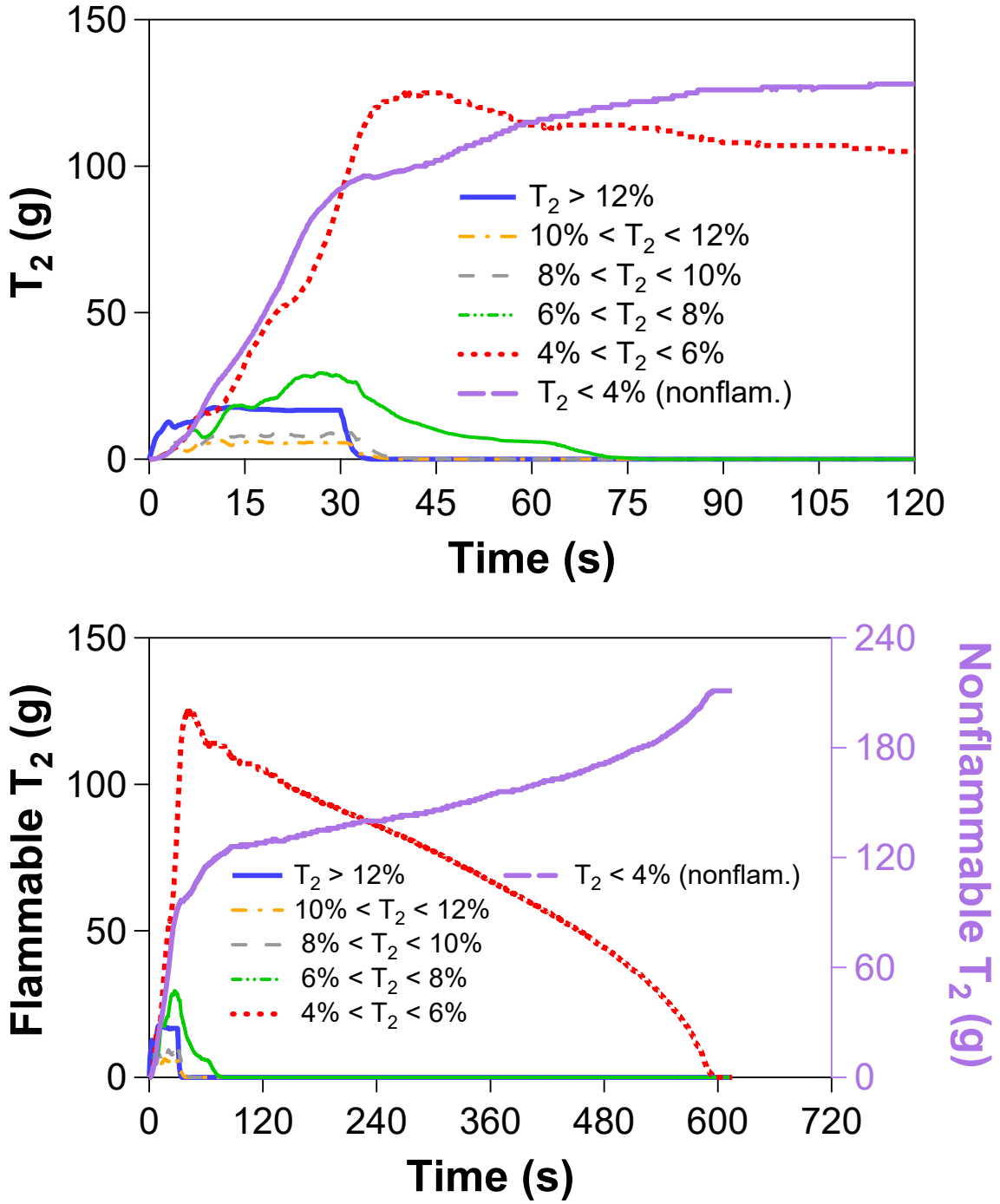

Figure 3-17. Concentration bins for 30 s release of 240 g T_2 into medium room with reduced inlet (4.1 m ceiling, 0.09265 m inlet length, M3). The top plot has a limited (zoomed-in) horizontal time scale with both flammable and nonflammable concentrations on the same vertical axis.

3.2.1. Follow-up Simulations of T_2 Release in the Medium Room

After the initial simulations in the three room sizes were complete (see Sections 3.1, 3.2, and 3.3) along with the preliminary analysis shown in Section 3.4.1, it was considered prudent to obtain more complete information regarding the threshold criteria for the formation and persistence of a ceiling layer. Such layers occur in simulated cases where a high-momentum jet forces a large amount of hydrogen isotope to the ceiling quickly enough to prevent full dispersion *en route*. Three additional cases were run in the medium room (4.1 m ceiling) with a release of 240 grams T_2. These additional cases were based on momentum metrics defined in Section 2.3 as a means to bracket the threshold for ceiling layer formation into a narrower range of conditions. These cases (M4, M5, and M6) were also designed to investigate whether the formation and persistence of a ceiling layer from the first round of simulations was an artifact of the turbulent momentum model that was used only for the cases with the highest inlet momentum. They are summarized in Table 2-2, with inlet metrics in Table 2-3.

Two of these cases simulated T_2 release occurring over 45 seconds (21.6 L/s) through the standard inlet (same inlet as M1 and M2). Case M4 used laminar solvers, while case M5 was modeled as turbulent; all other aspects of the model and inputs were identical for these two cases. The effective inlet Reynolds number for M4 and M5 was 1812, which approaches the turbulence transition number of 2300 for pipe flow. The third additional case designated as M6 simulated T_2 release occurring over 30 seconds (32.4 L/s) through the standard inlet with turbulent solvers (inlet Reynolds number of 2719). This release time is the same as case M3, but the standard inlet area used for case M6 exceeds the M3 inlet area by a factor of 16, with a corresponding reduction in the initial velocity and hence momentum.

Figure 3-18 is a modified version of Figure 3-9, showing the flammable mass and volume versus time for the four fastest release times of 240 g T_2 in the medium room (M3 plus the three new cases). Cases M4 and M5 differ only in terms of the laminar versus turbulent modeling approach, and they yield dispersion results in Figure 3-18 that are quite similar to each other. The turbulent case M5 does achieve a slightly higher flammable mass and volume than the laminar case M4, but the maximum "plateau" levels appear to be within a common noise band. Both M4 and M5 disperse towards a nonflammable condition with similar initial decay slopes, but M4 is dispersed to nonflammable in 13.8 s while M5 has a longer "tail" and disperses in 29.2 s.

The slower final dispersion rates for the turbulent case (M5) with respect to the laminar case (M4) appear to be a result of limitations from the simplified Schmidt number approach that was used for the turbulent simulations. The Schmidt number of 0.34 developed for T_2 at 1% concentration diffusing in N_2 as described in Chapter 3 of our previous report (Brown et al. 2022) was adopted for turbulent simulations in this study. However, the same chapter demonstrates that this modeling approach with a single Schmidt number is oversimplified; it overestimates diffusion rates at concentrations higher than 1% and underestimates diffusion rates at lower concentrations. This trend in the diffusivity means that concentration gradients for very dilute mixtures with the constant Schmidt model are not as steep as they would be with a more rigorous diffusion model. This effect tends to slow final dispersion, even though the LFL at 4% is higher that the optimal concentration of 1% for this model. However, the fact that the laminar case M4 with a more rigorous diffusion model and the turbulent case M5 with the simpler constant Schmidt diffusion model are visually quite similar in Figure 3-18 (with nearly identical initial dispersion rates) indicates that effects of model limitations are fairly minor, at least for these conditions.

Figure 3-18 also shows that case M6 is in-family with case M3, which shares the same volumetric or mass release rate with different inlet areas and velocities. The initial rise in flammable volume and mass are similar for these two cases. The peak values differ only modestly, with a higher peak occurring for the case with higher momentum (M3). Case M6 with lower initial momentum and lower peak flammable mass (and volume) than M3 also disperses about 3 minutes sooner.

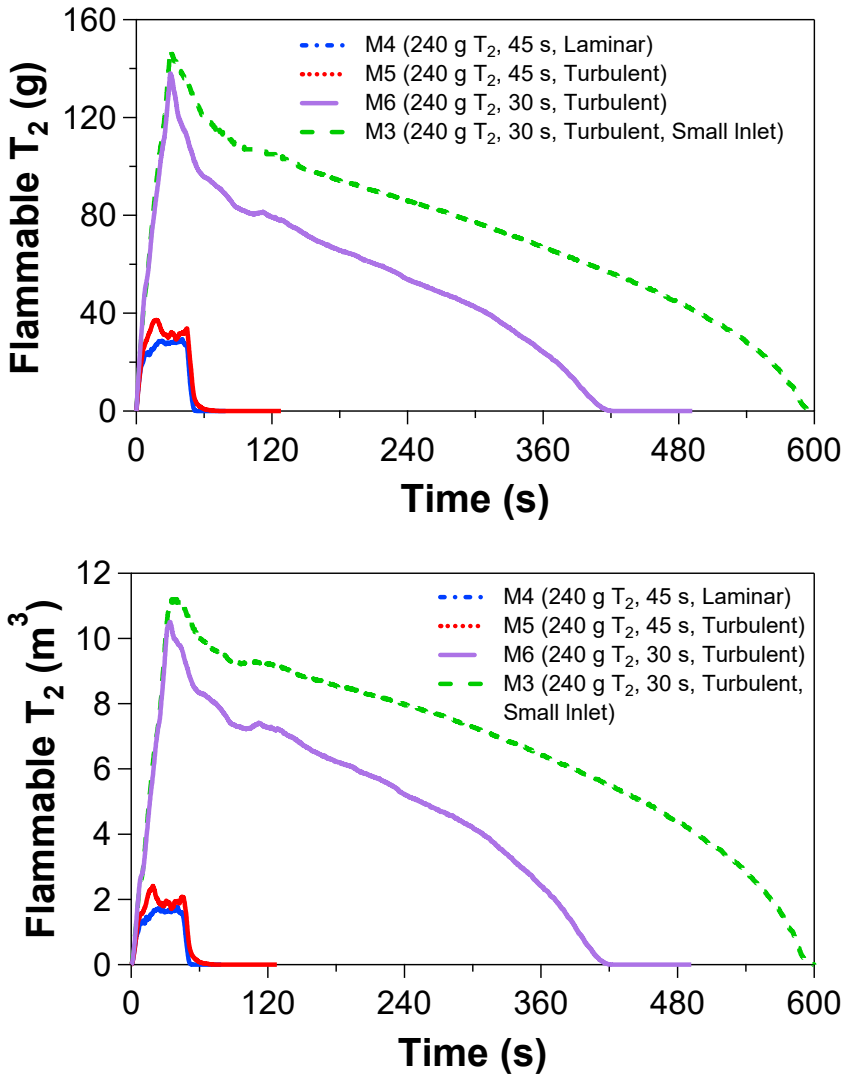

Figure 3-18. Flammable mass (top) and volume (bottom) for selected 240-g cases in the medium domain with room volume of 168.5 m^3

Figure 3-19 and Figure 3-20 show visualizations of the predicted T_2 plumes for cases M4 and M5, respectively, that are representative of the maximum ceiling coverage occurring for each of these simulations. The surfaces shown correspond to the 4% T_2 iso-contour (conservative LFL), which is colored by velocity magnitude. The laminar (Figure 3-19) versus turbulent (Figure 3-20) modeling of these two cases does not make much difference in terms of the ceiling coverage or the maximum velocity magnitude. The turbulent case M5 exhibits a smoother concentration iso-contour, with fewer features such as wrinkles and lobes with respect to the laminar case M4. These features appear to be a consequence of the turbulent flow dynamics and the resulting augmentation of diffusion through the notion of a turbulent viscosity, which is a sub-grid technique that models the small-scale

turbulent effect as a viscosity analog. These features may also relate to a flatter concentration gradient below the LFL resulting from use of a constant Schmidt number calibrated at 1% T_2.

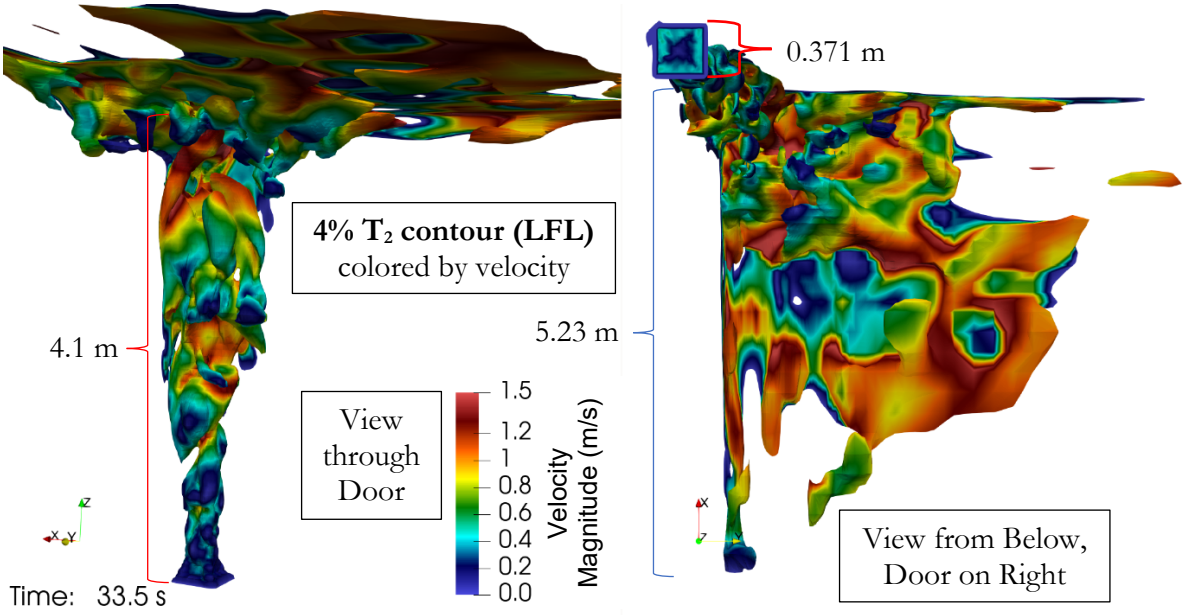

Figure 3-19. Flammable region (>4%) for 45 s laminar release of 240 g T_2 (4.1 m ceiling, M4)

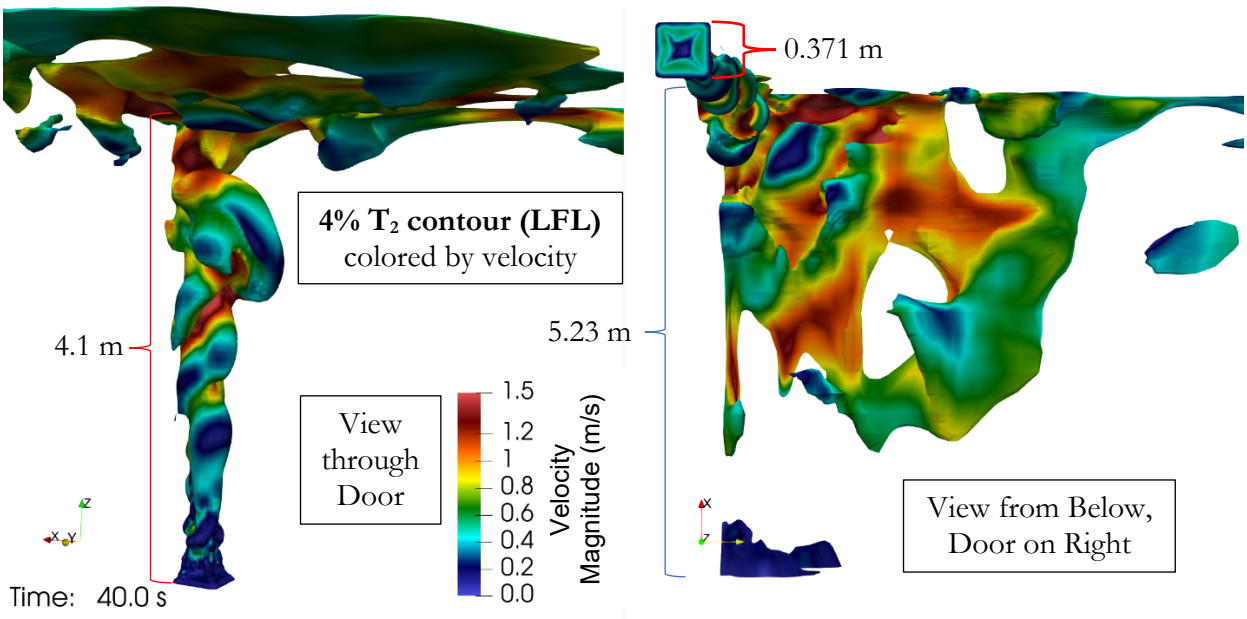

Figure 3-20. Flammable region (>4%) for 45 s turbulent release of 240 g T_2 (4.1 m ceiling, M5)

Figure 3-21 shows the behavior of case M6 in terms of the 4% T_2 iso-contour colored by velocity, which should be compared to case M3 in Figure 3-12. Both cases are modeled as turbulent and yield a layer of flammable T_2 that covers the ceiling. The larger injection area and lower momentum for case M6 in Figure 3-21 yields a jet with a less symmetrical shape and less uniform velocities on the

surface of the iso-contour compared to case M3 in Figure 3-12. Both of these jets are driven primarily by the initial momentum, but the less-uniform velocities (including higher velocity magnitudes) at the top of the plume in Figure 3-21 suggests that buoyancy with associated enhanced mixing plays a larger role for this case. The slightly lower peak flammable mass and volume for M6 relative to M3 in Figure 3-18 are likely attributable to the higher velocities in the jet and on the ceiling for M6, and buoyancy may drive some of these higher velocities.

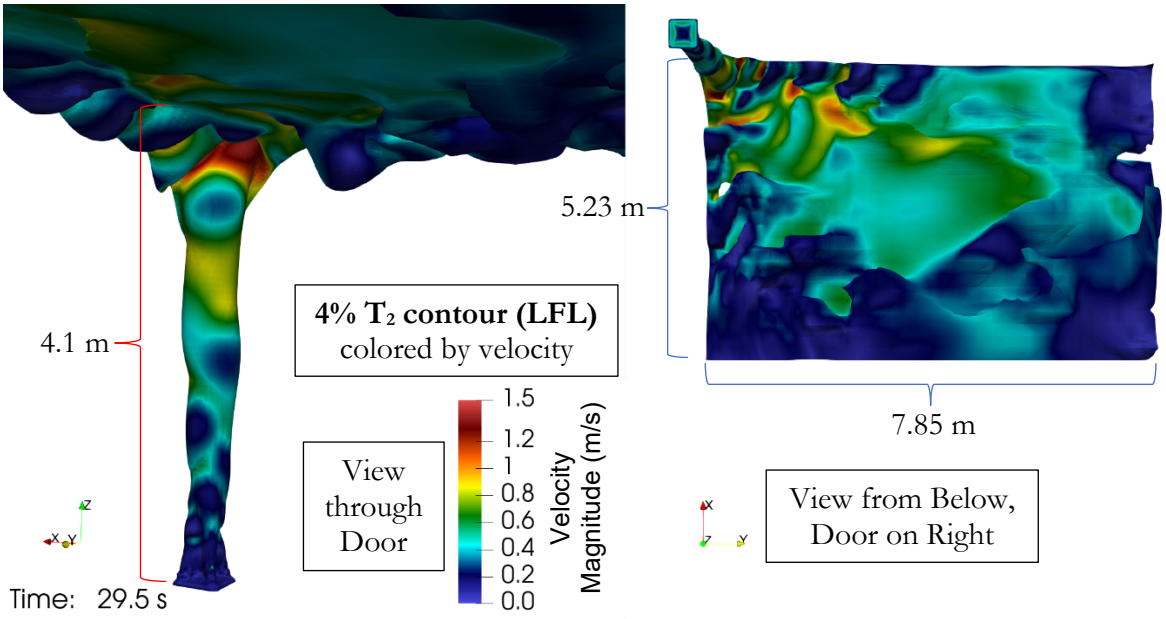

Figure 3-21. Flammable region (>4%) for 30 s release of 240 g T_2 with nominal inlet (4.1 m ceiling, M6)

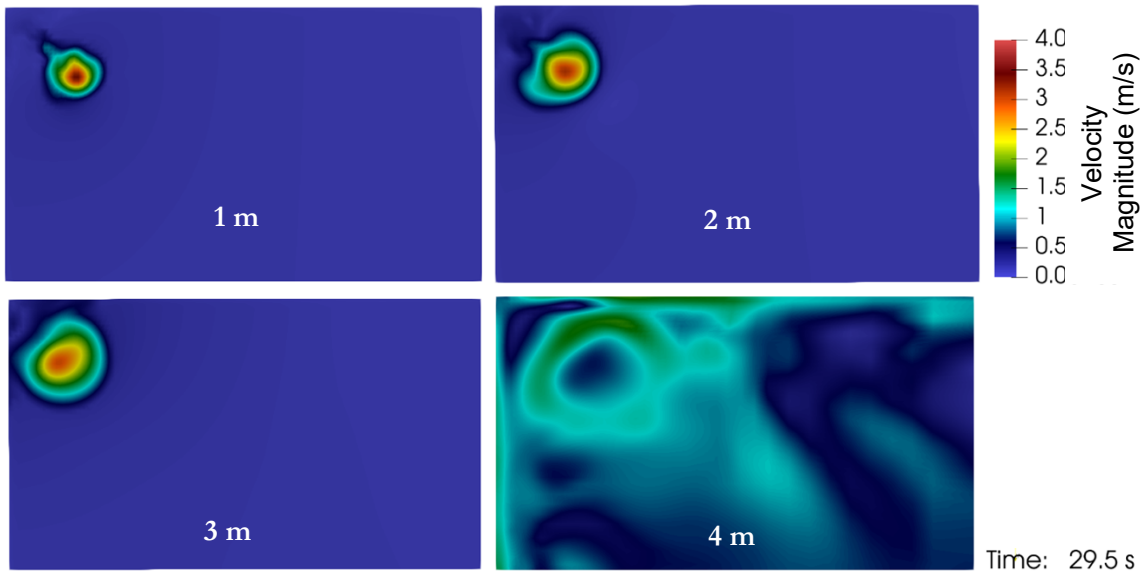

Figure 3-22. Horizontal slices of velocity magnitude through the jet from the 30 s release of 240 g T_2 through a nominal inlet into room with 4.1 m ceiling; heights from floor are designated in each frame

Horizontal cross sections of the jet for case M6 shown in Figure 3-22 display velocity distributions at different heights. Comparison to case M3 in Figure 3-13 confirms the observation from Figure

3-21 that case M6 with lower initial momentum produces a jet that is less uniform in shape. The region with highest velocity at 1 m above the floor is larger and faster for case M6 than for case M3. This difference is interesting because the larger M6 jet had lower initial velocity (0.24 m/s) compared to M3 (3.8 m/s). This observation suggests that buoyancy accelerates the core of the M6 jet as the periphery of the jet mixes with air. The maximum velocities at higher locations in both Figure 3-22 and Figure 3-13 are similar, and both are slightly lower than the initial velocity for case M3 at heights of 2 meters and 3 meters. These velocities suggest that the core of the M3 jet is slowed by viscous drag while buoyancy accelerates the core of the M6 jet to a similar "terminal velocity" somewhere between 1 meter and 2 meters. The influence of viscous drag is more spatially uniform than buoyancy, which explains the different degrees of symmetry for the M3 and M6 jets. Since the release location is near a corner and the jets for M3 and M6 have the same center location, the larger M6 jet also has more opportunity to interact with the walls, which is another potential source for the less uniform jet shape in Figure 3-21 and Figure 3-22.

Figure 3-23, Figure 3-24, and Figure 3-25 present more detailed views of the concentration distributions in the style of Figure 3-18 for cases M4, M5, and M6, respectively. The nonflammable masses for case M4 in Figure 3-23 and case M5 in Figure 3-24 begin to rise nearly linearly about 3 seconds after the release begins. The rise in the nonflammable mass continues until 51.6 seconds for M4 and 54.3 seconds for M5, when the flammable regions are fully dispersed. The steps towards lower nonflammable concentrations that occur after 60 seconds for M4 are indicative of gas pockets with considerable T_2 passing through the door and rapidly leaving the domain via buoyancy. The lack of such large steps for M5 may indicate that the turbulent case has higher effective viscosity, so the sloshing motion of the gas near the ceiling dissipates more quickly and less material is pushed out the door.

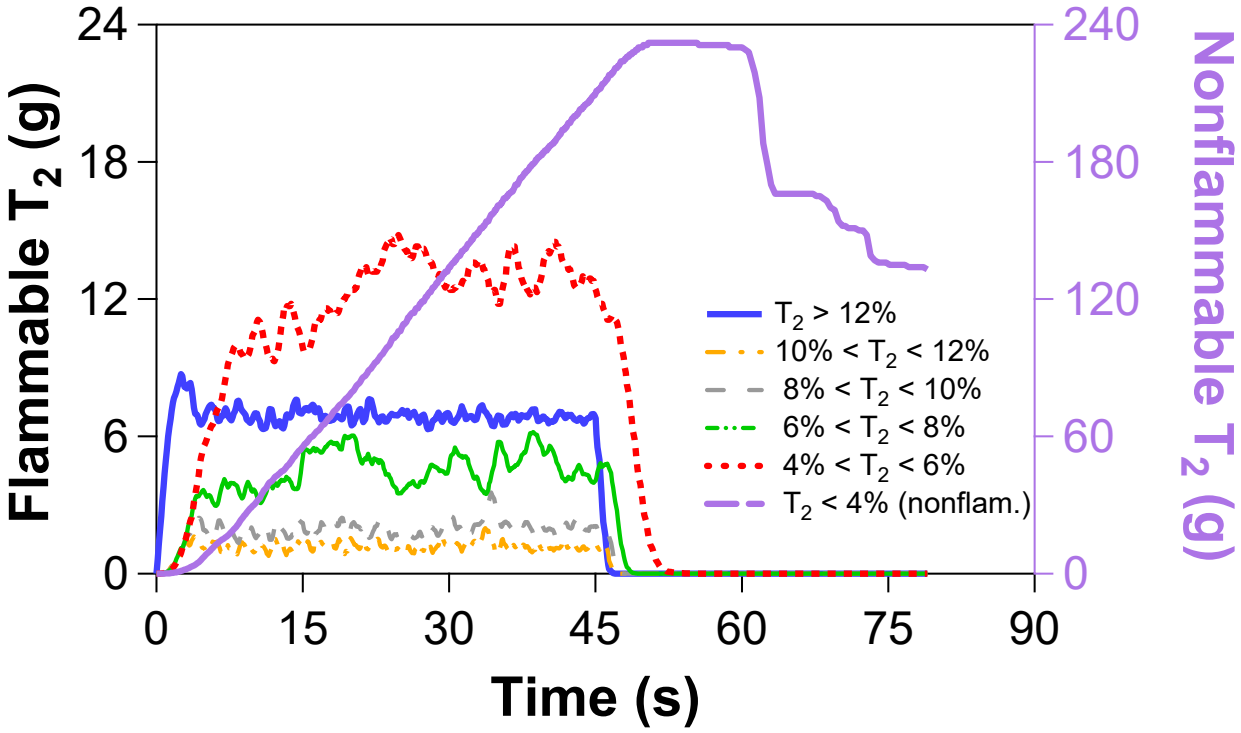

Figure 3-23. Concentration bins for 45 s laminar release of 240 g T_2 into room with 4.1 m ceiling (M4)

The trends in Figure 3-23 and Figure 3-24 with a 45-second release are similar to the 60-second release in Figure 3-15 in terms of the ranking of the concentration bins and the dispersion of higher concentrations before lower concentrations. The turbulent M5 case yields similar averages during the release with higher maximum concentrations for all bins below 10%, and these exhibit peaks at about 18 seconds that the laminar M4 case lacks. These features constitute a range of possible predictions, as transitional behavior in fluid mechanics is a challenging problem. The constant Schmidt number diffusion model used in the turbulent simulations can make gradients flatter at low concentrations, which appears to artificially reduce dispersion rates of the most dilute residual concentrations (below 1%, which is <LFL but on the same order of magnitude). This observation suggests that the simplified turbulent diffusion modeling approach used in this study may predict slow dispersion rates that are similar to or even more conservative than the laminar model; the laminar model should already be somewhat conservative compared to a higher-fidelity representation of a turbulent scenario.

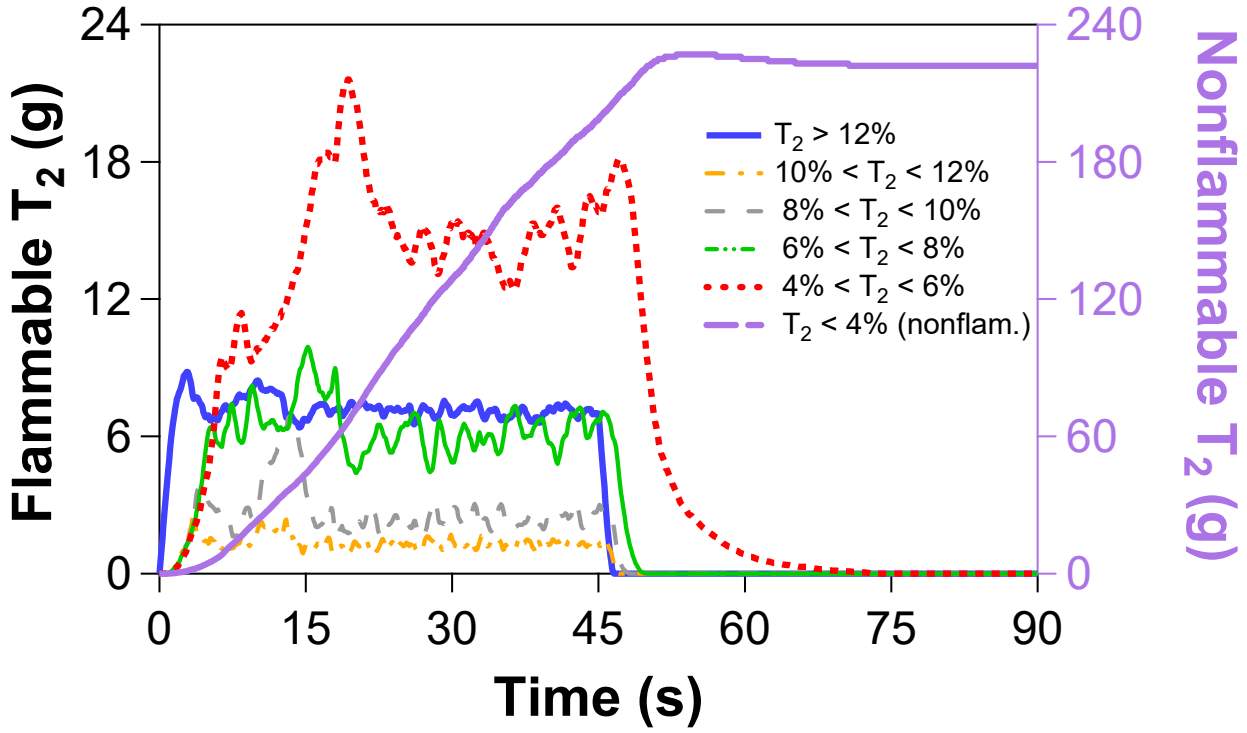

Figure 3-24. Concentration bins for 45 s turbulent release of 240 g T_2 into room with 4.1 m ceiling (M5)

Figure 3-25 should properly be compared to Figure 3-17 because the only difference between cases M3 and M6 are the inlet area and velocity, and the trends for the different concentration bins are largely comparable. In both cases, the flammable mass peaked just after the release ended at 30 seconds, with 138 grams for M6 compared to 148 grams for M3. Case M6 in Figure 3-25 with lower inlet momentum achieves 0.15 kg of T_2 at sub-flammable concentrations by about 85 seconds, while case M3 in Figure 3-17 does not do so until 330 seconds. For case M3, the T_2 mass in the 6% to 8% bin after 15 seconds exceeded the mass at concentrations >12% by close to a factor of 2, but these two bins remain comparable in terms of T_2 mass until the end of the release for case M6. The 6% to 8% concentration bin for M6 achieved a lower maximum T_2 mass of 21 grams (volume of 1.26 m^3) compared to 30 grams (1.82 m^3) for M3. Dispersion of the concentration bins higher than 4% to 6% occurred sooner for case M6 compared to M3; the 4% to 6% bin encompasses essentially all

flammable gas by 64 seconds for M6, but a comparable level of dispersion does not occur until 80 seconds for M3. Crossing this mixing threshold indicates that using the less conservative LFL of 6.6% for tritium (Cadwallader and Petti, 2002) yields a dispersion time between 1 minute and 1.5 minutes for both cases M3 and M6, which is considerably less than the dispersion times of 7 to 10 minutes predicted for the more conservative 4% LFL.

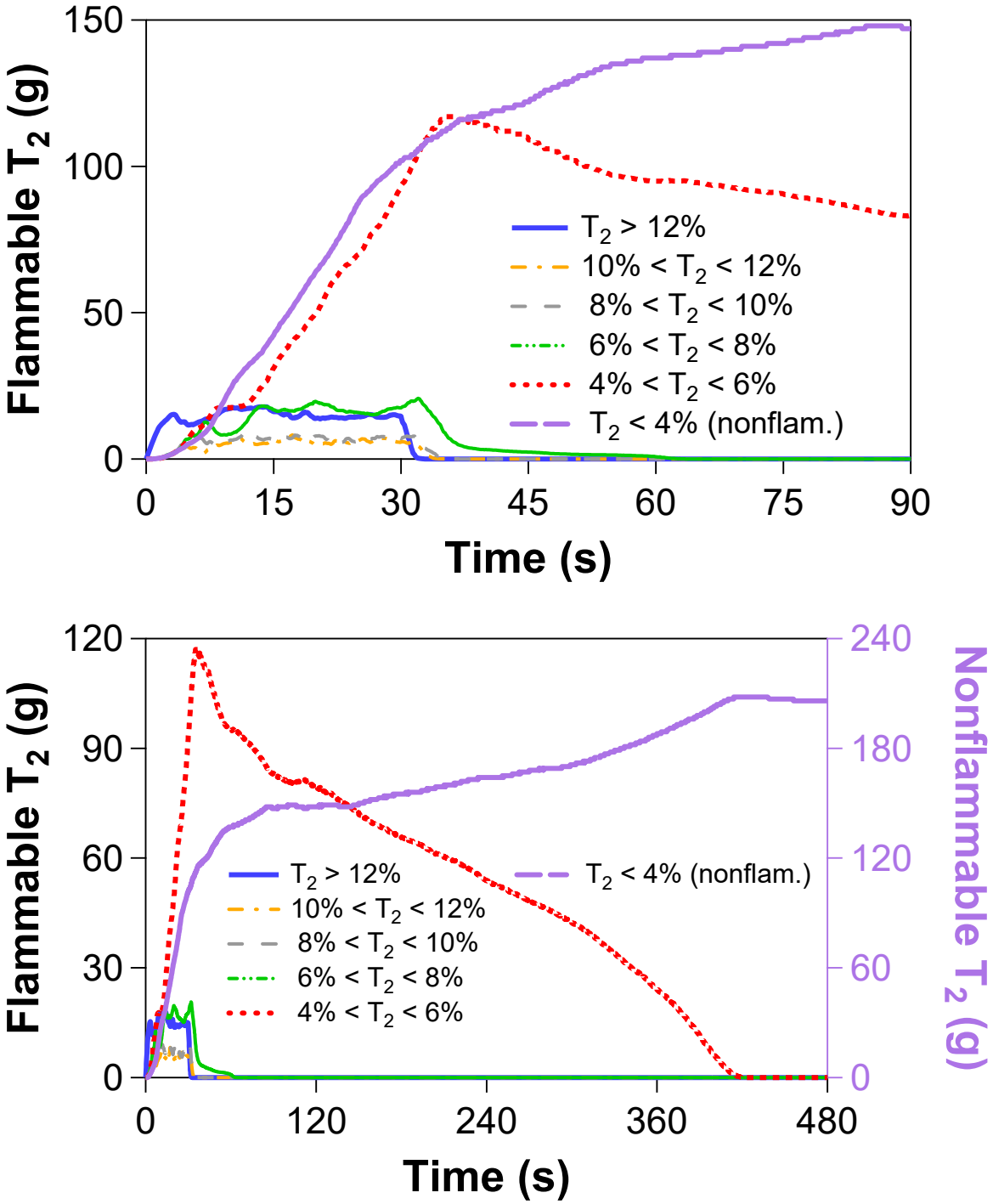

Figure 3-25. Concentration bins for 30 s turbulent release of 240 g T_2 into medium room with nominal inlet (4.1 m ceiling, 0.3706 m inlet length, M6). The top plot has limited (zoomed-in) time scale.

3.3. Large Room with 7.62 m (25 ft) Ceiling

The cases in the large room are defined as the last 2 rows of Table 2-2 and are designated with case numbers that start with "L." The mesh geometries for these cases are summarized in the last row of Table 2-1, and metrics are identified in the last 2 rows of Table 2-3. The rows pertaining to these cases in all three tables are shaded orange or tan.

Two simulations were executed to predict a 1.5-kg release of T_2 in the large room with a 7.62 m ceiling. At the time of this writing, these cases may be reflective of a release at a large Hazard Category 2 (HC2) facility (see DOE-STD-1027-2018). The case with a release duration of 5 minutes (300 seconds at 20 L/s, inlet velocity of 0.1 m/s, L1) was modeled as laminar. The case with a release duration of 8 seconds (762.5 L/s, inlet velocity of 3.9 m/s, L2) was modeled as turbulent.

The tritium mass and volume corresponding to the flammable portion of the domain for these two cases are shown in Figure 3-26 (>4% T_2 by volume), with striking differences. The methods used to produce the metrics shown in this plot are described in Section 2.3.1 and the beginning of Section 3.1. The 300-second release (L1) disperses rapidly, producing a maximum flammable mass and volume of 25 g (1.7% of total mass released) and 1.376 m^3, respectively. The 8-second release (L2) has a maximum flammable mass and volume of 1.48 kg (98.6% of total mass released) and 69.7 m^3, respectively. The flammable volume for L2 is about 16% of the total room volume, versus 0.3% of the room volume for L1. The full dispersion time to nonflammable conditions is 15.0 seconds after the 300-second L1 release ends, but dispersion takes 2270.3 seconds (37.84 minutes) after the 8-second L2 release. These comparisons with different release rates show that consideration of the released quantity of flammable gas alone is insufficient to characterize the potential hazard. These are more extreme manifestations of the trends with increasing release rate observed for small (30g) and medium (240 g) releases described in the preceding sections, including larger flammable volumes and slower dispersion times for faster release rates.

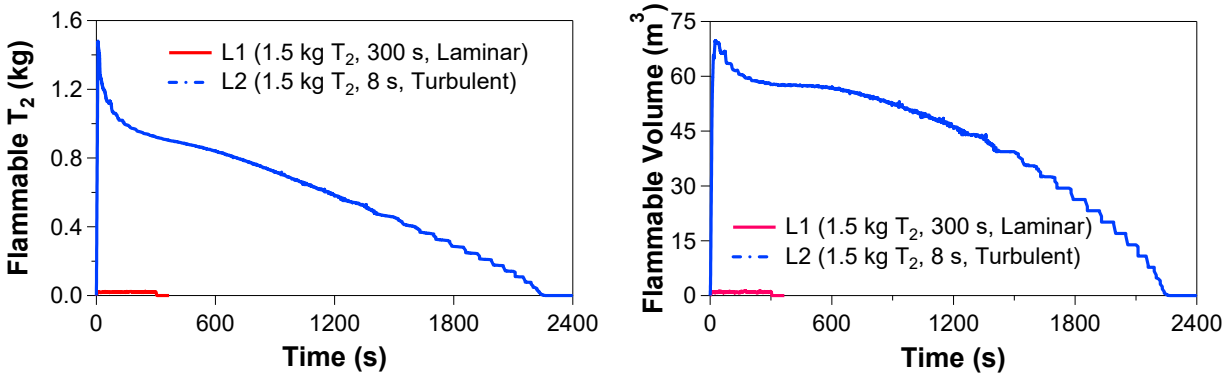

Figure 3-26. Flammable mass (left) and volume (right) for the two 1.5-kg cases in the large domain with room volume of 445.1 m^3

The plume associated with the slower release (300 s duration, L1) is visualized in Figure 3-27. This rate of release (20 L/s) is low enough for the buoyant plume to disperses completely below the LFL; the 4% T2 contour of the plume shown in Figure 3-27 only touches the ceiling intermittently. This observation is consistent with the very small flammable mass and volume shown in Figure 3-26. The ceiling does not cause slower dispersion, and no flammable layer is formed on the ceiling for case L1.

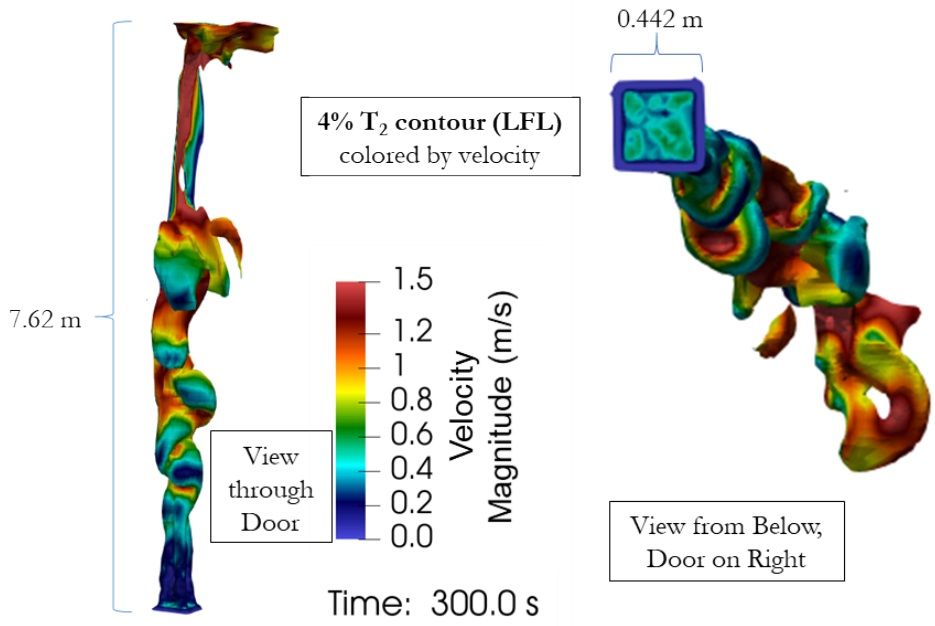

Figure 3-27. Flammable region (>4%) for 300 s release of 1.5 kg T_2 into room with 7.62 m ceiling (L1)

The simulation results visualized in Figure 3-28 for the large 8-second release (L2) initially resemble the jetting behavior of the fastest medium release (M3) shown in Figure 3-13, but Figure 3-28 shows that the velocities for this larger release are 2 to 3 times higher at the center of the jet. Figure 3-29 through Figure 3-33 show views of the L2 jetting release over time. Figure 3-29 shows a jet that is qualitatively similar to the M3 release in Figure 3-12; the ceiling for L2 is nearly covered with a rapidly spreading layer of flammable gas by the time the jetting release ends at 8 seconds. This rapid layer formation is consistent with the fact that 98.6% of the released tritium is flammable at this time. Figure 3-30 shows that the residual plume has nearly disappeared by 11.5 seconds through a combination of buoyant rise and dispersion through diffusion and mixing driven by residual velocities.

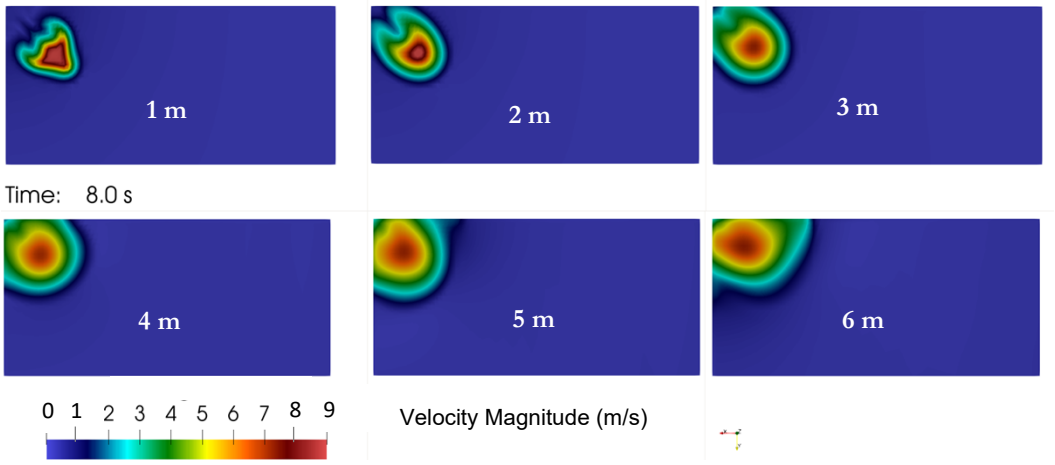

Figure 3-28. Horizontal slices of velocity magnitude through the jet from the 8 s release of 1.5 kg T_2 into room with 7.62 m ceiling (L2); heights from floor are designated in each frame

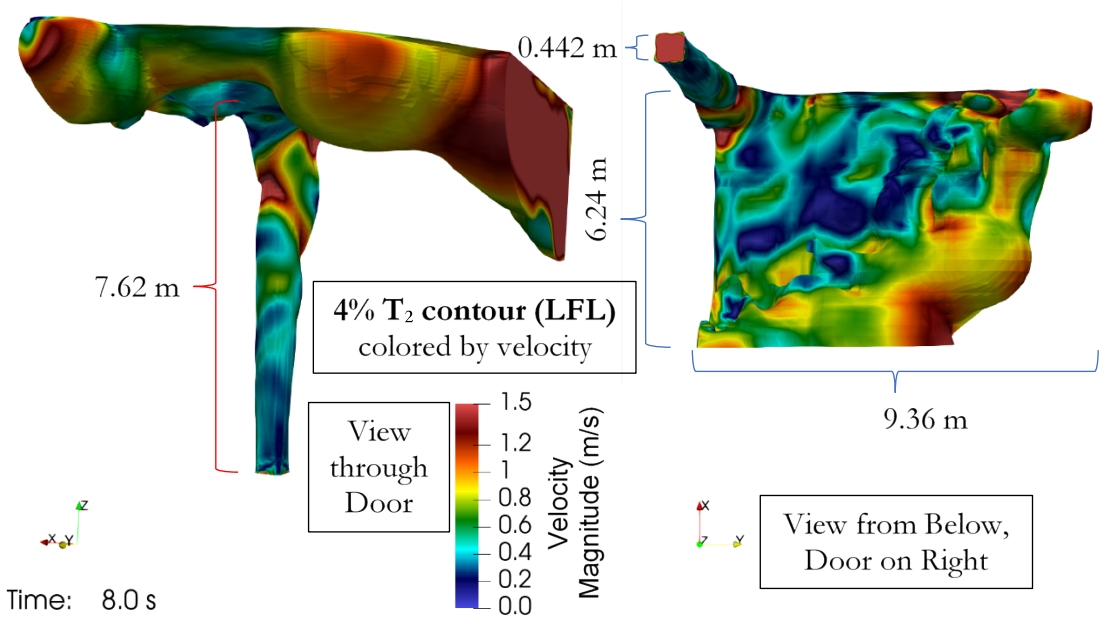

Figure 3-29. Flammable region for 8 s release of 1.5 kg T_2 into room with 7.62 m ceiling (L2) at 8 s

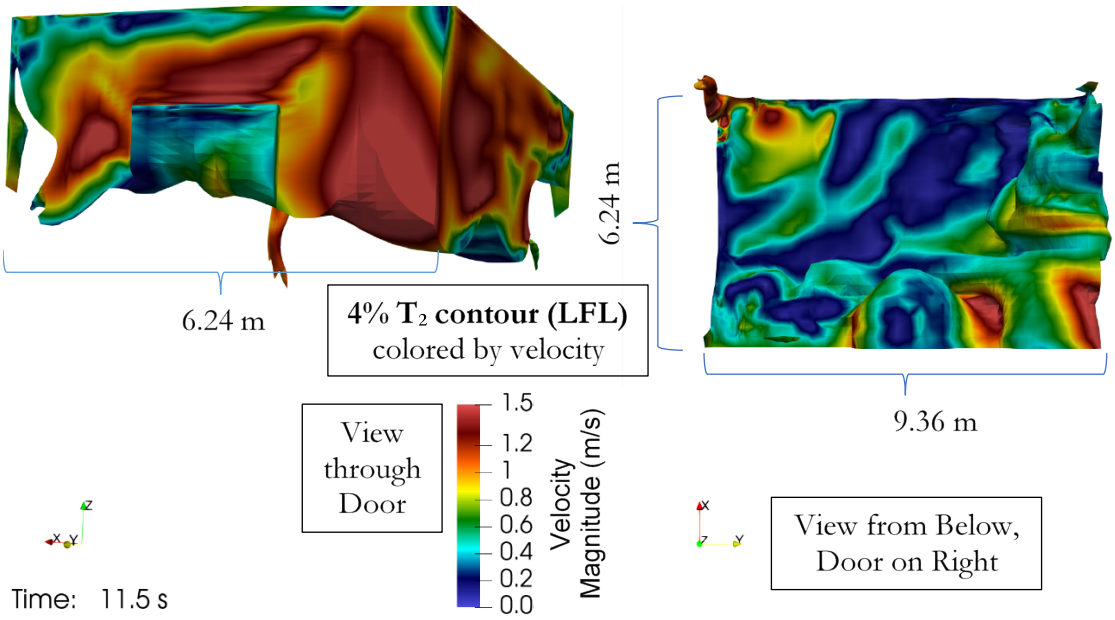

Figure 3-30. Flammable region for 8 s release of 1.5 kg T_2 into room with 7.62 m ceiling (L2) at 11.5 s

The initial momentum of the L2 jetting release and the displacement of air from the room triggers a "sloshing" motion within the room, like water in a bathtub when a large object enters or exits rapidly from one of the sides. By 11.5 seconds (Figure 3-30), this sloshing motion has caused a thick portion of the ceiling layer to approach the open doorframe; a large pocket of flammable gas from this wave is shown leaving the room in Figure 3-31 at 15 seconds and Figure 3-32 at 17.5 seconds. The sloshing motion of the air in the room, including the ceiling layer at the top, initially has a period of about 30 s. This sloshing causes several pockets of flammable gas to be expelled out the door as the motion subsides over about 12 minutes; one of these is shown at 75 seconds in Figure

3-33. Smaller-scale sloshing motion persists for many minutes afterwards, but the velocities decay and the flammable layer is approximately level with the top of the doorframe at later times, so the dissipation rate of the tritium-rich layer slows down. This dissipation of motion accounts for the step function-like curves in Figure 3-26.

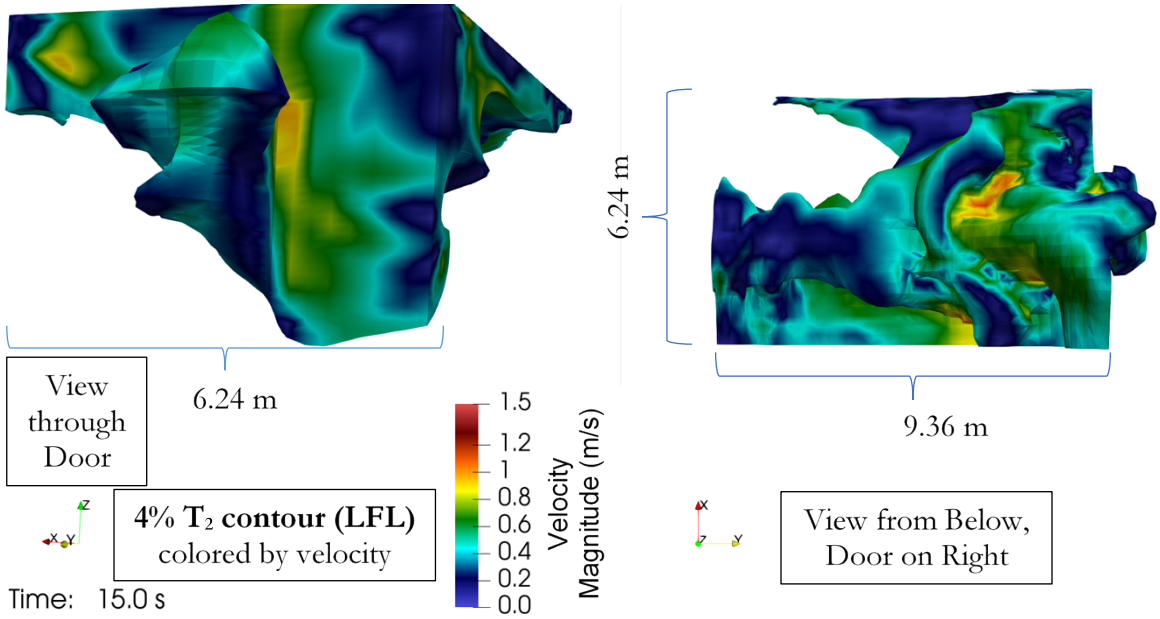

Figure 3-31. Flammable region for 8 s release of 1.5 kg T_2 into room with 7.62 m ceiling (L2) at 15 s

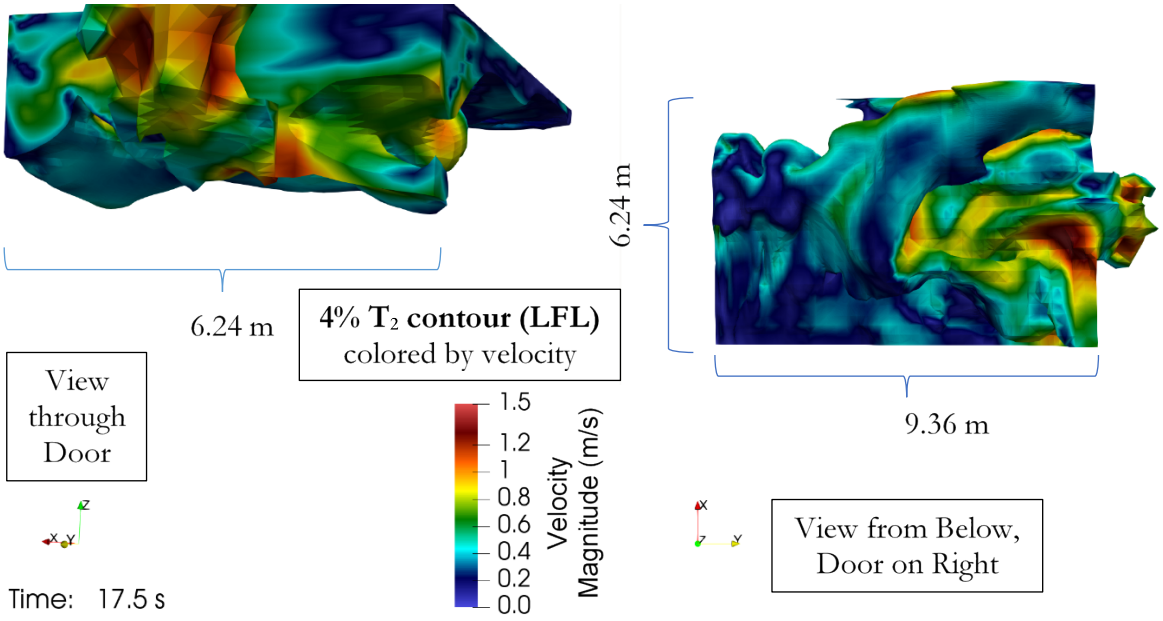

Figure 3-32. Flammable region for 8 s release of 1.5 kg T_2 into room with 7.62 m ceiling (L2) at 17.5 s

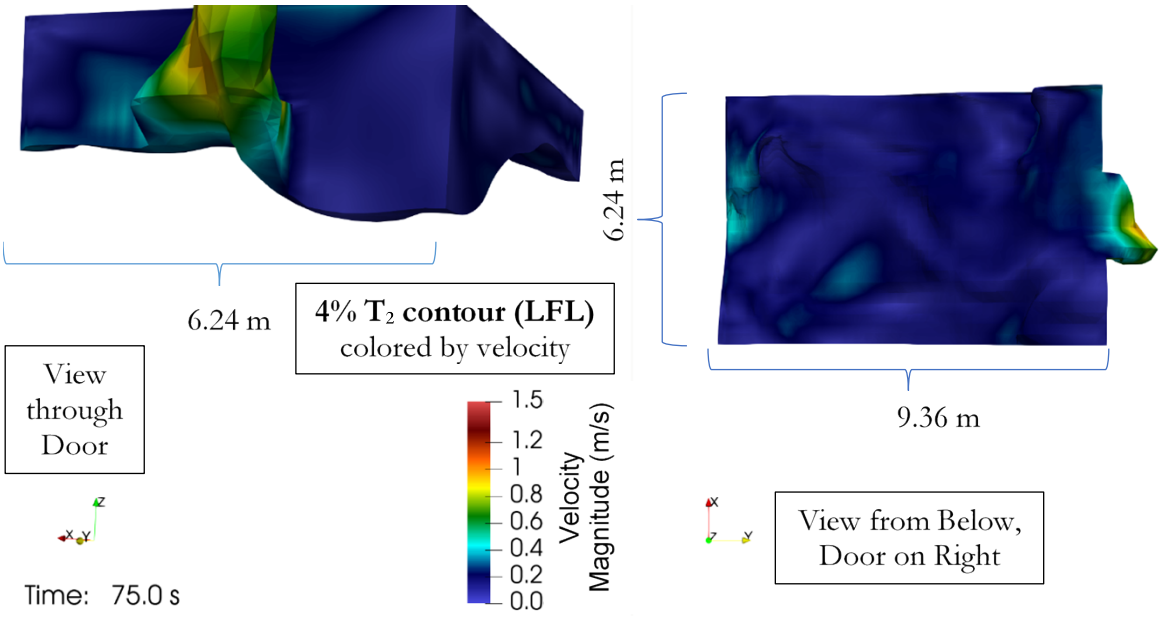

Figure 3-33. Flammable region for 8 s release of 1.5 kg T_2 into room with 7.62 m ceiling (L2) at 75 s

Figure 3-34 shows the detailed flammable concentrations corresponding to the 300-second L1 release from Figure 3-26. The nonflammable T_2 mass rises monotonically until the end of the release and begins to decline 3 seconds later as the tritium exits the door and leaves the computational domain (often as a buoyant plume). The reduction in the slope of the nonflammable <4% bin in Figure 3-34 shortly after 120 seconds suggests that tritium begins to leave the computational domain, which is confirmed by the sum of 0.978 kg for all T_2 in the domain at 300 s (65% of the full release). Figure 3-34 indicates that 37% of the flammable mass during the release (measured at 300 s) corresponds to the lowest concentration bin between 4% and 6% (65% of flammable volume). About 38% of the flammable mass during the release occurs at concentrations >12%, but this bin accounts for only 11% of the flammable volume. The volumes and masses in the bins between these extremes (6% to 12%) are all much less than the red 4% to 6% bin. The sum of the volumes at all concentrations above 6% is 35% of all flammable volume, or about half of the volume in the 4% to 6% bin. The mass in the intermediate bins is 24% of all flammable mixtures at 300 s.

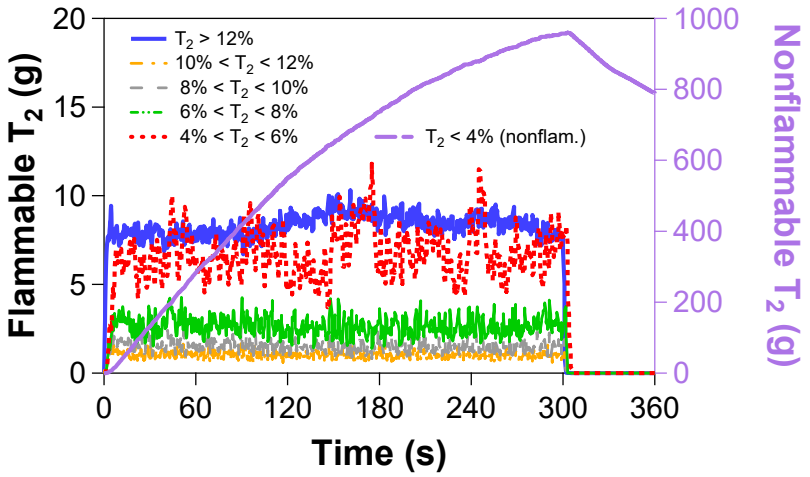

Figure 3-34. Concentration bins for 300 s release of 1.5 kg T_2 in room with 7.62 m ceiling (L1)

Figure 3-35 is a more detailed view in the style of Figure 3-26 with binned concentrations for the L2 high-velocity jetting release occurring over 8 seconds. The top panel of Figure 3-35 has a shorter time scale. Unlike the slower L1 release rate of 1.5 kg in Figure 3-34, the nonflammable T_2 mass for L2 does not begin to decline immediately after the release terminates. Instead, most of the L2 flammable mass in Figure 3-35 becomes trapped in a ceiling layer, and the nonflammable T_2 mass continues to increase as the flammable ceiling layer disperses over approximately 37 minutes; the nonflammable mass begins to decay only after the flammable mass is completely depleted.

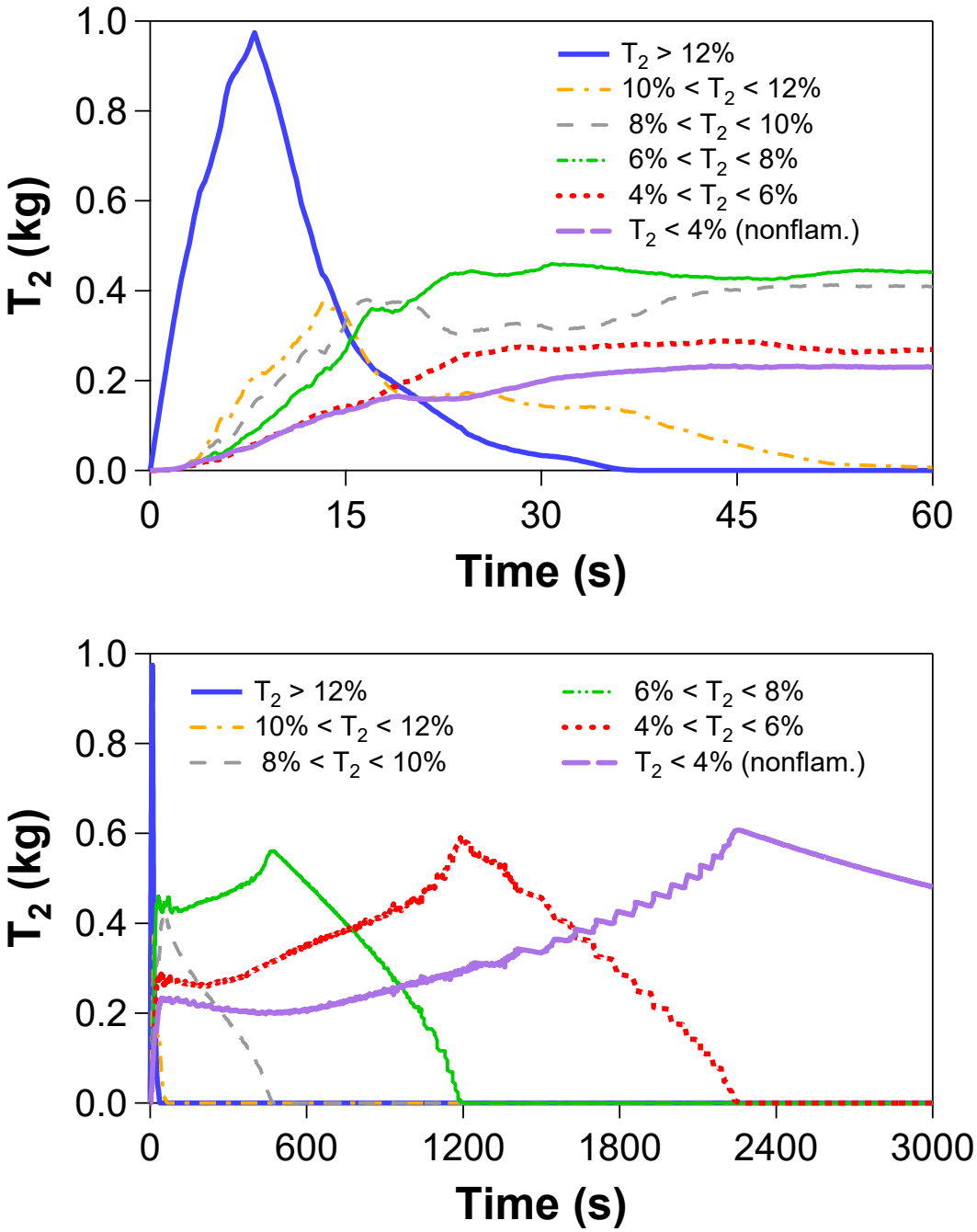

Figure 3-35. Concentration bins for 8 s release of 1.5 kg T_2 in room with 7.62 m ceiling (L2). The top plot has a limited (zoomed-in) time scale.

Unlike the other simulations in this report, the lowest concentration bin between 4% and 6% from Figure 3-35 takes a long time to become dominant (about 12 minutes) for the fastest release event (L2). At 8 seconds only 11% of the flammable volume or 4% of the flammable mass is in this bin. The lowest flammable bin increases to 33% of flammable volume and 24% of flammable mass at 68 seconds, after all concentrations >10% have decayed. This slow growth of the 4% to 6% bin occurs because the L2 tritium jet has much higher momentum than the other cases considered in this report. There is very little initial mixing of the high-momentum jet with the air, so the ceiling layer initially consists of high concentrations, as demonstrated by the initial dominance of the >12% blue curve in the upper plots of Figure 3-35.

The bin with >12% T_2 concentration in Figure 3-35 decays within 30 seconds after the jetting release event ends. This loss of higher concentrations and the subsequent decay to below 10% by 60 seconds after the jet stops suggests that the long persistence of the ceiling layer does not necessarily imply that a high risk of sustained ignition and efficient oxidation will persist for many minutes after the release (Shapiro and Moffette, 1957). The relatively fast dispersion of the highest concentrations in the L2 simulation (Figure 3-35) can be attributed to the residual gas momentum that causes the "sloshing" movement, as signified by the high velocities shown for early times in Figure 3-29 and Figure 3-30. Exploratory variants of the L2 simulation documented in Appendix B confirm this influence of residual sloshing or wave motion combined with turbulence, which significantly enhances the dispersion rate with respect to an otherwise comparable ceiling layer that is modeled as stagnant and simulated as laminar. However, the dissipation of this initial momentum (shown as decreasing velocities in Figure 3-31 through Figure 3-33) causes concentrations between 8% and 10% in Figure 3-35 to persist until 475 s (7.9 min), and concentrations between 6% and 8% persist until 1200 s (20 min).

Figure 3-35 indicates that high concentrations dominate early in the L2 simulation, unlike the other cases in this report. Only 4% of the flammable mass or 11% of the flammable volume at 8 seconds (the end of the release) corresponds to the lowest concentration bin between 4% and 6%. However, the high velocities at early times cause the highest concentrations to disperse quickly enough that all the flammable mass is <10% volume concentration by 80 seconds, and efficient combustion of hydrogen isotopes does not happen for these concentrations that approach the LFL (Shapiro and Moffette, 1957). All concentrations greater than 8% are dispersed by 8 minutes. Note that if a more accurate and less conservative LFL of 6.6% is assumed for tritium (Cadwallader and Petti, 2002), all flammable regions are dispersed in less than 20 minutes, whereas concentrations above the more conservative 4% LFL persist for nearly twice that long.

Some of the stair-stepping behavior in Figure 3-35 may be attributed to pockets of tritium-rich gas spilling out the doorway and leaving the domain, and this behavior may be influenced by mesh resolution for the largest domain (see Appendix A and Appendix B). The mesh was refined in the vicinity of the jet and the ceiling as shown in Figure 2-2 until the high-velocity behavior near the beginning of the simulation converged to mesh-independent solutions. However, parts of the mesh along tritium dispersion paths with less refinement (especially the upper doorframe and near the domain exit) may enhance the stair-stepping behavior that still appears after 1000 seconds (when velocities are relatively low) in Figure 3-35. Appendix A and Appendix B document mesh refinement studies showing that the rate of dispersion increases monotonically while stair-stepping becomes less severe when finer meshes are used, so any influence of coarse mesh in the dispersion path is expected to yield dispersion times that are conservatively long with respect to more refined solutions.

The simulations in this section are releases of 1.5 kg of tritium (HC2) with a 7.62 m ceiling and excess volume sufficient to preclude flammability once the room is fully mixed. The results are qualitatively similar to simulations in the previous sections with lower ceilings, in that the rate of release has a strong effect on whether a flammable zone persists after the source of the tritium release is exhausted. The buoyancy-driven plume for the slower release rate (5-minute duration, L1) causes flammable regions to disperse within seconds, with no flammable layer forming near the ceiling. The high-velocity jet that is directed towards the ceiling in case L2 moves too quickly to dissipate much tritium before it reaches the ceiling (3.9 m/s at the inlet in this case), so a flammable ceiling layer forms and then disperses slowly to a nonflammable condition. However, dispersion to concentrations low enough to preclude efficient oxidation to T_2O or HTO still occurs very rapidly for simulation L2 with a high-velocity tritium jet.

3.4. Discussion of Safety Metrics for Dispersion of Hydrogen Isotopes

The simulations in this report have shown that the rate of hydrogen isotope dispersion in many and perhaps most scenarios can be quite rapid, but a release that occurs near the ceiling or as the result of a high-velocity jet directed at the ceiling has the potential to create a flammable zone (>4%) that may persist for many minutes if the room is not ventilated (as in cases M3, M6 and L2). In contrast, slower releases result in lower peak concentrations, with the potential for shorter durations for localized flammable mixtures. These momentum effects mean that flammability metrics such as the ISF (which was greater than 1 for all simulations) is a useful but insufficient metric with respect to ignition safety for some scenarios. The MFLT metric is somewhat more informative than the ISF because it includes the effect of room height, but other metrics must be evaluated to account for momentum effects, such as those shown in Table 2-3.

Besides the 4% LFL assumption, the simulations in this work have an additional embedded conservatism in terms of the orientation of the hydrogen isotope jet. If a jet of gas is not oriented upward and/or the path of the jet towards the ceiling is obstructed, the effect of these momentum parameters could be quite different. A high-momentum jet (with large Re and large Fr) having a horizontal orientation will spread and mix the released gas over a large volume far from the ceiling. In the horizontal jet scenario, any of the released gas that ends up on the ceiling (e.g., via buoyancy) will be mixed to a much lower concentration than would be the case for the ceiling layer formed from an equivalent vertical jet, and flammable regions will disperse faster. These simulations can therefore be viewed as worst-case approximations given the vertical release assumptions.

The use of momentum metrics to describe thresholds for the formation of flammable ceiling layers is of interest, as this exercise yields safety criteria that can be used to quickly evaluate and screen hazards. The next two subsections use the framework of the momentum metrics introduced in Section 2.3.3 to evaluate the plume and dispersion behavior from the full suite of simulations. The initial simulations are used to define an initial range for the α parameter in Equation (10) and the results of follow-up simulations are used to narrow this range in a calibration exercise. The metrics summarized in Table 2-3 from Section 2.3.3 are used throughout this discussion.

3.4.1. Momentum Trends from Initial Simulations

As indicated in Table 2-3, the first round of simulations in the medium room did not include cases M4 through M6. These established that for the 4.1 m ceiling height, the threshold for formation of a ceiling layer occurs when the term $Re^{0.5}FrD$ is somewhere between 0.9 m and 40 m (see Table 2-3). A persistent ceiling layer formed for case M3 with $Re^{0.5}FrD$ = 40.7 m and a 4.1-m ceiling in Figure 3-12, which persisted for 9.5 minutes. Likewise, a higher initial momentum corresponding to

$Re^{0.5}FrD$ = 203.4 m for case L2 in Figure 3-29 formed a very thick layer below a 7.62-m ceiling that persisted for 37.8 minutes after the release ended. The ceiling layer was thicker and endured longer for L2 compared to M3 because the total release was more than 6 times larger (1.5 kg versus 0.24 kg), and also because the jet had higher momentum, as reflected in the term $Re^{0.5}FrD$. The term $Re^{0.5}FrD$ for L2 exceeded M3 by a factor of 5, which is substantially larger than the ratio of room heights (1.85). This higher momentum metric helps explain why nearly all of the L2 release became flammable, while less than 2/3 of the M3 release became flammable.

Figure 3-11 shows that case M2 with $Re^{0.5}FrD$ = 0.899 reaches the 4.1-m ceiling with insufficient momentum to form a thick layer, and the plume has a thin "neck" occurring at about 75% of the ceiling height. Case M2 is therefore below the momentum threshold for formation of a flammable ceiling layer. However, M2 appears to be closer to the threshold condition than case M3, which exceeds the threshold by a substantial margin with $Re^{0.5}FrD$ = 40.699. From inspection of the simulated behavior and $Re^{0.5}FrD$ values for cases M2 and M3, it appears that Equation (10) with $1 < \alpha < 4.1$ is a reasonable first estimate.

For the initial estimated range for α cited above, the smallest room with a 2.4-m ceiling has a corresponding momentum threshold in the range 0.59 m < $Re^{0.5}FrD$ < 2.4 m. Likewise, the medium room with a 4.1-m ceiling should have a threshold in the range 1 m < $Re^{0.5}FrD$ < 4.1 m. The large room with a 7.62-m ceiling should have a threshold in the range 1.86 m < $Re^{0.5}FrD$ < 7.62 m. The following paragraphs provide additional evidence for these ranges from the other cases in the first round of simulations.

With respect to the height of the smallest room, cases S1, S2, S3, and M1 all fall below the proposed lower momentum threshold for forming a flammable ceiling layer. Case S1 in Figure 3-3 shows that the flammable portion of the plume fails to consistently reach the 2.4-m ceiling when $Re^{0.5}FrD$ = 0.065 m. A plume that reaches 2.4 meters with insufficient residual momentum to form a thick ceiling layer is manifest for S2 with $Re^{0.5}FrD$ = 0.534 m in Figure 3-4 and for S3 with $Re^{0.5}FrD$ = 0.309 m in Figure 3-5. This is also the case for M1 with $Re^{0.5}FrD$ = 0.173 m in Figure 3-10, where the plume begins to taper near 2.4 m (58% of the room height).

Inspection of the plume heights and thicknesses from simulations in larger rooms supports the estimate that releases with momentum described by 0.59 m < $Re^{0.5}FrD$ < 2.4 m may form a flammable ceiling layer when the ceiling height is limited to 2.4 m. M2 with $Re^{0.5}FrD$ = 0.899 in Figure 3-11 has a robust plume at 2.4 m (58% simulated height). Likewise, L1 with $Re^{0.5}FrD$ = 0.886 in Figure 3-27 has a thick plume at 2.4 m (31% simulated height). The thickness of the plume for cases M2 and L1 at 2.4 meters is sufficient to suggest that formation of a semi-stable flammable layer is probable for these inlet conditions in the smaller room.

3.4.2. Momentum Effects and Parameter Tuning from Follow-up Simulations

Additional simulations were designed with the momentum parameter $Re^{0.5}FrD$ set to 1.385 m (cases M4 and M5) and 2.544 m (case M6) to determine whether the proposed range of 1 m < $Re^{0.5}FrD$ < 4.1 m (based on consideration of the initial simulations in the previous section) actually contains the threshold for the formation a thick ceiling layer with a 4.1 m ceiling (see Table 2-3). This exercise served to provide evidence to narrow the range for the momentum-based threshold identified from specific cases in the first round of simulations (0.899 m < $Re^{0.5}FrD$ < 40.7 m). Cases M4 and M5 formed plumes that only partially covered the ceiling with a thin layer that dispersed quickly in a manner qualitatively similar to case M2 with $Re^{0.5}FrD$ = 0.899. The use of a turbulent model in case M5 did not trigger different behavior in terms of the ceiling layer.

Case M6 did trigger the formation of a ceiling layer that persisted for 6.5 minutes, or about 70% of the dispersion time observed in case M3. This observation indicates that initial jet momentum is not a strong driver of average dispersion rates for 2.5 m < $Re^{0.5}FrD$ < 40.7 m (see metrics for cases M3 and M6 in Table 2-3). This result makes sense because mixing driven by the initial gas motion should dissipate fairly quickly, so slower diffusion processes should dominate the dispersion behavior of the ceiling layer soon after the release ends. This result also suggests that the largest changes in dispersion time must occur near the momentum threshold required for a ceiling layer to form.

The results of cases M4, M5, and M6 bracket the momentum threshold for a medium room with a 4.1-m ceiling to a much smaller range that rounds to 1.4 m < $Re^{0.5}FrD$ < 2.5 m. This narrower range for $Re^{0.5}FrD$ can be used with Equation (10) to revise the estimate for α to the reduced range of $1.6 < \alpha < 3.0$. For the smaller room with a 2.4-m ceiling, this proposed range reduction for α translates to a threshold for the shorter room of 0.8 m < $Re^{0.5}FrD$ < 1.5 m, which is consistent with the evidence noted in the previous section for cases M2 and L1 with $Re^{0.5}FrD \approx 0.9$. There is only minor overlap between the reduced momentum parameter ranges for the ceiling heights at 2.4 m and 4.1 m. Likewise, the threshold for the 7.62-m ceiling based on the revised range for α is reduced to 2.6 m < $Re^{0.5}FrD$ < 4.7 m, which has no overlap with the momentum ranges for the two lower ceilings considered in this study.

The ranges for these momentum metric thresholds could be reduced further with additional simulations, but detailed exploration of the near-threshold behavior is beyond the scope of the current work. Using the upper-bound $\alpha = 3.0$ in Equation (10) or the lower-bound values for $Re^{0.5}FrD$ with each ceiling height given in the preceding paragraph will produce a momentum threshold estimate that is conservatively low with respect to the simulations studied to date. These conservative limits are based on cases M4 and M5 with <25% coverage of the ceiling with a flammable layer, while the opposite limit is based on case M6 with a full ceiling layer that disperses over 7 minutes. It appears that a true momentum threshold is closer to case M4 than it is to M6. Assuming 1/3 of the total range designated from these simulations with respect to the conservative limit yields $\alpha = 2.5$ as a reasonable estimate for the threshold. For the ceiling heights considered in this study, this value for α corresponds to momentum parameter thresholds of $Re^{0.5}FrD$ = 0.96 m for a 2.4-m ceiling, $Re^{0.5}FrD$ = 1.6 m for a 4.1-m ceiling, and $Re^{0.5}FrD$ = 3.0 m for a 7.62-m ceiling.

Figure 3-36 illustrates penetration heights for a vertical jet or plume of tritium gas as predicted by Equation (10) with respect to the orifice size and velocity. Figure 3-37 presents the same information with fewer orifice diameters and without the logarithmic horizontal velocity or the symbols representing the simulations from this work. Both of these figures use the best parameter estimate of $\alpha = 2.5$ as developed in this section. The more conservative limit of $\alpha = 3.0$ does not change the trends much from these figures; it decreases the velocity required to reach the 7.62 m ceiling by about 13% for the two curves on the far right of Figure 3-37 with the smallest orifices.

The simulated tritium releases from this work are shown as open diamonds in Figure 3-36, where the nominal positions are defined in the same manner as the lines using Equation (10) with $\alpha = 2.5$. The case that formed a flammable ceiling layer (M6, see Figure 3-21) is designated in red with a lower-bound error bar estimated as ≥ 0.2 m above the actual medium ceiling height. The remaining cases show upper-bound error bars for the penetration height, which are visually estimated from the corresponding plume images shown in this report based on the assumption that a flammable ceiling layer can only form at a height lower than a thin "neck" in the plume (see S1 in Figure 3-3, M1 in Figure 3-10, M2 in Figure 3-11, and L1 in Figure 3-27). For cases where the flammable region of the

plume impacted the ceiling without spreading significantly, a height 0.2 m below the actual ceiling was assumed for the error bar (see S2 in Figure 3-4, M4 in Figure 3-19, and M5 in Figure 3-20). The other cases that formed flammable ceiling layers (L2 and M3) are excluded from Figure 3-36 because the predicted penetration heights are more than an order of magnitude higher than the remaining simulations (509 m and 102 m, respectively). These large, extrapolated values from Equation (10) suggest that a flammable layer will form for any practical ceiling height when the inlet momentum is comparable to the L2 or M3 conditions. All simulations from this work fall between the three lines corresponding to the highest jet diameters shown on the left side of Figure 3-36 (93 mm to 442 mm, see Table 2-1).

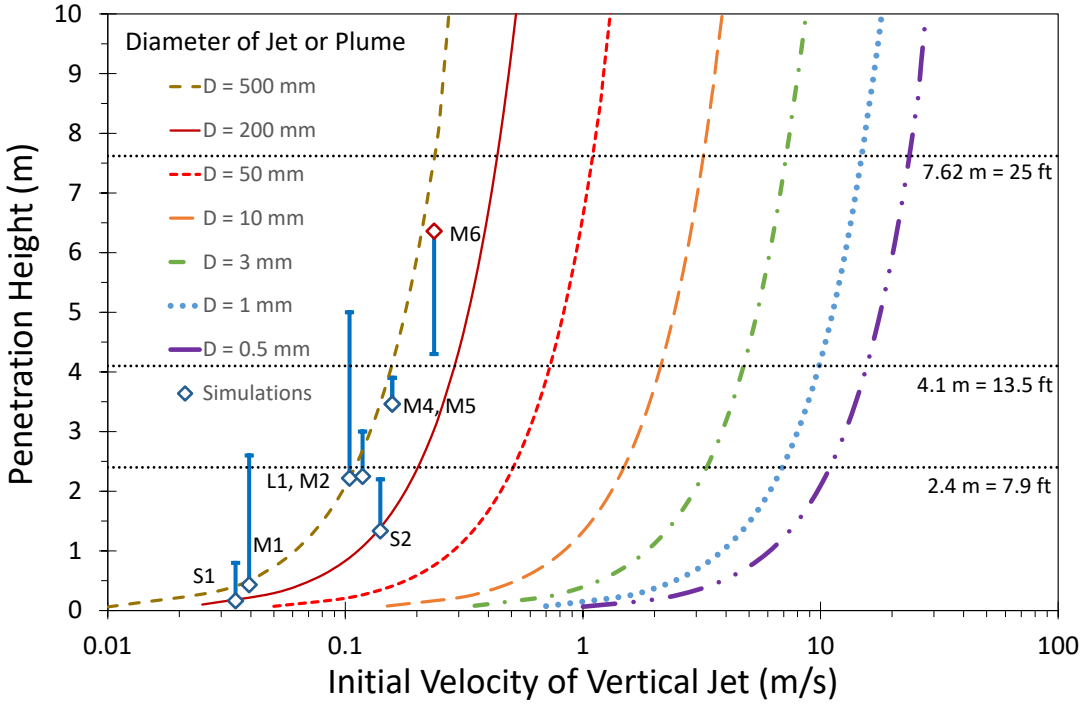

Figure 3-36. Penetration height from Equation (10) as a function of the velocity and diameter of the gas release orifice, using $\alpha = 2.5$ and a logarithmic horizontal axis for velocity. Diamonds with estimated error bars represent simulated conditions; a flammable ceiling layer was observed for the red diamond (M6).

The four lowest orifice diameters (< 10 mm) on the right side of Figure 3-36 and Figure 3-37 encompass leak scenarios that are much easier to imagine occurring for real tritium containment vessels in terms of failure modes such as cracked welds, leaky valves, etc. Leaks from features of such small sizes were not investigated in this study because the mesh resolution requirements would have increased the computational cost significantly (by orders of magnitude). Figure 3-36 and Figure 3-37 indicate that vertical penetration of a jet with a more probable orifice diameter (<10 mm) sufficient to form a flammable layer below the ceiling requires initial velocities between 1 and 2 orders of magnitude higher than the fastest inlet velocities simulated in this work (Cases M3 and L2 at slightly below 4 m/s; see Table 2-3). In other words, the optimized version of Equation (10) suggests that tritium leaks of reasonable size cannot form a ceiling layer unless they form jets with velocities on the order of 1.5 m/s to 25 m/s or higher. These velocity magnitudes can only develop and be sustained if the tritium storage pressure is elevated, so formation of a ceiling layer from a near-atmospheric tritium containment vessel can be ruled out.

The continued evaluation of Equation (10) and alternative momentum-based correlations with respect to more data and simulations is recommended to support safety assessments for release of light flammable gases like H_2 or T_2. The computational expense of simulations increases for higher velocities and smaller orifice diameters (which both require finer mesh resolution) and for larger rooms; these correspond to moving to the right and upward in Figure 3-36, respectively. Hence, ceiling heights on the order of 1 m or less would be most appropriate for future studies investigating whether the extrapolated trends for orifice diameters near 1 mm are reasonable.

The vertical error bars in Figure 3-36 suggest an alternative approach to calibrate the α parameter in Equation (10) that could be used in future simulation studies. In this alternative approach, estimates of initially observed plume characteristics would be used to specify reduced ceiling heights until a flammable ceiling layer is formed with a fixed inlet size and flow condition. Simulating smaller rooms in this manner could result in either faster computation with fewer computational elements or improved convergence due to finer spatial discretization. It is recommended that a postprocessing method be devised for future studies of this type to tabulate plume characteristics and average them over time, which would improve estimates for error bars of the kind shown in Figure 3-36.

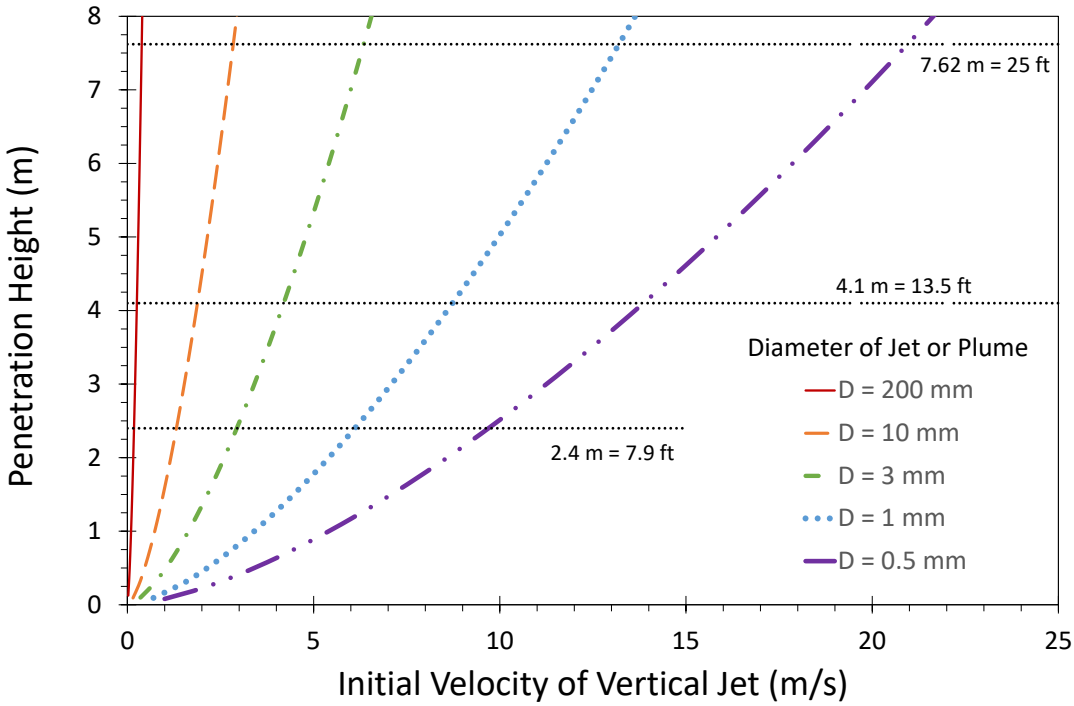

Figure 3-37. Penetration height from Equation (10) as a function of the velocity and diameter of the gas release orifice, using $\alpha = 2.5$

The trends in both Table 2-3 (simulations) and Table 2-4 (experiments) suggest that the Reynolds number by itself could also be a useful momentum metric for safety assessment purposes in rooms of normal to moderate heights (between 2.4 m and 4.1 m), with a critical value on the same order of magnitude as the turbulence transition at 2300. However, the comparison of Cases S2 and S3 in Table 2-3 suggests that Reynolds number should only be used for comparisons within a single gas type (or isotope), while the effect of gas type is less pronounced for $Re^{0.5}FrD$. Additionally, these momentum metrics assume a quasi-continuous release event, so flammability metrics such as ISF and MFLT should be used first to determine whether there is enough releasable flammable gas to

form a flammable region on the ceiling of the room under consideration. Appendix C contains a stepwise procedure to evaluate risk based on the flammability and momentum metrics as presented in this section.

3.5. Summarized Results from the Full Simulation Matrix

This section summarizes metrics, basic trends, and conservatisms based on the results and analysis of the simulations. The case matrix for the simulations executed and studied in this work is defined in Table 2-2. Simulation characteristics are listed in Table 2-1, including mesh resolution. Table 2-3 summarizes metrics related to flammability limits for the room as a whole (mixed room concentration, ISF and MFLT) and also momentum metrics (Re, Fr, and $Re^{0.5}FrD$). A flammable ceiling layer was produced in three simulations, and these persisted for 6 to 38 minutes. Flammable regions in the remaining eight cases dispersed within seconds, as summarized with other metrics from the simulations in Table 3-1. The cases that formed a flammable (or ignitable) layer below the ceiling are designated in Table 3-1 with asterisks next to the case numbers.

The maximum flammable mass in Table 3-1 refers to the dynamic mass of hydrogen isotope occurring in a region with a concentration >4% by volume during the transient jetting of the hydrogen. The maximum flammable mass is designated in Table 3-1 on a mass basis and also as a percentage of the total released mass. It is typical for cases that did not form a semi-stable flammable ceiling layer to achieve a maximum flammable mass that is less than about 20% of the total release, while more than 50% of the release was flammable when a ceiling layer formed for cases M3, M6, and L2.

The maximum volume occupied by a flammable mixture in Table 3-1 was divided by the ceiling area and normalized by the MFLT from Table 2-3 to see how simulations with different characteristics group together. This exercise shows that cases with a flammable ceiling layer all achieved flammable volumes above 40% of MFLT. Simulations exhibiting partial ceiling coverage that dispersed within seconds achieved 4% to 10% of MFLT. Simulations achieving 1% of MFLT or less did not form a layer on any portion of the ceiling. Therefore, only rapid releases with sufficient momentum to form a ceiling layer with achieve a substantial fraction of the idealized MFLT metric. Once a full ceiling layer forms, the dispersion times in Table 3-1 lengthen from a few seconds to several minutes. The dispersion time has an approximately exponential trend with the maximum % flammable mass release (correlation coefficient $R^2 = 0.96$). The dispersion time has a linear trend with momentum terms like the inlet Reynolds number ($R^2 = 0.98$) or $Re^{0.5}FrD$ ($R^2 = 0.97$).

Comparisons to experimental studies from the literature confirmed that both the magnitude of a hydrogen release with respect to the room volume (as reflected in ISF and MFLT) and the vertical momentum of the release are important considerations affecting the formation and persistence or dispersion of a flammable ceiling layer. The size of the release tends to dominate this behavior, but sufficiently high momentum (as reflected in the Reynolds number, the Froude number, or a combination such as $Re^{0.5}FrD$) can force formation of a semi-stable flammable ceiling layer even with ISF > 4 and MFLT < 0.7 m. These trends are broadly supported by both the simulations in this study and the available experimental measurements in the literature. A recommended stepwise procedure for using the metrics discussed in this report to evaluate the probability of forming an ignitable ceiling layer is contained in Appendix C.

Table 3-1. Metrics from simulated tritium and hydrogen releases

Case Num.	Release Mass (Duration)	Inlet Area (Momentum Model)	Max Flam. Mass (% Release)	Max Flam. Volume	Flam. Height as % of MFLT	Flam. Ceiling Layer (Y/N)	Time For Dispersion Below LFL (<4%)
S1	30 g T_2 (122 s)	0.0289 m^2 (Laminar)	0.6 g (2.0%)	0.032 m^3	1.0%	No	2.4 s
S2	30 g T_2 (30 s)	0.0289 m^2 (Laminar)	4.0 g (13.4%)	0.241 m^3	7.9%	No	7.3 s
S3	10 g H_2 (30 s)	0.0289 m^2 (Laminar)	1.1 g (10.7%)	0.178 m^3	5.8%	No	4.8 s
M1	240 g T_2 (180 s)	0.1373 m^2 (Laminar)	4.1 g (1.7%)	0.206 m^3	0.8%	No	6.2 s
M2	240 g T_2 (60 s)	0.1373 m^2 (Laminar)	19.3 g (8.0%)	1.175 m^3	4.8%	No	13.6 s
M3*	240 g T_2 (30 s)	0.0086 m^2 (Turbulent)	148.0 g (61.7%)	11.177 m^3	45.9%	Yes	570.1 s (9.50 min)
M4	240 g T_2 (45 s)	0.1373 m^2 (Laminar)	29.4 g (12.2%)	1.767 m^3	7.3%	No	13.8 s
M5	240 g T_2 (45 s)	0.1373 m^2 (Turbulent)	37.2 g (15.5%)	2.407 m^3	9.9%	No	29.2 s
M6*	240 g T_2 (30 s)	0.1373 m^2 (Turbulent)	138.2 g (57.6%)	10.476 m^3	43.0%	Yes	392.5 s (6.54 min)
L1	1.5 kg T_2 (300 s)	0.1954 m^2 (Laminar)	25.0 g (1.7%)	1.376 m^3	0.9%	No	15.0 s
L2*	1.5 kg T_2 (8 s)	0.1954 m^2 (Turbulent)	1.4793 kg (98.6%)	69.710 m^3	45.7%	Yes	2270.3 s (37.84 min)
*Asterisk next to case number indicates flammable layer at ceiling							

3.5.1. Summary of Conservatisms and Non-conservatisms

Since release characteristics from tritium containment vessels are not yet well-characterized, a wide variety of safety-related conservatisms were adopted or observed in this study. These conservatisms were intended to make the formation of a flammable ceiling layer more probable and extend the duration of any type of flammable zone compared to a more realistic release. Characterization of realistic release conditions from representative tritium containment vessels is recommended, followed by further studies with experiments and/or simulations to investigate how these release characteristics influence the dispersion behavior of light gases (including hydrogen isotopes) in air. The conservatisms identified and discussed in the methods and results sections above are restated here:

- The entire released mass was assumed to originate from a single location over a relatively short duration (8 s to 5 min), which implies a pressurized release.
    - Many facilities store sub-gram quantities of tritium in separate containers, which are often stored in various distributed locations rather than all together. Individual containers are unlikely to release their contents at the same time, and their finite spatial distribution also results in an effective spatial dilution of the T_2 prior to release. Releasing the full inventory from a single location maximizes the time required for dispersion to nonflammable conditions (< 4%)
    - Containers can be damaged in a variety of ways, so there is a considerable probability that even pressurized inventories could be released slower than the cases simulated in this study. This simulation study indicates that slower releases have a tendency to disperse faster. Release rates from pressurized vessels decay with time, so the rates near the end of a real release are likely to be very low, which differs from the step changes used in this study.
    - Many storage containers for tritium are at low or sub-atmospheric pressure, especially for small quantities (see analysis in Chapter 2 of Brown 2022). The most rapid release rates considered in this work are considered for completeness and are not necessarily representative of what would be possible at most tritium facilities.
    - The location of the release in a corner means that only about 50% of the plume area is exposed to fresh air, which reduces the dispersion rate for larger plumes with faster release rates.
- The simulations assume that the plume or jet of hydrogen isotope is directed upward.
    - Horizontal velocity components are expected to enhance mixing rates; a vertical jet is the configuration most likely to reach the ceiling while the mixture is still flammable
- The minimum LFL of 4% by volume (or moles) measured for normal hydrogen (protium) was used for all isotopes of hydrogen to assess whether ignition and conversion to the water form can occur.
    - The LFL for T_2 is estimated as 6.6% (Cadwallader and Petti, 2002).
    - The maximum LFL for H_2 is twice as high at 8% for downward propagation of flames compared to 4% for upward propagation of flames due to buoyancy. Sideways propagation yields an intermediate LFL (Shapiro and Moffette 1957, Kumar 1985, Bauwens and Dorofeev 2014).

- No safety credit is taken when hydrogen isotopes occur at concentrations above the UFL
    - Dispersion will reduce these concentrations to produce an ignitable mixture
- Concentrations near the LFL (i.e., < 10% for protium) do not yield high combustion efficiency (Shapiro and Moffette, 1957), so sustained ignition/explosion accompanied by 100% conversion to water is unlikely for concentrations between 4% and 10%.
    - No fire or ignition sources were modeled in this work. The maximum flammable mass fractions are higher than the anticipated true oxidation fractions.
- A homogeneous temperature is assumed in the room.
    - The temperature of the room was assumed to be homogeneous in the simulations. The analysis of the maximum flammable mass does not account for additional mixing that occurs due to the presence of temperature gradients from any fires in the vicinity.
- Laminar CFD solvers were used when practical (e.g., inlet Re < 2300).
    - This approach neglects turbulent mixing effects at the sub-grid scale that would otherwise be included via an advanced turbulent mixing model, so flammable regions may persist longer with this computational approach.
    - The back-to-back comparison of a laminar and turbulent case (M4 and M5) with Re slightly below 2300 (1812) suggests that the simplified constant Schmidt number method used for diffusive mixing in the turbulent simulations may predict dispersion rates that are conservatively slow compared to reality (comparable or even more conservative than the laminar model), at least near the turbulent transition threshold.
- The simulated domain represented paths available for tritium to leave the room as a single open door located on the side of the room opposite the release, with no obstacles in the room and all other room surfaces being free of leaks.
    - Enhanced mixing from any active ventilation systems is ignored. The air in the rooms is assumed to be initially stagnant at the time of release, which is unlikely given the force needed to compromise the largest types of tritium containers.
    - The presence of obstacles such as furniture in the room could potentially obstruct flow paths with respect to these simulations; obstacles could enhance mixing by inducing rotational motion.
    - Paths for gases to exit the room could easily be closer to the release location.
    - The distance between the ceiling and the top of the doorframe can trap buoyant tritium-air mixtures for extended periods under the right conditions, forcing final dispersion of a flammable ceiling layer to be limited by the slow rate of molecular diffusion. It is very common to have ventilation ducts in the ceiling that can allow buoyant hydrogen isotope mixtures to leave the room, even if the ventilation system is not actively flowing air.
    - Many ceiling and wall structures are not leak-tight
        - Drop-tile ceilings in particular provide many leak paths whereby tritium that rises to the ceiling can continue dispersing via buoyant rise and diffusion.

- The sizes of the rooms are conservatively small with respect to the mass of tritium released.
    - Our understanding of typical storage conditions suggests inventories in this study are high compared to the typically expected inventory given the volume of the rooms.
- Dispersion times for flammable regions in the largest rooms simulated (with coarser mesh resolution) are likely longer compared to results that would be obtained from comparable simulations using finer mesh resolution.
    - The mesh refinement studies in the appendices of this report indicate that dispersion time decreases monotonically with increasing mesh refinement and larger numbers of nonlinear iterations.
- An optional conservative limit has been identified for the momentum correlation given in Equation (10) based on the simulations.
    - The nominal estimate of $\alpha = 2.5$ was chosen to be closer to the conservative limit of $\alpha = 3.0$ than the limit of $\alpha = 1.6$ that is based on simulations where a flammable ceiling layer was formed.
- Preliminary application of Equation (10) as a screening tool (a momentum correlation) with respect to experimental measurements of H_2 release and dispersion yields conservative results (see Section 2.3.4).
    - Equation (10) correctly indicates that the H_2 release of Bauwens and Dorofeev (2014) has sufficient momentum to reach the ceiling, which is consistent with their measurements of concentrations between 4% and 8% next to the ceiling from about 7 seconds to sometime well beyond the 20 seconds of measurements they reported.
    - Equation (10) indicates that a flammable ceiling layer is likely for all four experimental conditions reported by Lacome et al. (2011). However, this calculated result is conservative because no flammable region was detected anywhere in the room for two of these cases. This absence of a flammable region appears to be attributable to the smaller size of these two release events.

It is acknowledged that some aspects of the simulated scenarios may be nonconservative, but efforts were taken to minimize these. It is quite possible that the following list is not comprehensive, but on a preliminary basis it appears that the nonconservative items below are neither as numerous nor as impactful as the conservatisms listed above. Nonconservative features of the simulations reported in this work with respect to realistic tritium release scenarios may include:

- A flat ceiling was assumed that allows a buoyant gas to spread horizontally until it reaches the walls, which provides a lot of surface area at the interface between the light gas on the ceiling and the surrounding air where mixing can occur.
    - Some ceilings are divided into concave structures that could capture gas from a buoyant plume within just a few small regions. This arrangement would interfere with horizontal spreading and provide less surface area between the light gas region and the surrounding air where mixing can occur.

- The releases were assumed to occur on the floor of the room with no barriers in the vertical path to the ceiling.
    - Flammable ceiling layers are more probable for releases occurring at higher elevations within a room because they have less time and space to mix before they rise via buoyancy to the ceiling.
    - Semi-stable flammable layers could also occur for releases within stagnant cabinets or under tabletops (where the vertical distance is much smaller than the open rooms studied here), especially if there is a lip or other concave structure around the edge of a table that can prevent sideways motion or diffusion.
- It is assumed that there is no ignition source within the relatively small flammable region of the released plume
    - An ignition source in such an optimized location would likely result in a high value for the tritium-to-water CF for almost any realistic tritium release conditions.

4. CONCLUSIONS

This work uses theory and CFD simulations to investigate conditions required for tritium and other hydrogen isotopes to form a flammable (or ignitable) layer below the ceiling and characterize the time required for flammable regions of different types to disperse. The pertinent physics mechanisms are identified as buoyant rise, dispersion via molecular diffusion, and more rapid mixing associated with gas motion. Mixing driven by advective gas motion may originate from the jetting release, buoyant rise, or other sources, and the motion may be laminar or turbulent (turbulent mixing is faster). These physics mechanisms do not allow for gravitational enrichment of a light gas within buildings of any realistic size. Hydrogen isotopes will not form a flammable region once they have been mixed to concentrations below the lower flammability limit.

Flammability metrics were found to be a useful screening tool to assess whether there is enough flammable gas to create a serious risk of a high conversion factor (CF) from gaseous tritium to the more hazardous heavy water forms (T_2O or THO). Previous work indicates that CFs are likely to be lower than ~10% for sub-flammable mixtures, which have T_2 concentrations lower than the conservative LFL of 4% by volume. However, it is probable that the CF will be considerably higher for flammable mixtures that encounter an ignition source. Thresholds of concern based on flammability metrics were identified in this work for ISF (ignition safety factor) and MFLT (defined in this work as maximum flammable layer thickness). Both metrics account for the effect of room size, and MFLT accounts for the effect of room height with the assumption of a flat ceiling.

The probability of an ignition event that results in a high conversion factor (CF) increases as the extent of a flammable region increases in space and time (larger volume and longer duration). Because potential ignition sources are spatially distributed, a scenario with a very large flammable volume of almost any duration is more hazardous than a scenario with a small flammable volume and an extended duration. The simulations in this work demonstrate that for releases of the same total mass of T_2, slower release rates produce a lower hazard by minimizing the volume of the ignitable mixture and expediting dispersion to non-flammable conditions once the release event has terminated. Simulations that formed flammable layers next to the ceiling were observed to disperse below the LFL over timescales of minutes, whereas simulations with no flammable ceiling layer dispersed much faster, achieving nonflammable conditions within seconds.

Metrics associated with the momentum of a plume or jet were used to further bound the risk of a release event for cases with high values of MFLT that indicate increasingly risky quantities of T_2 relative to the room size. The $Re^{0.5}FrD$ metric was used to recommend momentum thresholds for jetting release events. Tritium jets that exceed the $Re^{0.5}FrD$ threshold for a specified room height have enough momentum for high concentrations to penetrate the full room height and form a flammable layer next to the ceiling. In contrast, flammable regions will be restricted to a tritium plume that is mostly dispersed to non-flammable concentrations by the time it reaches the ceiling if the momentum of the release is sufficiently low. Summarized procedures to evaluate risks with recommended thresholds for both flammability and momentum metrics are provided in Appendix C.

This page left blank

REFERENCES

[1] Badino, G. (2009) "The legend of carbon dioxide heaviness," *Journal of Cave and Karst Studies*, 71(1), 100–107.

[2] Blake, T. R. Webb, H., and Sunderland, P. B. (1990), "The nondimensionalization of equations describing fluidization with application to the correlation of jet penetration height," *Chemical Engineering Science*, 45(2), 365-371, https://doi.org/10.1016/0009-2509(90)87022-K

[3] Briens, C., Li, F. Berruti, F. and McMillan, J. (2010), "Penetration of High Velocity Horizontal Gas Jets into a Fluidized Bed at High Temperature," presented at the *13th International Conference on Fluidization - New Paradigm in Fluidization Engineering*.

[4] Brown, A. L., Shurtz, R. C., Takahashi, L. K., Coker, E. N., Hewson, J. C. and Hobbs, M. L. (April 2022), "Tritium Fires: Simulation and Safety Assessment," Sandia National Laboratories, SAND2022-4187, https://doi.org/10.2172/1862102

[5] Cadwallader, L. C., Petti, D. A. (2002). Deuterium and Tritium Safety Issues in IFE Target Fabrication. *Fusion Science and Technology*, 41(3P2), 635-641, https://doi.org/10.13182/FST02-A22665

[6] Cashdollar, K. L., Zlochower, I. A., Green, G. M., Thomas, R. A. and Hertzberg, M. (2000) "Flammability of methane, propane, and hydrogen gases," *Journal of Loss Prevention in the Process Industries*, 13(3), 327-340, https://doi.org/10.1016/S0950-4230(99)00037-6

[7] De Stefano, M., Rocourt, X., Sochet, I. and Daudey, N. (2019), "Hydrogen dispersion in a closed environment," *International Journal of Hydrogen Energy*, 44(17), 9031-9040, https://doi.org/10.1016/j.ijhydene.2018.06.099

[8] DOE-STD-1027-2018, "Hazard Categorization of DOE Nuclear Facilities," United States Department of Energy, Washington, D.C., (2018).

[9] DOE-STD-1129-2015, "Tritium Handling and Safe Storage," United States Department of Energy, Washington, D.C., (2015).

[10] ISO 9705-1:2016(E), "Reaction to fire tests - Room corner test for wall and ceiling lining products - Part 1: Test method for a small room configuration," Swedish Institute for Standards, Vernier, Geneva, Switzerland, (2016), https://www.iso.org/standard/59895.html

[11] Kazachkov, I. (2011), "The Mathematical Models for Penetration of a Liquid Jets into a Pool," *WSEAS Transactions on fluid mechanics*, 2, 71-91.

[12] Kim, J., Jung, E. and Kang, S. (2015), "Large eddy simulation of hydrogen dispersion from leakage in a nuclear containment model," *International Journal of Hydrogen Energy*, 40(35), 11762-11770, https://doi.org/10.1016/j.ijhydene.2015.04.156

[13] Koroll, G. W. and Kumar, R. K. (1991), "Isotope effects on the combustion properties of deuterium and hydrogen," Combustion and Flame, 84(1), 154-159, https://doi.org/10.1016/0010-2180(91)90044-C

[14] Kumar, R. K. (1985), "Flammability Limits of Hydrogen-Oxygen-Diluent Mixtures," *Journal of Fire Sciences*, 3(4), 245-262, https://doi.org/10.1177/073490418500300402

[15] Kuznetsov, M., Yanez, J., Grune, J., Friedrich, A. and Jordan, T. (2015), "Hydrogen combustion in a flat semi-confined layer with respect to the Fukushima Daiichi accident," *Nuclear Engineering and Design*, 286, 36-48, https://doi.org/10.1016/j.nucengdes.2015.01.016

[16] Lacome, J. M., Jamois, D. Perrette, L. and Proust, C. H. (2011), "Large-scale hydrogen release in an isothermal confined area," *International Journal of Hydrogen Energy*, 36(3), 2302-2312, https://doi.org/10.1016/j.ijhydene.2010.10.080

[17] Liang, Z., Clouthier, T., MacCoy, R. and Chin, Y.-S. (2018), "Overview of hydrogen combustion experiments performed in a large scale vented vessel at Canadian Nuclear Laboratories," *Nuclear Engineering and Design*, 330, 272-281, https://doi.org/10.1016/j.nucengdes.2018.02.002

[18] Mishima, J. and Steele, C.M. (2002), "Oxidation of Tritium Gas under Accident and Transport Conditions," Los Alamos National Laboratory, Report to DOE, LA-UR-02-3803.

[19] Philippe, P., Raufaste, C., Kurowski, P. and Petitjeans, P. (2005), "Penetration of a negatively buoyant jet in a miscible liquid," *Physics of Fluids*, 17(5), 053601, https://doi.org/10.1063/1.1907735

[20] Shapiro, Z. M. and Moffette, T. R. (September 1957), "Hydrogen Flammability Data and Application To PWR Loss-Of-Coolant Accident," Westinghouse Electric Corp., Pittsburgh, PA, USA, WAPD-SC-545. https://doi.org/10.2172/4327402

[21] Sierra Thermal Fluids Development Team (2022a), "Sierra Low Mach Module: Fuego Theory Manual – Version 5.6," Sandia National Laboratories, SAND2022-3961.

[22] Sierra Thermal Fluids Development Team (2022b), "Sierra Low Mach Module: Fuego User Manual – Version 5.6," Sandia National Laboratories, SAND2022-3960.

[23] Svantesson, J. L., Ersson, M. and Jönsson, P. G. (2021), "Effect of Froude Number on Submerged Gas Blowing Characteristics," *Materials (Basel)*, 14(3), 627, https://doi.org/10.3390/ma14030627

[24] Theilacker, J. C. and White, M. J. (2005), "Diffusion of gases in air and its affect on oxygen deficiency hazard abatement, Fermi National Accelerator Lab, FERMILAB-CONF-05-635-AD, https://www.osti.gov/servlets/purl/897228

[25] Tieszen, S.R., Domino, S.P., and Black, A.R. (June 2005), "Validation of a simple turbulence model suitable for closure of temporally-filtered Navier-Stokes equations using a helium plume," Sandia National Laboratories, SAND2005-3210, https://doi.org/10.2172/923079

APPENDIX A. MESH AND TIMESTEP RESOLUTION STUDIES

This appendix presents effects of mesh refinement and nonlinear iterations for each of the room sizes modeled in this study. Representative residuals for each of the scaled R4 meshes is also presented to show the effect of nonlinear iterations. The most refined regions of these meshes near the T_2 inlet are shown in Figure 2-2, and mesh dimensions are listed in Table 2-1.

Figure A - 1 shows the effects of mesh refinement and nonlinear iterations on the flammable volume (>4% T_2) in the smallest room (ISO-9705 standard) for case S2. This flammable volume is obtained from the simulations using Equation (4) as defined in Section 2.3.1. Increased refinement and nonlinear iterations both reduce the maximum flammable mass and volume. Greater spatial or temporal refinement also reduce the time required for full dispersion to occur. The differences between the cases become indistinguishable with respect to the stochastic noise level when the mesh is refined to the R4S level or higher with at least four nonlinear iterations (NL).

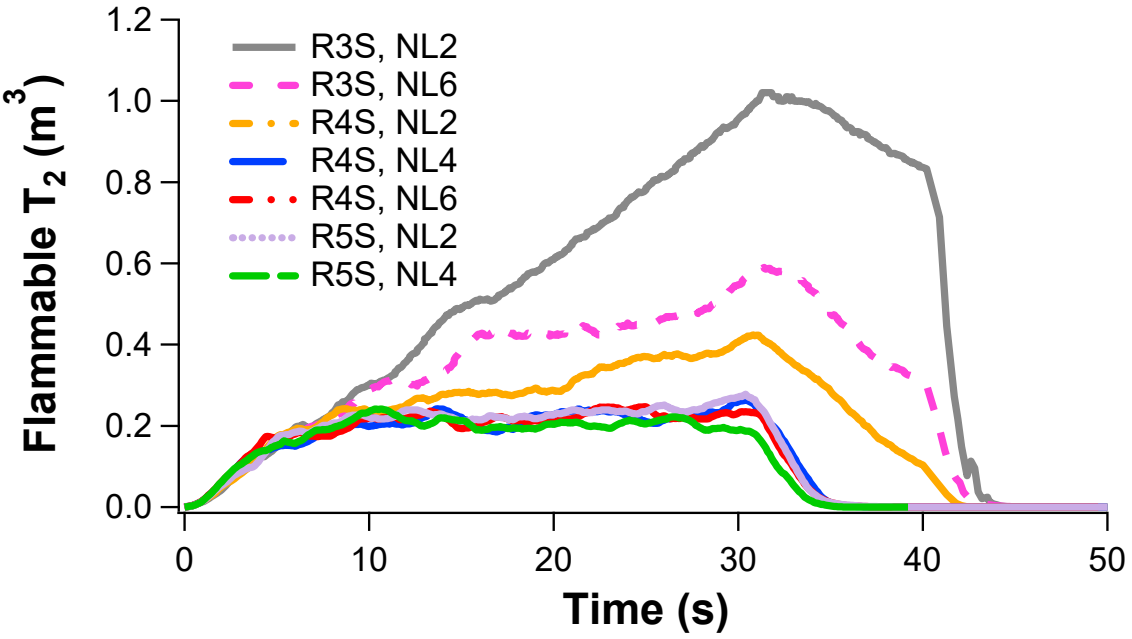

Figure A - 1. Flammable volume (>4% T_2) with increasing mesh refinement (R#S) and nonlinear iterations (NL#) for case S2 (30 g T_2 released in 30 s, small domain)

The final results presented in the main body of this report for case S2 used the R5S mesh with four nonlinear iterations. However, since the R4S mesh used three different nonlinear iterations and yielded similar results in Figure A - 1, the residuals with the R4S mesh are shown as qualitatively representative of final results on the more refined R5S mesh. Figure A - 2 highlights residuals for the overall momentum continuity, species continuity for T_2 (representative of species continuity for O_2 and N_2 as well), and momentum in the vertical Z-direction (representative of X and Y momentum). The enthalpy residuals are not relevant because these simulations were isothermal. The vertical drops in Figure A - 2 indicate the improvement in residuals of at least 2 orders of magnitude with increasing nonlinear iterations for a single timestep. All of the residuals for the small room are significantly better with four nonlinear iterations compared to 2 and increasing nonlinear iterations from four to six significantly improves continuity and momentum without producing much benefit for species.

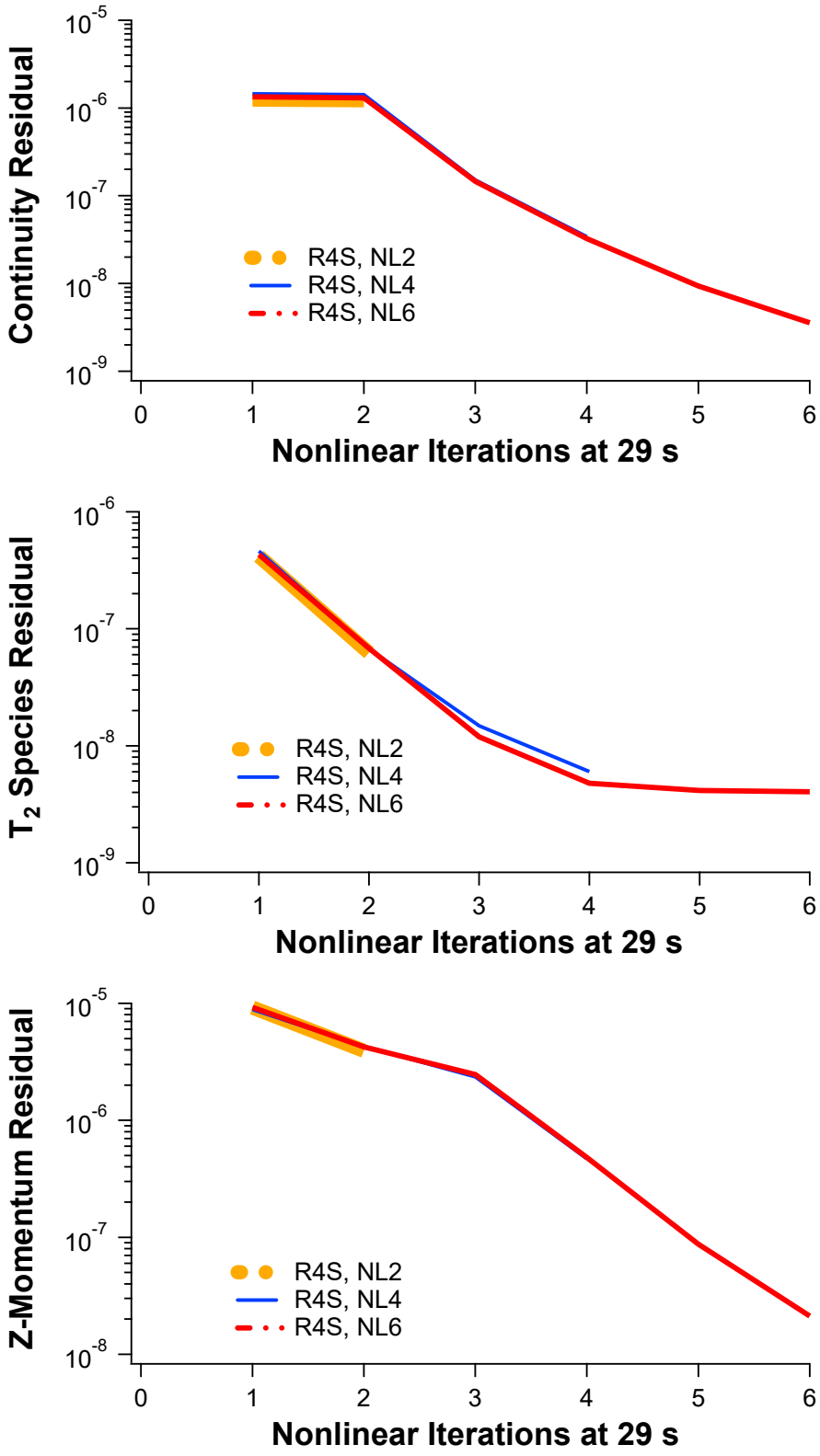

Figure A - 2. Representative residuals on the R4S mesh versus nonlinear iterations (NL#) for case S2 (30 g T_2 released in 30 s, small domain)

Figure A - 3 shows the effects of mesh refinement and nonlinear iterations on the flammable volume (>4% T_2) in the medium room for case M2. An initial simulation shown in Figure A - 3 used a scaled-up version of the base ISO9705 mesh from the previous study (see Brown 2022) is designated as RbM, which has less refinement than the R3M mesh. This initial case with 2 nonlinear iterations yielded extraordinarily long dispersion times, which were reduced by refining the mesh (especially near the gas inlet and the ceiling) and increasing the number of nonlinear iterations until the solution behavior stabilized. As with the smaller room size, the differences between the cases become indistinguishable with respect to the stochastic noise level when the mesh is refined to the R4M level or higher with at least four nonlinear iterations in the medium room.

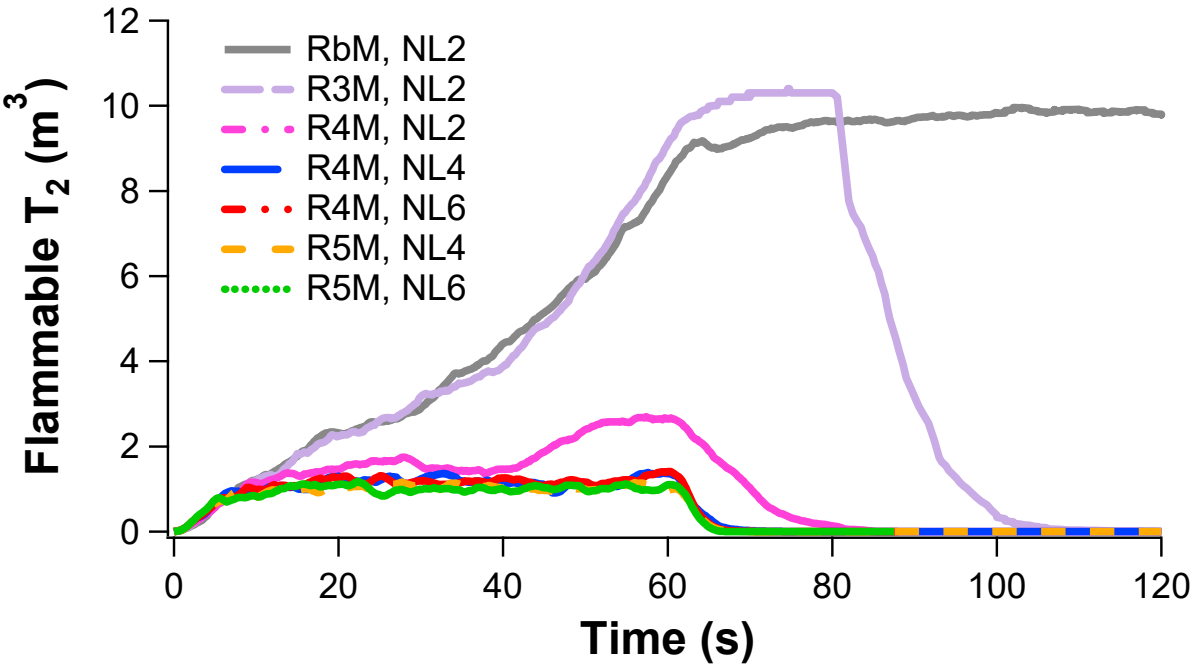

Figure A - 3. Flammable volume (>4% T_2) with increasing mesh refinement (R#M) and nonlinear iterations (NL#) for case M2 (240 g T_2 released in 60 s, medium domain)

The final results presented in the main body of this report for case M2 used the R5M mesh with six nonlinear iterations. However, since the R4M mesh used 3 different nonlinear iterations and yielded similar results in Figure A - 3, the residuals with the R4M mesh are shown as qualitatively representative of final results on the more refined R5M mesh. Figure A - 4 highlights representative residuals for the medium room in the same manner as Figure A - 2 does for the small room. All of the residuals for the medium room are significantly better with four nonlinear iterations compared to 2 and increasing nonlinear iterations from four to six also results in some improvement. The residuals with six nonlinear iterations in the medium geometry decrease ~2 orders of magnitude, which is similar to the small geometry.

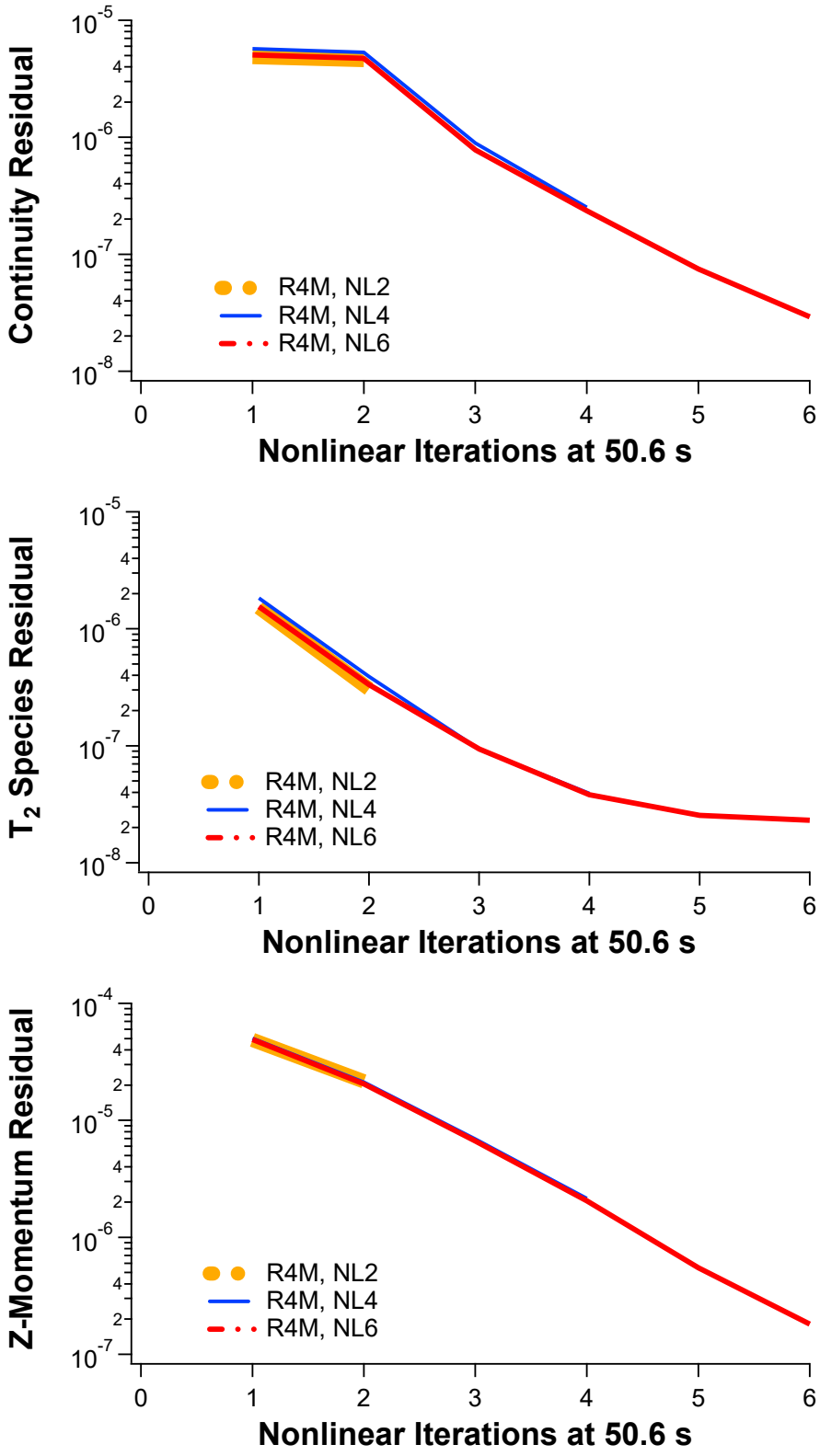

Figure A - 4. Representative residuals on the R4M mesh versus nonlinear iterations (NL#) for case M2 (240 g T_2 released in 60 s, medium domain)

Figure A - 5 shows how mesh refinement and increasing nonlinear iterations (NL) both decrease the dispersion time for flammable regions in case L2, similar to the results in the medium and small rooms. Nonphysical phenomena such as the increased flammable volume (without any increase in flammable mass) between 300 s and 1000 s disappear when the mesh is refined from R3L to R4L. The variants of simulation L2 in the large domain that were refined to R4L took more than 6000 processor hours to predict the full dispersion time. Attempts were made to use the more refined R5L mesh with four nonlinear iterations, but Figure A - 5 shows that only 306 seconds were simulated for this case using 3500 processor hours. Likewise, a case with six nonlinear iterations per timestep with the R5L mesh (not shown) only simulated 21 seconds in over 5000 processor hours. Since the results using the R5L mesh with four nonlinear iterations prior to this time were similar to the R4L case with six nonlinear iterations, the R5L cases were discontinued and the less-refined R4L mesh was used with six nonlinear iterations per timestep, which is expected to produce a dispersion time that is somewhat longer than would be predicted using a more optimal mesh resolution. Since longer dispersion times are conservative for the purpose of a safety analysis and the initial behavior is very similar to computed results with higher resolution, this approach was deemed acceptable for the purpose of this study.

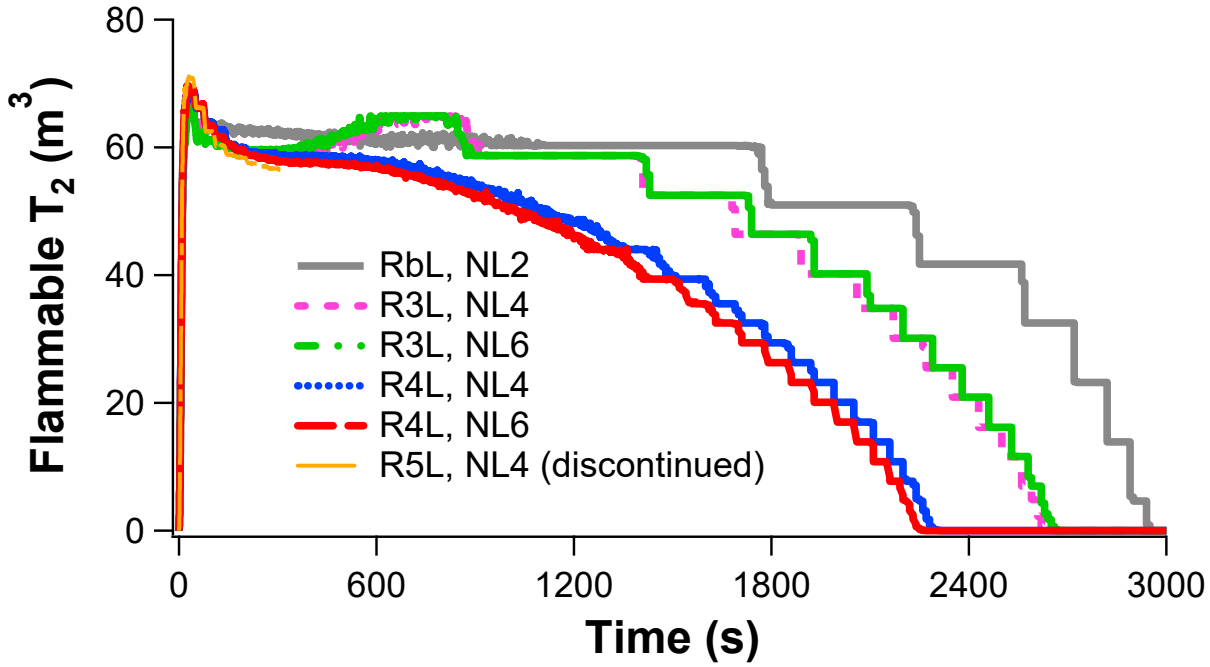

Figure A - 5. Flammable volume (>4% T_2) with increasing mesh refinement (R#L) and nonlinear iterations (NL#) for case L2 (1.5 kg T_2 released in 8 s, large domain)

The residuals for case L2 with the R4L mesh are shown in Figure A - 6; these residuals improve considerably when nonlinear iterations for each timestep are increased from four to 6. Despite this large improvement in the behavior of the residuals, the corresponding response in terms of the flammable volume shown in Figure A - 5 is minor for these two cases. In addition to the residual metrics shown for the smaller rooms, this turbulent case (L2) includes residuals for turbulent kinetic energy as well as dissipation of turbulent kinetic energy. A residual is also included for the momentum in the Y-direction to show it is comparable to the Z-direction. Momentum residuals

actually get worse up through 3 iterations for this turbulent case, so using six NL is strongly preferred. The residual for turbulent kinetic energy dissipation is poor at four NL and nonmonotonic up through 5 NL, which is another reason to choose six or more nonlinear iterations.

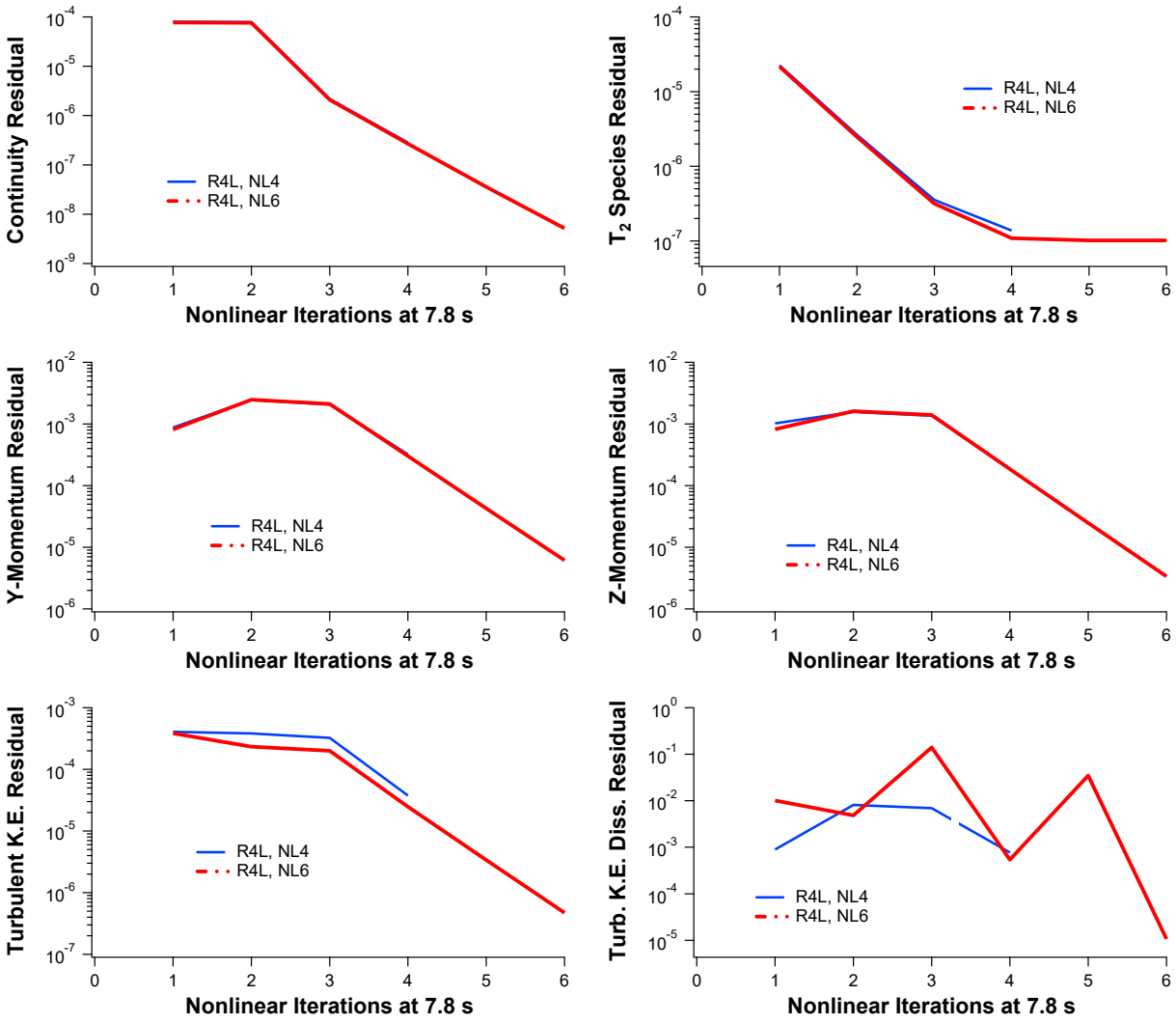

Figure A - 6. Representative residuals on the R4L mesh versus nonlinear iterations (NL#) for case L2 (1.5 kg T_2 released in 8 s, large domain)

APPENDIX B. EFFECTS OF MOTION AND EXIT PATH MESH ON DISPERSION RATES

A few exploratory variants of the L2 simulation (8-second release of 1.5 kg T_2 in the largest room) were conducted. One of these is designated as L2a, and its purpose was to explore how much the residual motion in the ceiling layer (sloshing back and forth) affected the rate of T_2 dispersion. Another case designated as L2b was used to investigate the influence of mesh resolution near the domain outlet, including the upper portion of the door frame.

Case L2a was defined as a simplification of the conditions existing in case L2 at 180 seconds to consider the limiting case of a stagnant flammable ceiling layer. The following steps were used to define these simplified initial conditions:

- The concentration outside the door was assumed to be zero.
- A stagnant velocity field was assumed (zero velocity everywhere).
- Laminar momentum solvers only (stagnant implies no turbulence).
- A completely stratified scenario was assumed, where the highest concentration occurs at the ceiling and decays linearly with decreasing height.
- The tritium masses associated with the L2 concentration bins (see top of Figure 3-35) were used to define a linear concentration profile versus height within the large room. Regions with nonzero tritium concentrations were defined as follows:
    - Applies for z > 5.792 m (height with nonzero concentrations)
    - Applies for y < 9.36 m (inside the room)
    - Mass fraction T_2 = 1.11605E-2*z-6.45936E-2
    - Deviation of the N_2 mass fraction from the standard 7.67083E-1 within the range of y and z listed above is defined as -8.56103E-3*z+4.95486E-2
    - Deviation of the O_2 mass fraction from the standard 2.32917E-1 within the range of y and z listed above is defined as -2.59947E-3*z+1.50449E-2

This definition results in an initial condition for case L2a with 1.003 kg flammable T_2 (> 4% by volume or moles) and 0.2073 kg nonflammable T_2 (< 4%). In other words, less than 0.3 kg out of 1.5 kg left the domain in the first 3 minutes of simulation L2. This linear concentration profile was also consistent with the associated concentration volumes from case L2 at 180 seconds, as well as the average height of the 4% iso-contour at 180 s (similar to Figure 3-33 with less residual motion).

The results of case L2a with respect to case L2 in terms of flammable T_2 mass are shown in Figure B - 1, where the initial behavior before 180 seconds is assumed to be identical. These flammable masses (> 4%) are obtained from Equation (3) as defined in Section 2.3.1. The slope or dissipation rate for case L2a is nearly constant and much lower than any dissipation rate occurring for case L2 prior to 2200 seconds. These slope differences in Figure B - 1 show that the residual motion in case L2 contributes strongly to the dissipation of tritium within 38 minutes.

The two step-changes in T_2 mass for case L2a occur because the initial condition specifies that some of the tritium mass occurs below the level of the doorframe at 6.35 m, which is close to the flammable interface (4% T_2 by volume or 0.85% by mass) occurring at 6.54 m. Some of the nonflammable tritium at the bottom of the stratified layer (5.792 m < z < 6.35 m) can spread

sideways via diffusion through the doorframe and then form a pocket enriched in tritium that to leaves the domain faster than the rate of diffusion because it can rise buoyantly outside the doorframe. This buoyant rise introduces some nonzero velocity to the computational domain and replaces some tritium mass with pure air, both of which contribute to the step changes shown for case L2a. Similar events occur for case L2, which also exhibits step changes in concentration near the beginning and end of the dispersion process.

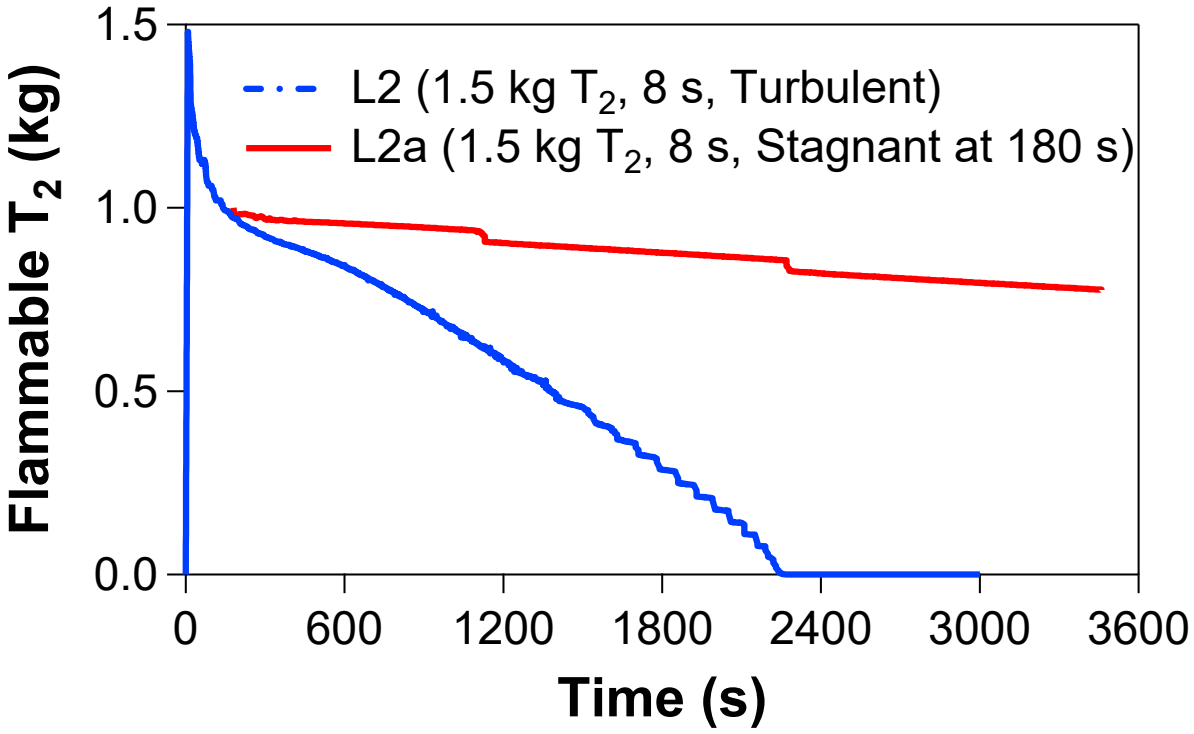

Figure B - 1. Flammable mass for cases L2 and L2a (stagnant and laminar at 180 seconds)

The dispersion slope for the last portion of the L2a curve after 2400 s in Figure B - 1 is -9.6332 kg/s, which represents a pure diffusion limit. This rate suggests that case L2a will take 650 days to disperse (neglecting any additional step changes). This result with an artificially stagnant ceiling layer is much slower than practical scenarios and even well-controlled scenarios such as the experimental studies of helium and hydrogen dispersion by Bauwens (2014), Theilacker (2005), and Lacome (2011). Case L2a is not considered a realistic scenario, as such a large release of hydrogen suggests a pressurized source, which means large releases are more likely to occur fast enough to produce significant gas motion. Even if a large release occurs slowly, it will need to happen very near the ceiling to avoid producing significant dispersive motion from buoyancy.

These results and other simulations from this study exhibiting stair-stepping dispersion suggest that low mesh resolution in the upper doorframe and outside the room near the ceiling could cause relatively few cells to have a large influence on aspects of the simulations such as the rate at which tritium leaves the domain. Case L2b was devised to investigate effects of mesh refinement in the upper doorframe and in the upper regions outside the door where buoyant plumes exit the domain. Case L2b is identical to case L2, but it uses extra refinement in these regions along the path where most of the tritium exits the domain. The mesh dimensions and simulation parameters designated in Table 2-1 for case L2 remain applicable, but the nonlinear iterations for the new mesh (designated as

R7L) were reduced from six to 4. The same min and max mesh sizes apply for L2 and L2b, but the number of mesh nodes increased by about 30% (from 330808 to 429472) when the regions that include the exit path for tritium were refined. The differences in mesh refinement near the doorframe are illustrated in Figure B - 2; the elements for R7L used near the door in case L2b are of higher quality in terms of having lower aspect ratios and smaller average mesh sizes. The higher mesh density on the ceiling near the foreground wall in Figure B - 2 occurs because this wall is adjacent to the release plume (on the lower left). This wall in the left foreground of the top panel of Figure B - 2 corresponds to the lower left wall shown in the top right view of Figure 2-2 (where the highlighted release surface is on the floor).

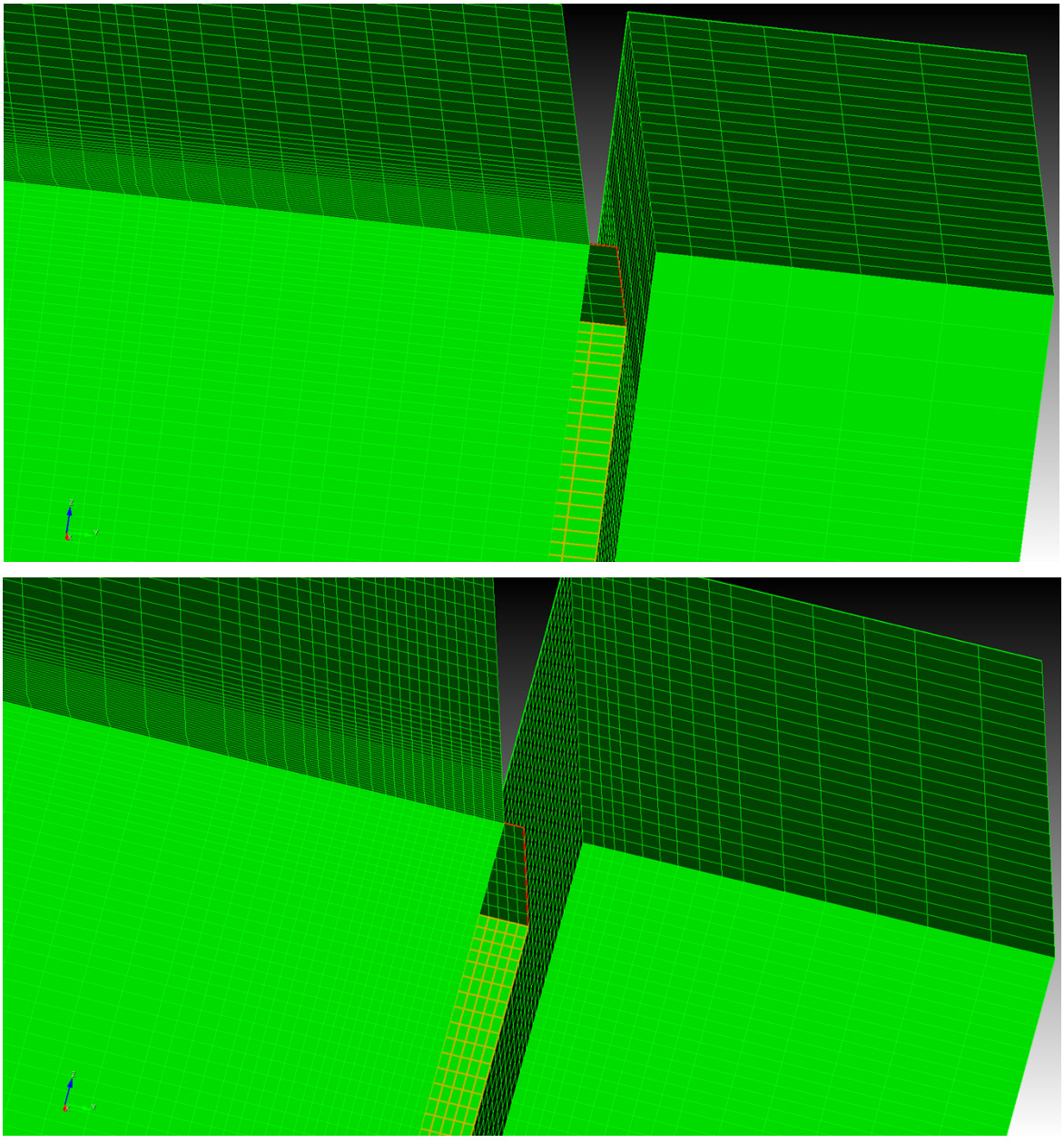

Figure B - 2. Door frame highlighted on R4L mesh used for case L2 (top) and R7L mesh used for case L2b (bottom)

The results of the L2b simulation with respect to L2 are shown in Figure B - 3. The initial behavior during the 8-second release is identical. Thereafter, case L2b closely follows the behavior of case L2, but the "bubble" behavior illustrated for case L2 in Figure 3-31 at 15 seconds is damped, so that L2b produces a smoother curve in Figure B - 3. For this event and others like it, a tritium-enriched region exits the room through the top of the doorframe and then rapidly leaves the domain via buoyant rise.

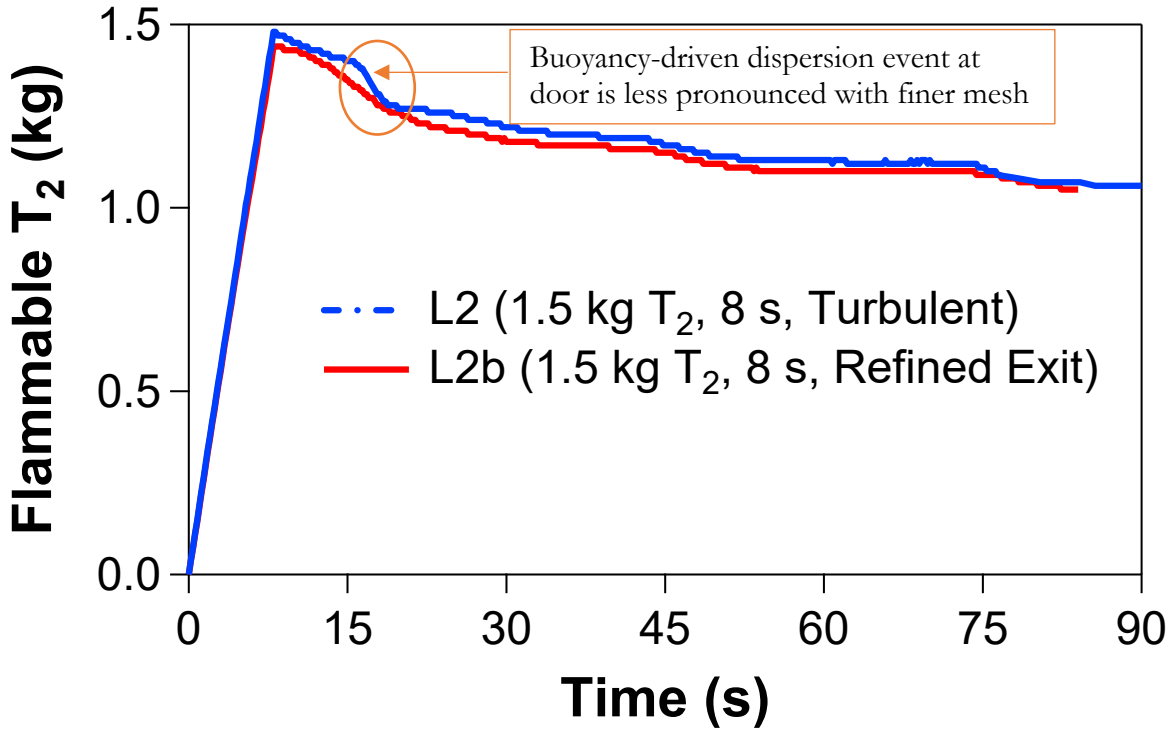

Figure B - 3. Flammable mass for cases L2 and L2b (refined along the path of buoyant dispersion)

The non-ventilated CFD study of Bauwens and Dorofeev (2014) found that hydrogen disperses faster with a coarser mesh, which appears to be related to buoyancy-driven events since they also released hydrogen near the floor and the largest mesh effects occur at locations just above the release where buoyant effects dominate. It makes sense that buoyant events can be artificially enhanced with coarse meshes because buoyant rise of a gas pocket from one computational volume to the next volume above it could introduce light gas to the next "ceiling" interface more quickly if the volumes are large. However, the overall trend in Figure B - 3 for the dispersion of L2b appears to be similar or slightly faster than L2. Similar to the results shown in Appendix A, refinement has the net effect of making the T_2 concentration drop faster or at least sooner. This enhanced dispersion with mesh refinement is presumably dominated by diffusion rather than buoyancy.

APPENDIX C. PROCEDURE TO ASSESS RISK OF FORMING A PERSISTENT FLAMMABLE ZONE

A stepwise procedure to assess the flammability risk associated with gas releases in enclosed spaces based on the metrics in Table 2-3 and the discussion in Section 3.4 is recommended as follows:

1. Check the initial concentration and pressure of the gas in its storage container(s).
    a. Initial concentrations that are low (below the LFL) will not auto-enrich to form a flammable mixture (see Section 1.1).
    b. Concentrations near the flammability limit (<10%) will not convert efficiently to the water form when ignited (Shapiro 1957).
    c. As described in our previous report (see Chapter 2 of Brown 2022), a flammable release from sub-atmospheric storage is not a credible scenario.
2. Check whether the ISF > 1.
    a. A scenario with a larger ignition safety factor is inherently safer and has more propensity to disperse to a nonflammable state.
    b. If ISF < 1, a flammable mixture will occur and persist until the room is ventilated.
3. Check the magnitude of MFLT.
    a. The MFLT will be less than the room height when ISF > 1.
    b. MFLT < 0.1 meter indicates that formation of a real flammable layer is unlikely.
    c. Intermediate values of MFLT (estimated between 0.1 m and 0.5 m) correspond to cases where formation of a flammable zone large enough to be of concern would require the released gas to be constrained by geometric factors and/or stagnant conditions to disperse slowly from a localized zone. In a worst-case (rapid release) scenario that has an MFLT falling in this range, the flammable mass percentage has an intermediate value that is still significantly less than 100%.
    d. MFLT ≥ 0.5 meter indicates that there is a potential to form a continuous flammable zone near the ceiling wherein a high percentage (approaching 100%) of the released gas is present in flammable concentrations. A flammable gas layer of this type may persist for timescales on the order of minutes rather than seconds.
4. To improve bounds on any hazards not eliminated by other criteria, estimate momentum-based parameters such as Re or $Re^{0.5}FrD$ based on the geometry and most probable failure modes of the gas container for a range of realistic release scenarios as indicated in the previous section.
    a. Use Equation (10) with the compound momentum parameter $Re^{0.5}FrD$ and $\alpha = 2.5$.
        i. Data or detailed simulations may be used to specify a better correlation or coefficient value. A more conservative estimate can be obtained using $\alpha = 3.0$ (limit from the simulations in this report without interpolation).
    b. Check whether the resulting penetration height H_p exceeds the room height. If it does, the release event under consideration has enough initial momentum to reach the ceiling and form a semi-stable flammable layer.

i. Re > 2300 may be considered as a secondary or backup momentum criterion that does not account for the effect of room size.

c. These momentum approaches couple with the amount of mass released, so the MFLT criterion should be checked first. If MFLT < 0.1 m, any flammable layer formed is expected to disperse rapidly enough to not be of concern.

5. Further Considerations

a. For the momentum criteria to be meaningful, the flammable gas must be stored in such a manner that a pressure-driven jet directed towards the ceiling is a relevant failure mode.

b. Estimating a range of relevant Froude and Reynolds numbers typically requires knowing the gas pressure and a range of possible orifice sizes for a release event, which requires detailed knowledge of the container shape, dimensions, failure mechanism, and materials.

DISTRIBUTION

Email—Internal

Name	Org.	Sandia Email Address
Russell Jarek	07576	rljarek@sandia.gov
Richard Karnesky	08341	rakarne@sandia.gov
Carlos Lopez	01532	carlope@sandia.gov
Clark Snow	07585	cssnow@sandia.gov
Rajan Tandon	07576	rtandon@sandia.gov
Technical Library	01977	sanddocs@sandia.gov

Email—External

Name	Company Email Address	Company Name
Brandon Chung	chung7@llnl.gov	LLNL
Nanette Founds	nanette.founds@nnsa.doe.gov	US/DOE/NNSA
Matthew Kesterson	Matthew.Kesterson@srs.gov	SRS/SRNL
James Klein	james.klein@srnl.doe.gov	SRNL
James Laurinat	james.laurinat@srnl.doe.gov	SRNL
Haylie Lobeck	haylie.lobeck@nnsa.doe.gov	US/DOE/NNSA
Chandra Marsden	chandra@lanl.gov	LANL
Adrian Mistreanu	adrian.mistreanu@srnl.doe.gov	SRNL
Marlene Moore	marlene.moore@srs.gov	SRS/SRNL
David Pinkston	pinkston1@llnl.gov	LLNL
Jorge Sanchez	sanchez3@llnl.gov	LLNL
Gregory Staack	gregory.staack@srnl.doe.gov	SRNL
Jacob Tuia	jacob.tuia@nnsa.doe.gov	US/DOE/NNSA
Bill Weaver	bill.weaver@em.doe.gov	US/DOE

This page left blank

This page left blank

Sandia National Laboratories

Sandia National Laboratories is a multimission laboratory managed and operated by National Technology & Engineering Solutions of Sandia LLC, a wholly owned subsidiary of Honeywell International Inc. for the U.S. Department of Energy's National Nuclear Security Administration under contract DE-NA0003525.